

Alma Mater Studiorum – Università di Bologna

DOTTORATO DI RICERCA IN

Scienze Biomediche e Neuromotorie

Ciclo XXXI

Settore Concorsuale: 05/D1

Settore Scientifico Disciplinare: BIO/09

**RECEPTOR ARCHITECTURE OF THE MACAQUE MONKEY
SUPERIOR PARIETAL LOBULE**

Presentata da: Dott. Daniele Impieri

Coordinatore Dottorato

Prof. Pietro Cortelli

Supervisore

Prof. Claudio Galletti

Esame finale anno 2019

INDEX

1. INTRODUCTION	1
<i>Associative cortices</i>	1
<i>Posterior parietal cortex (PPC)</i>	4
2. PURPOSE OF THE THESIS	22
3. MATERIALS AND METHODS	23
<i>Histological procedures</i>	23
<i>Receptor autoradiographic labelling</i>	23
<i>Image analysis</i>	25
<i>Statistical analysis</i>	26
4. RESULTS	27
<i>Cyto-architecture of SPL areas</i>	28
<i>Receptor-architecture of SPL areas</i>	32
<i>Receptor fingerprints and insights into functional organization of SPL areas</i>	35
5. DISCUSSION	41
<i>Parcellation schemes of the SPL</i>	41
<i>Receptor-architecture and functional organization of SPL areas</i>	44
<i>Comparison with the human SPL</i>	47
<i>Concluding remarks</i>	48
REFERENCES	50

Colour Table 1	61
Colour Table 2	62
Colour Table 3	63
Colour Table 4	64
Colour Table 5	65
Colour Table 6	66
Colour Table 7	67
Colour Table 8	68
Colour Table 9	69

1. INTRODUCTION

Although the scientific research in the field of neuroscience is exponentially upgrading in the last years, the anatomical and functional characteristics of the brain are still far away from being definitely revealed. The new frontier represented by the Brain Machine Interfaces (BMIs), born with the intention to allow to people losing their motor capabilities to reobtain the use, even if partial, of the motion, in particular way referred to the forelimbs, gave a new impulse on the studies of the brain. In particular, the capability that a robotized machine has in reproducing the fine and precise movements proper of the hands subtends the same fine and precise knowledge of all the possible features of the cerebral areas involved in the movement of the arms. The act of reaching or prehension of an object is the result of the integration of different stimuli coming from the external environment: usually, the object has to be seen in order to analyse characteristics such as shape and dimension; then, if you decide to grasp it, the arm starts to move going towards the object, and hand and fingers have to display so that the object can be correctly grasped. All these steps are possible because the brain is able to integrate visual, sensory, and motor stimuli, so that the movement directed to the object is precise as most as possible. The lack, even partial, of only one of these inputs dramatically impairs the success of the motor act. Equally dramatic is the lack of brain capability to integrate the above-mentioned information. This integration process is the prerogative of the associative cerebral cortices.

Associative cortices

As shown in Fig. 1, the associative cortices occupy the major part (about 80%) of the cortical mantle, while primary motor and sensory cortices constitute only the remaining 20% of the cerebral cortex. In spite of this, the primary motor and sensory cortices are the most studied and known regions of the brain, while the organization and functional role of associative cortices are at present still partly unknown.

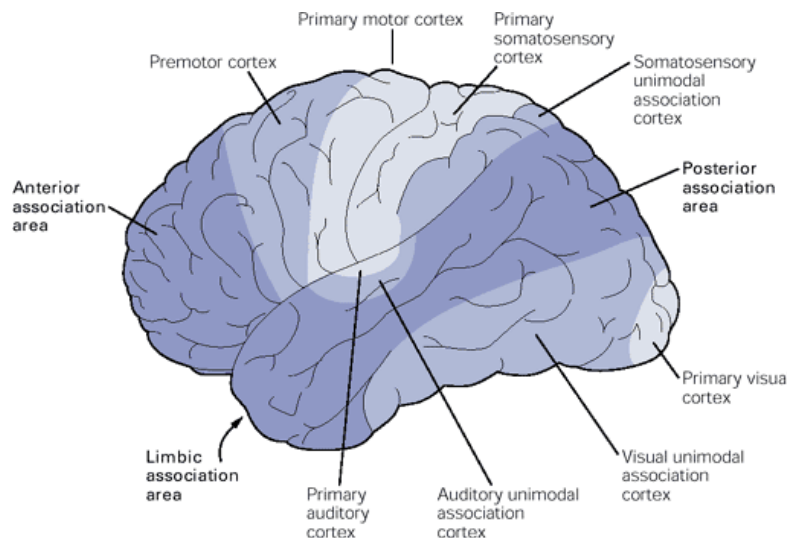


Figure 1. Location and extent of primary sensory, unimodal and multimodal associative areas in the human brain. In this lateral view of a reference human brain, primary sensory (light blue), unimodal as well as multimodal associative cortex (darker blue) are shown. The limbic association area extends in the mesial surface of the hemisphere (arrow), and it is not shown here. (From Kandel E.R., Schwartz J.H., Jessell T.M., Principles of Neural Science, 4/e, Copyright © 2000 by The McGraw-Hill Companies, Inc. All rights reserved.)

It is generally reported that the associative areas of the cerebral cortex are involved in “cognitive functions” (Purves et al., 2013). The term “cognitive functions” means the capability to pay attention to external stimuli, or internal motivational boosts to identify the meaning of these stimuli and, finally, to generate appropriate responses. Because of the high complexity that these tasks require, it is not surprising that the associative areas receive and integrate information coming from multiple sources, affecting a wide range of cortical and subcortical structures. The afferences directed to cortical associative areas comprise projections from motor and sensory cortices, either primary or secondary, from thalamus, and brainstem as well. The associative cortical areas project, in turn, to other cortical areas, hippocampus, basal ganglia, cerebellum, and thalamus.

About the anatomical connectivity, the main difference between primary motor-sensory areas and associative cortices is that the former receive main inputs from peripheral neurons, deputy to capture internal (proprioception) and external stimuli from the surrounding environment; on the contrary, associative cortices are mainly connected with other cortical regions, without a direct interaction with the extra-personal space. In other words, the primary sensory cortices receive information directly from the peripheral sense organs, while the signals that achieve the cortical

associative areas are sensory and motor information that have been elaborated in the primary sensory and motor areas of the cerebral cortex.

Primary sensory cortical areas project to the adjoining higher-order sensory cortical areas, known as unimodal associative areas, which integrate different information concerning single sensory modalities. The unimodal associative areas, in turn, project to multimodal associative areas, that receive also copies of the motor signals and transform sensory-motor information in an action plan. The multimodal associative areas establish the necessary internal programs useful for movement execution, which are transmitted to premotor and primary motor areas for the definitive implementation of motor programs. This flow of information acts in synergy with an opposite one, useful for the modulation of the afferent input. This bidirectional flow of information allows online corrections of the movement to make and maintain it as precise as possible.

Three multimodal associative areas are of the utmost importance (see Figure 1):

- The anterior associative area (prefrontal cortex), located anterior to the pre-central gyrus, governs the planning of movements.
- The associative limbic area, located along the mesial margin of the cerebral hemispheres, presides to the emotional behaviour and memory storage.
- The posterior associative area (posterior parietal cortex), comprising parietal, temporal, and occipital lobes, links information coming from different sensory modalities for the purpose of perception for action.

For the purpose of this work, the organization of the posterior associative area, better known as posterior parietal cortex (PPC), will be discussed more in detail.

Posterior parietal cortex (PPC)

As shown in Fig. 2, the PPC is located in the caudal part of the parietal lobule in both humans and non-human primates, just posteriorly to the postcentral gyrus, which is the seat of the primary somatosensory cortex. It occupies two lobules, the inferior parietal lobule (IPL), laterally, and the superior parietal lobule (SPL), medially and on the mesial surface of the cerebral

hemisphere. IPL and SPL are separated by the intraparietal sulcus, whose walls are part of the posterior parietal cortex. The parieto-occipital sulcus represents the caudal border of the superior parietal cortex. The parieto-occipital sulcus represents the caudal border of the superior parietal lobule in both humans and non-human primates, dividing the posterior parietal cortex from the occipital cortex, which contains the cortical visual areas.

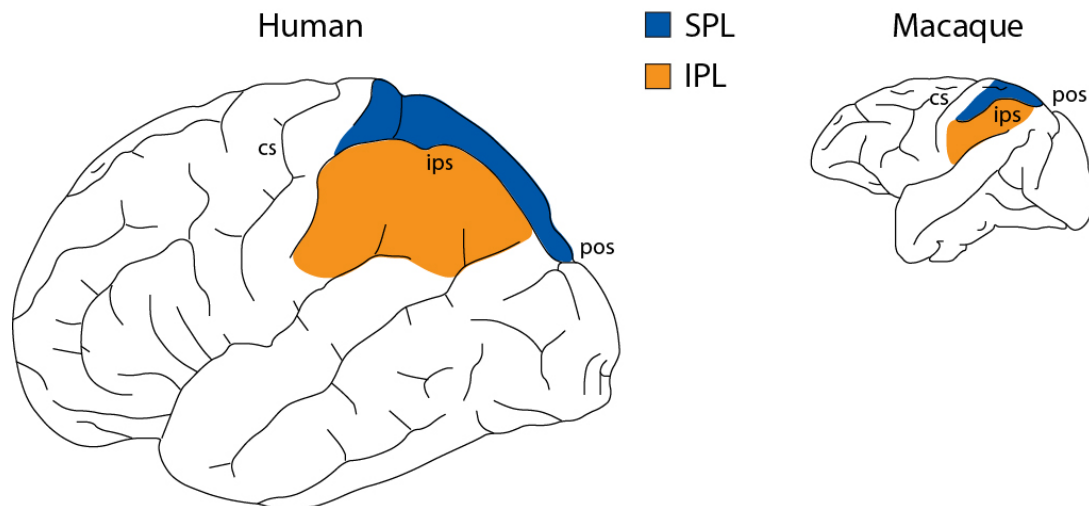


Figure 2. Location and extent of posterior parietal cortex in human and macaque brain. cs: central sulcus; ips: intraparietal sulcus; pos: parieto-occipital sulcus.

The SPL is part of a neuronal network involved in the association of information coming from frontal and visual cortices, useful to plan and control the execution of reaching and grasping movements (Goodale and Milner 1992; Rizzolatti and Matelli 2003; Galletti and Fattori 2017). This brain region hosts several cyto- and myelo-architecturally defined areas (see Figure 3), some of them extensively investigated and others much less studied to date (Pandya and Seltzer 1982; Colby et al. 1988; Luppino et al. 2005). Functional and anatomical studies showed that within the SPL there are two heavily interconnected flows of information, a visual one moving from the posterior areas to the anterior ones, and a somatosensory one moving in the opposite direction. The more central areas within SPL, where the two sensory streams overlapped, are typically sensory-motor areas.

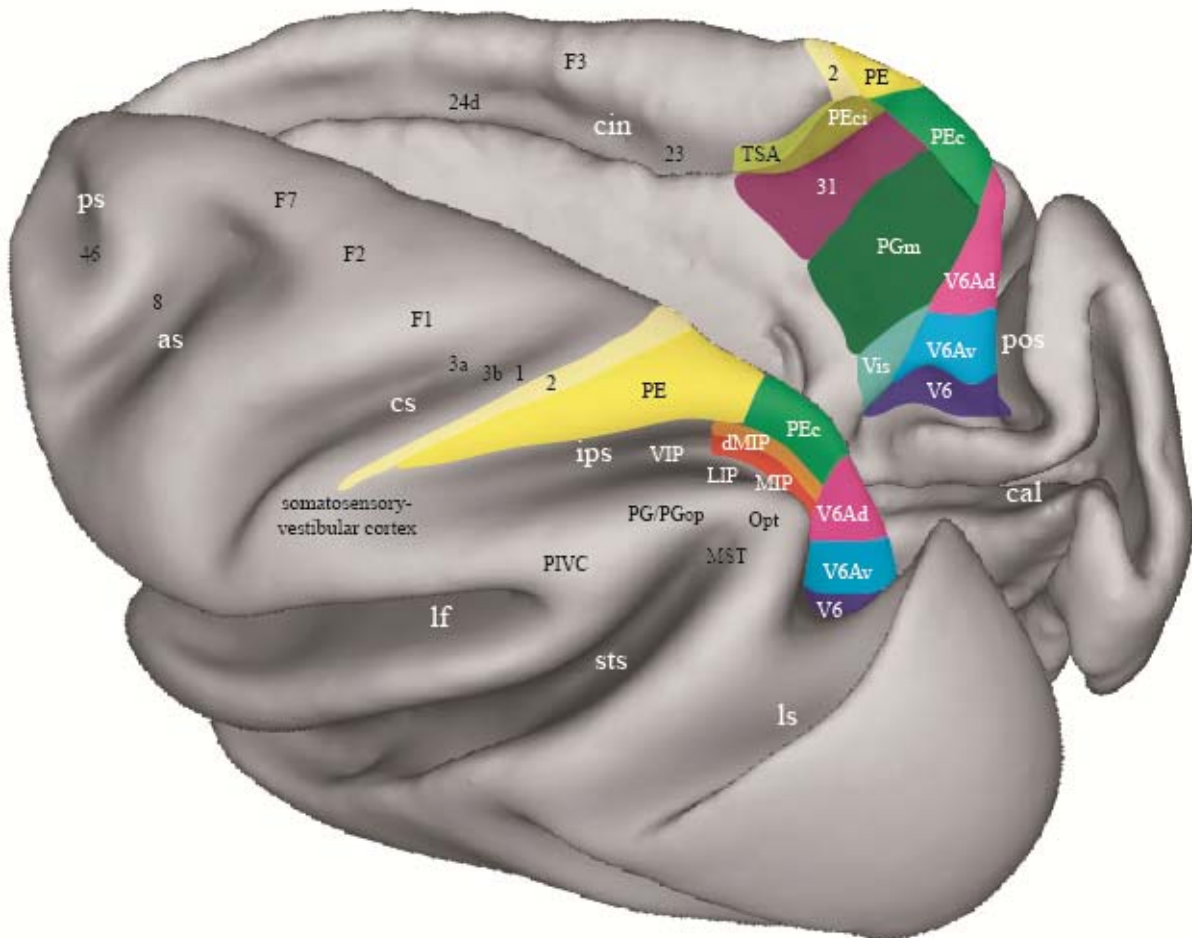


Figure 3. Location and extent of SPL and adjoining areas in the macaque brain. 3D reconstruction of the left hemisphere (in dorsal view) and of the right one (in mesial view) of a macaque monkey brain obtained using CARET software (<http://brainvis.wustl.edu/wiki/index.php/Caret:Download>) showing the location and extent of the areas composing the SPL, as well as of directly adjacent areas. as: arcuate sulcus; cal: calcarine sulcus; cin: cingulate sulcus; cs: central sulcus; ips: intra-parietal sulcus; lf: lateral fissure; ls: lunate sulcus; ps: principal sulcus; pos: parieto-occipital sulcus; sts: superior temporal sulcus.

As shown in Fig. 3, the areas of the SPL are areas V6 (visual motion area; Galletti et al. 1999, 2001; Gamberini et al. 2015), V6Av and V6Ad (visuo-motor areas; Gamberini et al. 2009, 2011, 2015, 2018; Passarelli et al. 2011; Galletti and Fattori 2017), PEc (visuo-motor area; Breveglieri et al. 2006, 2008; Bakola et al. 2010; Piserchia et al. 2017; Gamberini et al. 2018), PE (somato-motor area; Mountcastle et al. 1975; Pandya and Seltzer 1982; Padberg et al. 2007; Seelke et al. 2012; Bakola et al. 2013), PGm, mainly involved in oculomotor activity, spatial navigation (Olson et al. 1996; Thier and Andersen 1998; Leichnetz 2001; Passarelli et al. 2018) and visually guided limb movements (Ferraina, Garasto, et al. 1997; Passarelli et al. 2018), and PEci, with somato-motor properties (Murray and Coulter 1981; Morecraft et al. 2004).

The anatomo-functional characteristics of each of the above-mentioned areas will be discussed in the following sections.

Area V6

Area V6 is located in the caudalmost aspect of the SPL (Figure 3). It occupies a “C”-shaped belt of cortex whose lateral branch is within the depth of the pos, in the ventral part of the anterior bank of the sulcus, while the medial one is in the medial surface of the brain at the level of the medial parieto-occipital sulcus (Galletti, Fattori, Gamberini, et al. 1999). In the lateral dimension, area V6 goes down from the anterior bank to the fundus of the pos, where it borders area V3A, moving up again along the posterior bank of the same sulcus, merging with the cortex of area V3 laterally (see Fig. 17 in Galletti, Fattori, Gamberini, et al. 1999). Dorsally and anteriorly, area V6 borders on the ventral subdivision of area V6A, while ventrally and posteriorly it borders on the medial-most part of areas V3A and V3 (see Fig. 6 in Gamberini et al. 2015).

The Nissl staining method shows that this area presents an occipital cyto-architectonic pattern, similar to that of the adjoining area V3, characterized by a thick layer IV in which densely packed granular cells take place, a light layer V populated by small pyramidal cells, and a layer VI composed by two sub-layers, with a very dense layers VIb (Figure 4; Luppino et al. 2005). Other specific features that help to discriminate area V6 from area V3 are an evident layer II with densely packed small cells and a dense layer III in which medium-sized pyramids are visible in its lowest part. Furthermore, layer VI shows a clear radial cellular organization, constituted by thin vertical columns very close to each other (Figure 4; Luppino et al. 2005).

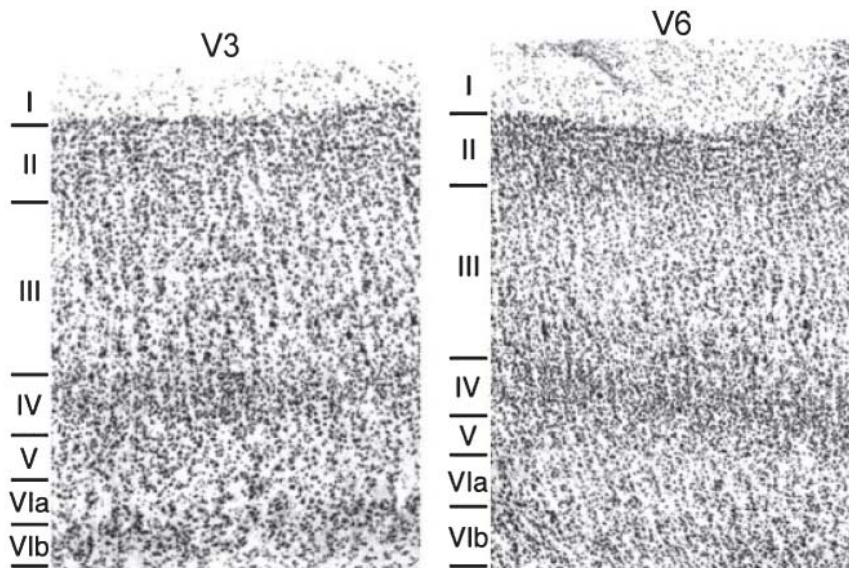


Figure 4. Cyto-architectonic pattern of area V6 and adjoining area V3. High magnification views of a Nissl-stained segment of areas V3 and V6 are shown. (Modified from Luppino et al. 2005).

Looking at immune-architecture (Figure 5, to the left), area V6 shows a relatively high immunoreactivity in the lower part of layer III, whilst layer V presents very few, small and weakly positive pyramidal cells (Luppino et al. 2005). Myelo-architecture analysis (Figure 5, to the right) allow to observe that area V6 is highly myelinated, with the inner and outer Baillarger bands densely impregnated (Luppino et al. 2005).

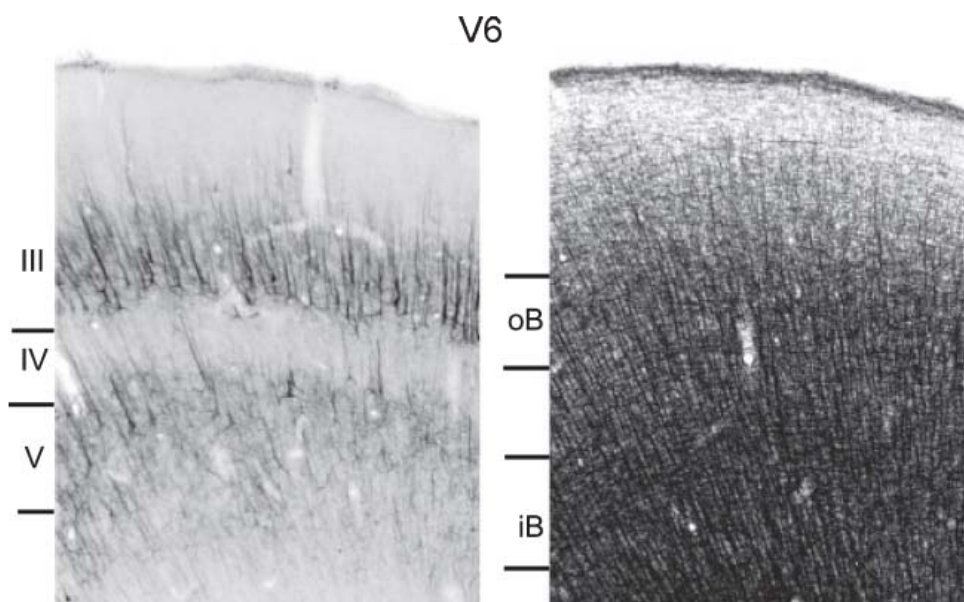


Figure 5. Immuno- and myelo-architecture of area V6. High magnification views of a SMI-32-immunoreactivity stained (to the left) and a myelin-stained segment (to the right) of area V6 are shown. (Modified from Luppino et al. 2005).

On a functional point of view, area V6 is a cortical visual area where the entire contralateral visual field is point-to-point represented up to an eccentricity of at least 80°, with the lower visual field representation located in the ventral-most part of the anterior bank of the pos, and the upper one within the medial pos, on the mesial surface of the hemisphere. The periphery of the visual field is represented medially, and the centre laterally (Galletti, Fattori, Gamberini, et al. 1999). The representation of the central part of the retina is not magnified, as it is usual for all the cortical visual areas. Area V6 represents central and peripheral parts of the retina in a quite uniform way, contrary to all other cortical visual areas (Galletti, Fattori, Gamberini, et al. 1999).

Area V6 is recognized as a visual motion area due to the high sensitivity to which its neurons respond to the direction and speed of motion (Galletti et al. 1996), as well as to real object movement in the visual space (Galletti and Fattori 2003). Cortico-cortical connections obtained using both anterograde and retrograde neuronal tracers corroborate this evidence: area V6 shows half of its reciprocal connections with the primary visual area (area V1) and with the extrastriate areas V2, V3, and V3A in the occipital lobe. The other half is shared with visual areas V6Av in the ventral part of the anterior bank of the pos, V4T, MT/V5 and the high-order visual area MST at the level of the superior temporal sulcus (sts), and with areas LIPv, MIP and VIP at the level of the intraparietal sulcus (ips; Galletti et al. 2001). All these areas are involved in the encoding of visual stimuli with different specificity. Thalamo-cortical pattern of connections is also in agreement with the visual properties associated to area V6: purely visual thalamic nuclei, namely lateral geniculate nucleus and lateral and inferior pulvinar nuclei, represent the bulk of the thalamic projections directed towards this cortical area (Gamberini et al. 2016). Like area V6, all these nuclei are retinotopically organized (Jones 2007; Kaas and Lyon 2007).

All these data strongly suggest that area V6 represents the gateway through which visual information from the occipital lobe reaches the areas of the parietal lobe (Galletti et al. 2001).

Area V6A

Dorsal to area V6 there is area V6A (Figure 3), that occupies most of the anterior bank of the pos as well as the caudal-most part of the precuneate cortex on the mesial surface of the hemisphere (Galletti, Fattori, Kutz, et al. 1999). This area has been subdivided into two different sectors, named V6Av (ventral) and V6Ad (dorsal), based on architectural, functional and connectional characteristics (Luppino et al. 2005; Gamberini et al. 2009, 2011; Passarelli et al. 2011).

Cyto-architectonic analysis (Figure 6) demonstrated that both areas V6Av and V6Ad are homotypic parietal areas (Luppino et al. 2005). They have well developed layers III and V, with a relatively large presence of medium sized pyramidal cells, a relatively dense layer IV, that could be subdivided in a less dense upper part and a denser lower part, and a layer VI in which the identification of sublayers appears to be quite hard and the border with the white matter is rather blurred (Luppino et al. 2005). By the way, several aspects allowing discerning between area V6Av and V6Ad counterbalance the common architectural characteristics mentioned before. In area V6Av, layer II is clearly distinguishable, and in layer III a size gradient of pyramidal cells is present, with larger pyramids located in its lower part (Luppino et al. 2005). More, layer V is quite developed, containing medium sized pyramidal neurons. Layer VI shows two subdivisions, and the border with the white matter is not as clear as in area V6 (Luppino et al. 2005). On the contrary, area V6Ad is characterized by a poorly definable layer II, and a layer III with a more homogeneous neuronal population (Luppino et al. 2005). Layer V is more stained compared to area V6Av, containing larger pyramids, while layer VI shows itself more homogeneous, with a less evident border at the level of white matter (Luppino et al. 2005). More, in area V6Av, layer III is denser compared to area V6Ad, displaying a more evident gradient in cellular size, layer V is less rich, and a differentiation of layer VI in two sublayers is clearer (Luppino et al. 2005).

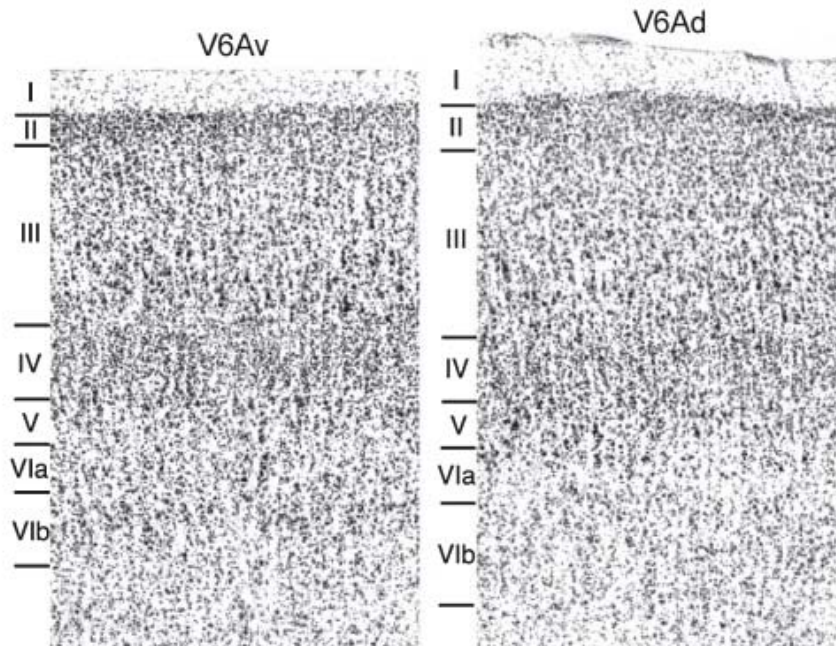


Figure 6. Cyto-architectonic pattern of areas V6Av and V6Ad. High magnification views of a Nissl-stained segment of areas V6Av and V6Ad are shown. (Modified from Luppino et al. 2005).

Looking at the distribution of SMI-32 immunoreactivity (Figure 7, to the left), layer III of area V6A is less stained compared to area V6, due to a loose arrangement in sublayer IIIc of the immune-positive pyramidal cells, which are larger than in area V6 but with a smaller amount of apical dendrites (Luppino et al. 2005). Another difference between area V6 and area V6A is the presence of large stained pyramidal cells in layer V of the latter (Luppino et al. 2005). The greatest difference between the two cyto-sectors of area V6A using the SMI-32 antibody is the presence of larger and more numerous cell bodies in layers III and V of area V6Ad compared to area V6Av (Luppino et al. 2005). Myelo-architecture analysis (Figure 7, to the right) shows that area V6Av is well stained, even if less than area V6, with clearly recognizable Baillarger bands. In area V6Ad, the Baillarger bands are less stained with respect to area V6Av (Luppino et al. 2005).

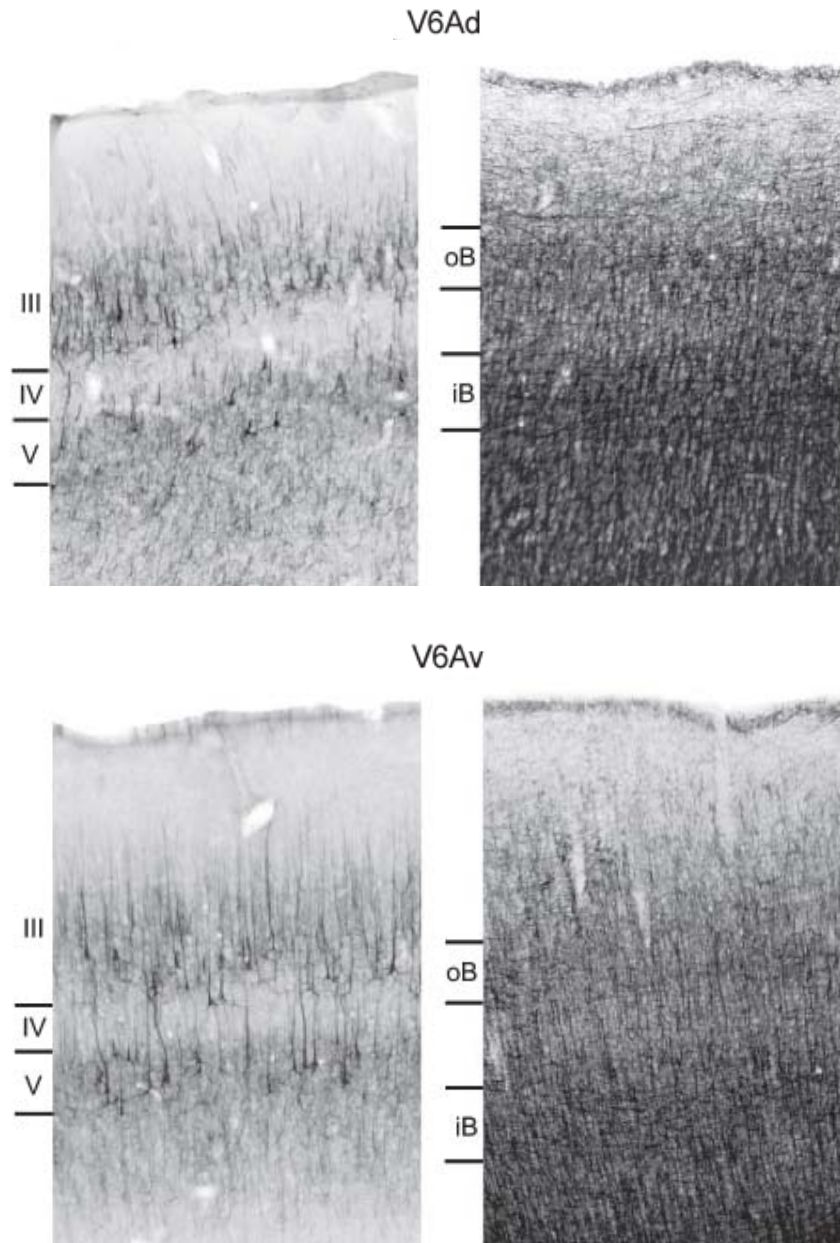


Figure 7. Immuno- and myelo-architecture of areas V6Ad and V6Av. High magnification views of a SMI-32-immunoreactivity stained (to the left) and a myelin-stained segment (to the right) of areas V6Ad and V6Av are shown. (Modified from Luppino et al. 2005).

Although both sectors of area V6A are not point-to-point retinotopically organized, area V6Av mainly represents the peripheral part of the contralateral visual field, whereas area V6Ad the central part of it; more, area V6Av represents almost exclusively the lower visual field, whereas area V6Ad represents both upper and lower visual fields, with a prevalence for the latter (Gamberini et al. 2011, 2015). Cells responsive to visual stimuli are more present in area V6Av than in area V6Ad and, on the contrary, somatosensory cells are more common in V6Ad than in V6Av; in

addition, cells in area V6Av respond to simple visual stimuli, whilst in area V6Ad more complex visual stimuli are required to activate neurons (Gamberini et al. 2011). Another difference in visual properties between the two sectors of area V6A is the location of a particular class of visual cells named “real-position” cells (Galletti et al. 1993, 1995). This type of cells, characterized by a visual receptive field that remains constant in space regardless of eye movements, is a prerogative of area V6Av (Galletti et al. 1995, 1996; Gamberini et al. 2011). Differences between the two sectors of V6A are also present in the distribution of somatosensory cells. The majority of somatosensory cells are located in area V6Ad, where they are twice as compared to those in area V6Av (Gamberini et al. 2011). In both sectors of area V6A, somatosensory cells represent the arm, in particular the joints, and body parts nearby (Breveglieri et al. 2002; Gamberini et al. 2011). Bimodal cells sensitive to both visual and somatosensory stimuli were mainly distributed in area V6Ad (Gamberini et al. 2011). Many cells in both areas V6Ad and V6Av are modulated by reaching (Galletti et al. 1997; Fattori et al. 2001, 2004, 2005, 2017; Gamberini et al. 2011) and grasping (Fattori et al. 2004, 2009, 2010, 2017; Gamberini et al. 2011) arm movements.

Cortico-cortical connections of areas V6Av and V6Ad reflect the different functional characteristics mentioned before. The ventral sector of area V6A is mainly connected with extrastriate visual areas, as well as parietal and frontal areas enrolled in the encoding of sensorimotor integration (Passarelli et al. 2011). Specifically, the visual areas connected with area V6Av are the extrastriate areas V2, V3, V4, V6, and MST, and the visuo-motor area V6Ad, suggesting that area V6Av plays a pivotal role in transferring the visual input from extrastriate visual areas to area V6Ad, that uses this information to control the movement of the upper limb (Passarelli et al. 2011). Other inputs to area V6Av come from the eye/arm-movement related areas PGm in the mesial cortex, MIP in the ips, and FEF, 46, and F7 in the frontal lobe (Passarelli et al. 2011). The fact that area V6Av receives inputs from parietal areas involved in the encoding of reaching and grasping arm movements, and that these areas are connected with frontal premotor areas, indicate that this area is a node of a neuronal network that is involved in the visuo-motor

process that controls the visual guidance of prehension in extra-personal environment (Passarelli et al. 2011). Also thalamic inputs to area V6Av, primarily coming from lateral posterior and medial pulvinar nuclei, support the view of an integrative role of visual and somato-motor information proposed for this cortical area (Gamberini et al. 2016).

Regarding the cortico-cortical connections of area V6Ad, minor afferents come from visual areas MST and V6Av, as well as from areas 31 and 23 of the mesial cortex and area 46 of the frontal lobe (Gamberini et al. 2009). Strong inputs come from parietal areas involved in processing of visual and somato-sensory stimuli useful to control reaching and grasping movements, that is areas MIP, LIP, VIP, and AIP hidden within the ips, PEc located in the exposed surface of the SPL, PGm in the mesial precuneate cortex, and PG and Opt in the IPL (Gamberini et al. 2009). Another strong input comes from the frontal lobe, in particular from area F2, which is involved in reaching and grasping activity (Raos et al. 2003, 2004), and area F7, mainly involved in oculomotor activity (Boussaoud et al. 1998; Gregoriou et al. 2005). In agreement with the functional properties of V6Ad neurons, the strong inputs coming from areas showing arm-reaching activity suggest that area V6Ad takes part in a parieto-frontal network involved in the control of prehension (Gamberini et al. 2009). Thalamic projections to area V6Ad are in agreement with this view, showing that the major inputs come from lateral posterior and medial pulvinar nuclei, while minor inputs from ventral lateral and medial dorsal nuclei (Gamberini et al. 2016). The integrative visuo-motor role of lateral posterior and medial pulvinar nuclei (Grieve et al. 2000), as well as the motor function of the ventral lateral nucleus (Ilinsky and Kultas-Ilinsky 1987), and the eye-related activity of medial dorsal nucleus (Watanabe and Funahashi 2004), well agree with the functional characteristics of area V6Ad (Gamberini et al. 2016).

Despite several differences can be appreciated comparing the architectural, functional, and connectional properties, as described above, nowadays it is believed that the two cyto-sectors of area V6A work as a single functional entity in the control of reach-to-grasp movements, V6Av

mainly presiding the visual aspect of this control and V6Ad its somato-motor aspect (Gamberini et al. 2011).

Area PEc

Area PEc lies anterior to area V6A, on the exposed surface of SPL (Figure 3; Pandya and Seltzer 1982; Luppino et al. 2005). Area PEc occupies the caudalmost third of a region originally indicated as area 7 by Brodmann (Brodmann 1909). It extends onto the mesial surface of the hemisphere up to the border with area PGm, and laterally into the medial wall of the ips up to the border with area MIP (Pandya and Seltzer 1982; Bakola et al. 2010).

Proper cyto-architectural features that distinguish area PEc from area V6Ad are the presence of a clear gradient in cellular size in layer III, with the lower part heavily populated by medium-sized pyramids, and a dense layer V in which large pyramidal neurons are present (Fig. 8; Pandya and Seltzer 1982; Luppino et al. 2005). Using SMI-32 monoclonal antibody, area PEc showed a decrease in the number of immune-positive pyramidal cells in layers III and V in respect to area V6Ad, even if the size of these cells is considerably larger than in area V6Ad (Fig. 8; Luppino et al. 2005).

Area PEc is a bimodal somato-visual area dominated by the somatic input. In area PEc there is an incomplete map of the body, principally focused on the four limbs, without any evident sign of topographical organization, and a rough, non-retinotopic representation of the contralateral visual field (Breveglieri et al. 2006, 2008; Gamberini et al. 2018). PEc neurons respond to visual or tactile stimuli, and/or to passive single-joint rotations (Squatrito et al. 2001; Raffi et al. 2002; Breveglieri et al. 2006, 2008; Gamberini et al. 2018), with some neurons capable of bimodal responses (Breveglieri et al. 2008; Gamberini et al. 2018). PEc neurons also show arm and eye movement-related activity (Battaglia-Mayer et al. 2001; Ferraina et al. 2001; Piserchia et al. 2017), including sensitivity to the direction and depth of arm movement (Bhattacharyya et al. 2009; Hadjidimitrakis et al. 2015).

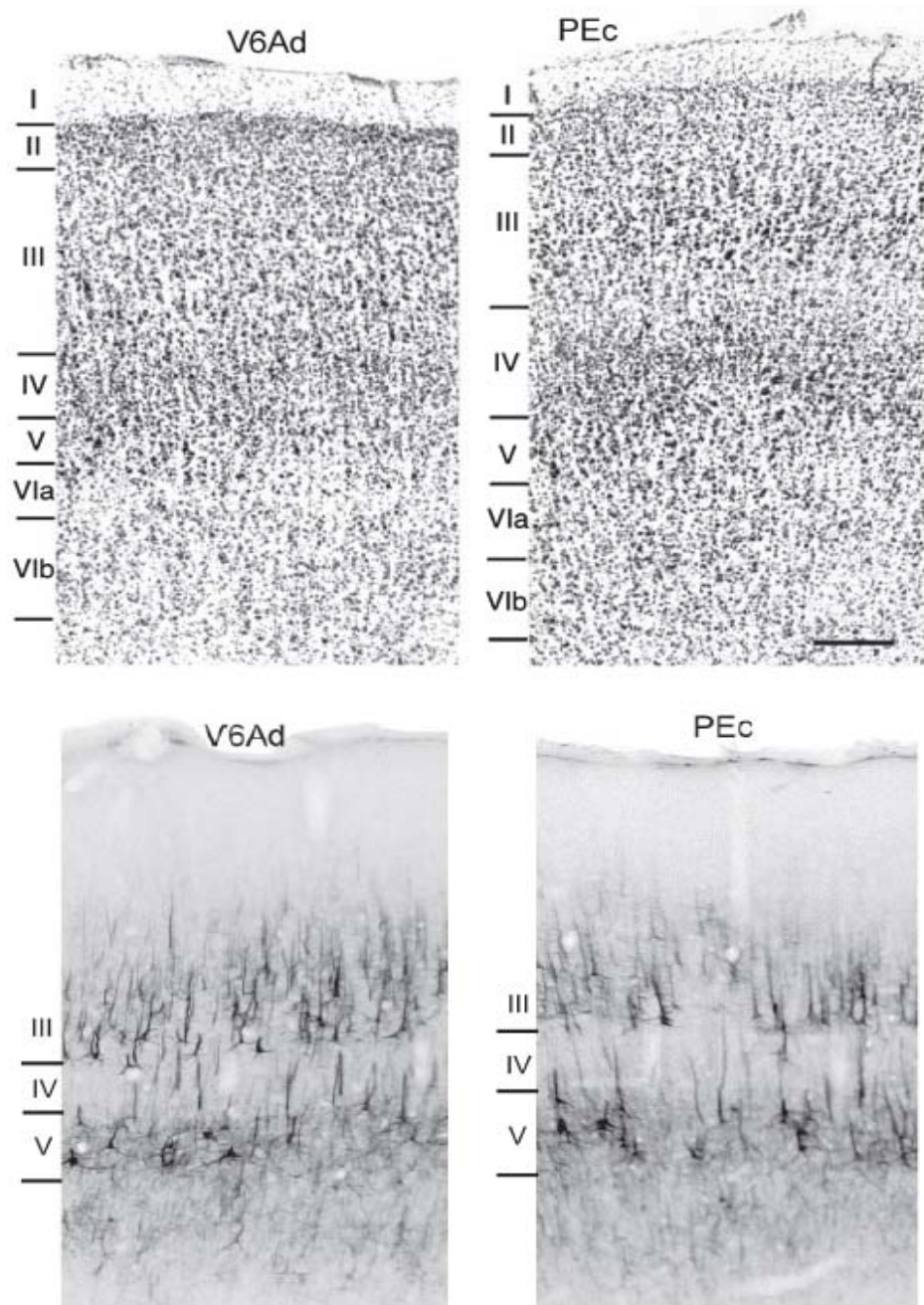


Figure 8. Cyto- and immuno-architecture of areas V6Ad and PEc. High magnification views of Nissl-stained (at the top) and SMI-32-immunoreactivity stained (at the bottom) segments of areas V6Ad and PEc are shown. (Modified from Luppino et al. 2005).

As expected by the functional properties of PEc neurons, the analysis of the cortical connections revealed that the majority of projections to area PEc comes from somatosensory-related cortices. In particular, PEc receives inputs from area PE, that occupies the anterior two thirds of the exposed surface of the SPL, and area PEci or SSA (Supplementary Somatosensory Area) located within the caudal tip of the cingulate sulcus (Duffy and Burchfiel 1971; Morecraft et al. 2004).

Another strong input to PEc originates in the caudal part of the medial bank of the ips, and in particular in its dorsal-most part, termed dMIP to distinguish it from area MIP proper, which sends only minor labelling to PEc (Bakola et al. 2010). Minor afferents to area PEc come from the somatosensory area 2 and the somatosensory-vestibular cortex of the lateral fissure, both located in the anterior part of the parietal lobe (Fig. 3; Bakola et al. 2010). The main visual information directed to area PEc comes from the visuo-motor area V6A, and in particular from its dorsal subdivision (Bakola et al. 2010), while motor information comes from areas F1, F2 (the main input), and F3 in the frontal lobe (Matelli et al. 1998; Bakola et al. 2010). Other cortical areas connected with area PEc are PGop, PG, and PIVC in the lateral parietal cortex, and areas 23, 24d, 31, and PGM in the mesial surface of the hemisphere (Bakola et al. 2010). Since area PEc is mainly connected with somatosensory and somato-motor areas of parietal and frontal lobes, it has been suggested that it is functionally involved in the skeleto-motor control (Bakola et al. 2010). Evidences coming from the analysis of the connectional pattern, together with the functional properties of the neurons located in area PEc, suggest a specific role of this area in locomotion and in coordination of movements in natural environments (Bakola et al. 2010).

The functional considerations derived by the analysis of claustral (Gamberini et al. 2017) and thalamic (Impieri et al. 2018) afferents to area PEc are in line with the above mentioned proposed role of area PEc. For a more exhaustive examination of the subcortical connections of area PEc, please refer to the specific articles reported at the end of the thesis.

Area PE

Area PE lies anterior to area PEc, on the exposed surface of the anterior two thirds of the SPL (Figure 3; Pandya and Seltzer 1982). The cortical region occupied by PE was originally indicated as area 5 by Brodmann (Brodmann 1909).

The analysis of the cyto-architectonic material (Figure 9) revealed that in area PE layer II is less differentiated, on the contrary layer III is well definable because of its thickness and the presence of a size gradient in the pyramidal cells population (Pandya and Seltzer 1982). About

myelo-architecture, area PE presents a weakly stained outer band of Baillarger and a moderately developed plexus of fibers in deeper layers (Pandya and Seltzer 1982).

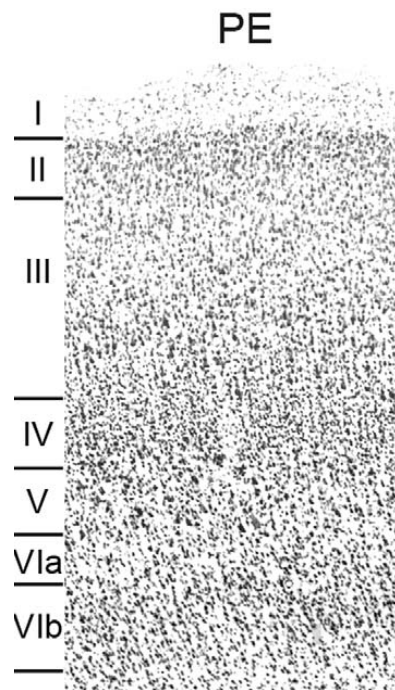


Figure 9. Cyto-architecture of area PE. High magnification view of a Nissl-stained segment of area PE is shown. (Modified from Impieri et al. 2018).

Area PE hosts a rough topographical representation of the body, with an over-representation of the arms and hands (Taoka et al. 1998, 2000; Padberg et al. 2007; Krubitzer and Disbrow 2008; Seelke et al. 2012). PE neurons are mainly activated by proprioceptive stimulation, although some of them respond to tactile stimulation (Duffy and Burchfiel 1971; Sakata et al. 1973; Mountcastle et al. 1975). These neurons are involved in the preparation and control of limb movements (Burbaud et al. 1991; Ferraina and Bianchi 1994; Lacquaniti et al. 1995; Kalaska 1996; Ferraina et al. 2009; Bremner and Andersen 2012) and become active during skilled actions (Maimon and Assad 2006; Chen et al. 2009; Shi et al. 2013).

The cortical inputs to area PE come from somatosensory-related and motor-related areas of parietal and frontal lobes (Bakola et al. 2013). About the somatosensory input, most come from the nearby areas 2, PEc, and PEci, as well as the opercular areas PGop and PPop, and the retro-insular cortex at the level of the lateral fissure (Bakola et al. 2013). Minor inputs originate from other

sectors of the somatosensory cortex as areas 1, 3a and 3b (Bakola et al. 2013). In addition, areas dMIP and PEip in the medial bank of the ips are connected with area PE, as well as areas 23 and 24 in the mesial cortex (Bakola et al. 2013). The motor input to PE mainly comes from F1 and, to a less extent, from premotor areas F2 and F3 (Bakola et al. 2013). The cortico-cortical connective pattern of area PE fits well with the proposed functional role for this area, that is the planning and guidance of reaching movements (Bakola et al. 2013). As for area PEc, claustral (Gamberini et al. 2017) and thalamic (Impieri et al. 2018) inputs corroborate the functional role proposed for area PE. For a more exhaustive examination of the subcortical connections of area PE, please refer to the specific articles reported at the end of the thesis.

Area PGm

The precuneate cortex on the mesial surface of the SPL is mostly occupied by area PGm (Figure 3; Pandya and Seltzer 1982; Passarelli et al. 2018). Area PGm occupies a cortical region originally indicated as area 7 by Brodmann (Brodmann 1909), and area 7m by other authors (Cavada and Goldman-Rakic 1989; Kobayashi and Amaral 2003).

The characteristic cyto-architectural feature of area PGm is an evident columnar organization with well-developed and defined layers IV, V, and VI (Figure 10; Luppino et al. 2005). Layer II is relatively thin, while layer III is thick and presents an increase in size gradient of the pyramidal cell population going towards its base (Passarelli et al. 2018). About myelo-architecture, PGm seems to be moderately stained, presenting well distinct inner and outer bands of Baillarger, all characteristics that allow an easy differentiation from the adjoining and more densely myelinated areas V6A and PEc (Passarelli et al. 2018).

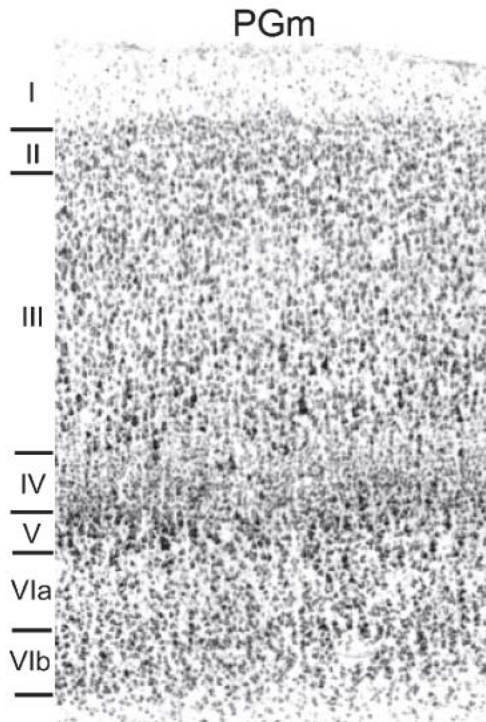


Figure 10. Cyto-architecture of area PGm. High magnification view of a Nissl-stained segment of area PGm is shown. (Modified from Luppino et al. 2005).

Area PGm is reported to be involved in eye movement control (Olson et al. 1996; Thier and Andersen 1998; Leichnetz 2001), visually-guided reaching (Ferraina, Garasto, et al. 1997; Ferraina, Johnson, et al. 1997; Leichnetz 2001), in navigation, scene perception, and spatial working memory (Sato et al. 2006, 2010; Baumann and Mattingley 2010; Kravitz et al. 2011; Hutchison et al. 2015). According to a recent work that revisited the PGm cortical afferences (Passarelli et al. 2018), the major cortical inputs come from area V6A and retrosplenial cortices; other strong inputs come from mesial (areas 23 and 31), frontal (area 8), and inferior parietal (areas Opt and PG/PGop) cortices; weaker connections come from extrastriate (area V6 and MST), intraparietal (areas LIP and VIP), prefrontal (area 46), and premotor (area F7) cortices. The fact that area PGm is mostly connected with the lateral rather than the medial bank of the ips, as well as with areas V6A and MST, suggests that area PGm is a node of a visuo-spatial processing network (Kravitz et al. 2011; Passarelli et al. 2018). The strong inputs coming from frontal areas suggest that area PGm is involved in abstract aspect of action planning, while the connection with limbic cortex could reflect an involvement in episodic memory retrieval (Passarelli et al. 2018). The overall cortico-cortical connectional pattern

suggests that area PGm plays an important role in the integration of sensory and mnemonic information in the context of visually-guided navigation (Baumann and Mattingley 2010; Passarelli et al. 2018).

Area PEci

Area PEci is hidden into the depth of the caudal tip of the cingulate sulcus (Figure 3; Pandya and Seltzer 1982; Morecraft et al. 2004). It is also known as supplementary sensory area, or SSA, and has been reported to host neurons involved in sensory and motor control (Murray and Coulter 1981).

The study of the cyto-architectonic material (Figure 11) shows a “limbic pattern”, in the sense that the cellular density of the infra-granular section of the cortex of area PEci, composed by the fusion of layers V and VI, is higher than that of its supra-granular section, in which pyramidal cells are visible only in layer IIIc, however in small number (Pandya and Seltzer 1982). The analysis of myelo-architecture shows a pattern similar to that of area PE, because of the presence of a single outer band of Baillarger and an inner plexus of myelinated fibers, even if less developed than that of area PE (Pandya and Seltzer 1982).

Cortical connections to area PEci come from frontal (areas 4, 6, 8, F2, and 46), sensory (areas 1, 2, and 3), superior parietal (areas PE, PEa, PEc, PO), inferior parietal (areas SII, paAc, PGop, PG, Tpt, and MST), insular, and medial (areas PGm, 31, TSA, 23a/b, 24a/b, F3 and F4) cortices (Morecraft et al. 2004).

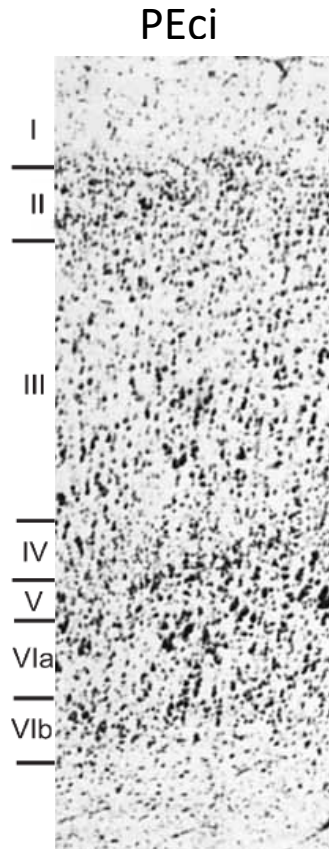


Figure 11. Cyto-architecture of area PEci. High magnification view of a Nissl-stained segment of area PEci is shown. (Modified from Pandya and Seltzer 1982).

The functional characterization of area PEci is still lacking. The only work reporting functional properties (Murray and Coulter 1981) suggests an involvement of area PEci in sensory-motor activity. Further functional studies will be needed to increase the knowledge on the function of this cortical area.

2. PURPOSE OF THE THESIS

As described above, the SPL of humans and non-human primates is a complex entity where several areas are involved in different steps of planning and execution of reaching and grasping arm movements. To date, the definition of the anatomical and functional characteristics of these areas come from data collected after injections of retrograde and anterograde neuronal tracers into the cortical areas, and after extracellular recordings of single cell activity, of macaque monkey SPL. This PhD thesis is aimed at increasing our knowledge of the macaque monkey SPL organization and functional role(s) by investigating the distribution of membrane receptors of SPL neurons, which represent the tools through which the cells play their specific functional roles. The chemo-architecture of the cortex of the SPL has not yet studied so far, and the present study could confirm or not the functional roles described until now for the SPL, and suggest other functional roles for this structure not yet proposed at present.

3. MATERIALS AND METHODS

All the experimental protocols were in accordance with the guidelines of the European laws for the care and use of animals for scientific purposes.

Four hemispheres of three *Macaca fascicularis* brains were used to collect the data shown in this study (animal ID #11539, left and right hemispheres; animal ID #11543, left hemisphere; animal ID #11530, left hemisphere). All the animals were male specimens between 6 and 8 years old, with a body weight between 5.2 and 6.6 kg.

Cyto- and myelo-architectural analysis of the Superior Parietal Lobule (SPL) and adjoining cortices was performed in order to define the anatomical borders existing between the different cortical areas taken in exam. Analysis of colour coded autoradiographs in the same hemispheres was subsequently carried out to identify the same architectonic borders previously defined thanks to cyto- and myelo-architectural material.

Histological procedures

The animals were sacrificed receiving a lethal dose of sodium pentobarbital (i.v. injection). Then, the brains were removed from the skull, and brainstem and cerebellum were dissected off in close proximity to the cerebral peduncles. The brains were divided into hemispheres cutting the corpus callosum, and then in a rostral and a caudal block making a cut in coronal plane of sectioning between the central and arcuate sulci. The unfixed tissue blocks were frozen in isopentane at -40°C to -50°C, and then stored in airtight plastic bags at -70°C. Each block was then sectioned in the coronal plane using a cryostat microtome (CM 3050, Leica, Germany), obtaining slices of 20 µm thickness, which were thaw-mounted on gelatine-coated slides and freeze-dried overnight. Alternating sections were stained for cell bodies (Merker 1983) or myelin (Gallyas 1979), or processed for the visualization of neurotransmitter receptor binding sites.

Receptor autoradiographic labelling

Quantitative *in vitro* receptor autoradiography was applied to label fifteen different receptors for the transmitters glutamate (AMPA, Kainate, NMDA), GABA (GABA_A, GABA_B, GABA_A

associated benzodiazepine [GABA_A/BZ] binding sites), acetylcholine (muscarinic M_1 , M_2 , M_3), noradrenaline (α_1 , α_2), serotonin (5-HT_{1A} , 5-HT_2), dopamine (D_1), and adenosine (A_1) by incubating the sections in solutions of respective tritiated ligands. The name and property of ligands used are specified in Table 1.

Table 1. Name and property of ligands used for receptor autoradiographic labelling

Transmitter	Receptor	Ligand (nM)	Property
Glutamate	AMPA	[^3H]-AMPA (10.0)	Agonist
	Kainate	[^3H]-Kainate (9.4)	Agonist
	NMDA	[^3H]-MK-801 (3.3)	Antagonist
GABA	GABA_A	[^3H]-Muscimol (7.7)	Agonist
	GABA_B	[^3H]-CGP 54626 (2.0)	Antagonist
	GABA_A/BZ	[^3H]-Flumazenil (1.0)	Antagonist
Acetylcholine	M_1	[^3H]-Pirenzepine (1.0)	Antagonist
	M_2	[^3H]-Oxotremorine-M (1.7)	Agonist
	M_3	[^3H]-4-DAMP (1.0)	Antagonist
Noradrenaline	α_1	[^3H]-Prazosin (0.2)	Antagonist
	α_2	[^3H]-UK 14,304 (0.64)	Agonist
Serotonin	5-HT_{1A}	[^3H]-8-OH-DPAT (1.0)	Agonist
	5-HT_2	[^3H]-Ketanserin (1.14)	Antagonist
Dopamine	D_1	[^3H]-SCH 23390 (1.67)	Antagonist
Adenosine	A_1	[^3H]-DPCPX (1.0)	Antagonist

Further details have been described in previous publications (Zilles, Palomero-Gallagher, et al. 2002a; Zilles, Schleicher, et al. 2002b; Palomero-Gallagher and Zilles, 2018). In short, the labelling protocol included a washing step to rehydrate the sections and remove endogenous substances, a main incubation, and a final rinsing step to remove the surplus ligand. In the main incubation, sections were incubated with either a tritiated ligand alone (in nM concentrations) to determine total binding, or with the tritiated ligand (also in nM concentrations) accompanied by a non-labelled specific displacer (in μM concentrations) to determine the proportion of displaceable, non-specific binding. Specific binding is the difference between total and non-specific binding. Since the used ligands and binding protocols resulted in a displaceable binding that was less than 5% of the total binding, total binding was considered to be equivalent of specific binding. The

sections processed for receptor autoradiography were then exposed together with plastic samples of known radioactivity against tritium-sensitive films (Hyperfilm, Amersham) for a period of 4-12 weeks based on the ligand used.

Image analysis

The ensuing autoradiographs were processed by densitometry with a video-based image analysing technique described in already published studies (Palomero-Gallagher and Zilles, 2018; Zilles, Schleicher et al., 2002b). Briefly, the autoradiographs were digitized using a CCD-camera, and stored as 8-bit grey value images. The plastic scales of known radioactivity were used to create a transformation curve to linearize the autoradiographs, i.e., to transform the grey values in each pixel of the autoradiograph into concentrations of radioactivity in the tissue. These concentrations of radioactivity were then converted into binding site densities, B_{\max} values (concentration values in fmol/mg protein at saturation of the ligand-receptor complex) by multiplying the grey values of the linearized autoradiographs by $(K_D + c)/c$ (where K_D is a dissociation constant of the ligand-receptor binding kinetics at the equilibrium phase, and c the free concentration of labeled ligand in the incubation buffer). Additionally, linearized autoradiographs were subjected to linear contrast enhancement, colour coding and median filtering for visualization purposes. These final steps were useful to obtain images that could be analysed by visual inspection, in order to subdivide the SPL into different cortical areas.

The mean areal density value for each area was calculated using in house software (AnaRec), which extracted the mean of the grey values contained in a specific cortical area over a series of 3–5 sections per animal and receptor type, and transformed it into a receptor concentration per unit protein (fmol/mg protein). The ensuing receptor densities were represented as multi-receptor fingerprints, i.e., as polar coordinate plots simultaneously depicting the concentrations of all examined receptor types within a given cortical area (Zilles, Palomero-Gallagher et al., 2002a). After that, all the data available were analysed to obtain a “receptor fingerprint” for each identified cortical area.

For each identified area, a Grey Level Index (GLI) value was also obtained from sections stained with the Nissl method to quantitatively compare the cytoarchitecture of the areas examined in this study. This analysis was performed choosing the best cytological segment of each cortical area, where the plane of sectioning was perpendicular to all cortical layers. The GLI, which quantifies the volume of cell bodies relative to the total brain volume, was computed using in house MATLAB scripts (for further details, see Zilles, Palomero-Gallagher, et al. 2002a and Zilles, Schleicher, et al. 2002b).

Statistical analysis

Hierarchical cluster and Multi-Dimensional Scaling (MDS) analyses were carried out with MATLAB (The MathWorks, Inc., Natick, MA) as previously described (Palomero-Gallagher et al. 2009) to determine the degree of (dis)similarity of the receptor fingerprints of SPL areas. The number of stable clusters was determined by a subsequent k-means analysis and the elbow method. Due to the large differences in the absolute expression levels of the different receptor types examined, receptor densities were normalized by z-scores prior to these analyses. In house MATLAB scripts were also used to compute Mahalanobis distances (Mahalanobis 1936) to determine the (dis)similarity in GLI values between areas of the SPL. This method is based on the correlation between variables through which different patterns can be identified and analysed. It differs from Euclidean distance as it takes into account correlations within the data set.

4. RESULTS

Fifteen different receptor types were analysed in order to provide insights into the molecular organization of SPL areas. These receptors were heterogeneously distributed, both at the regional and at the laminar level, throughout the cortex of the SPL. Some receptors (e.g. AMPA and α_1 receptors; Figure 12) were particularly useful to map the SPL, because the inter-areal differences in their expression levels clearly revealed cortical borders, whereas for other receptors (e.g., D₁ receptor; Figure 12), inter-areal differences were more subtle.

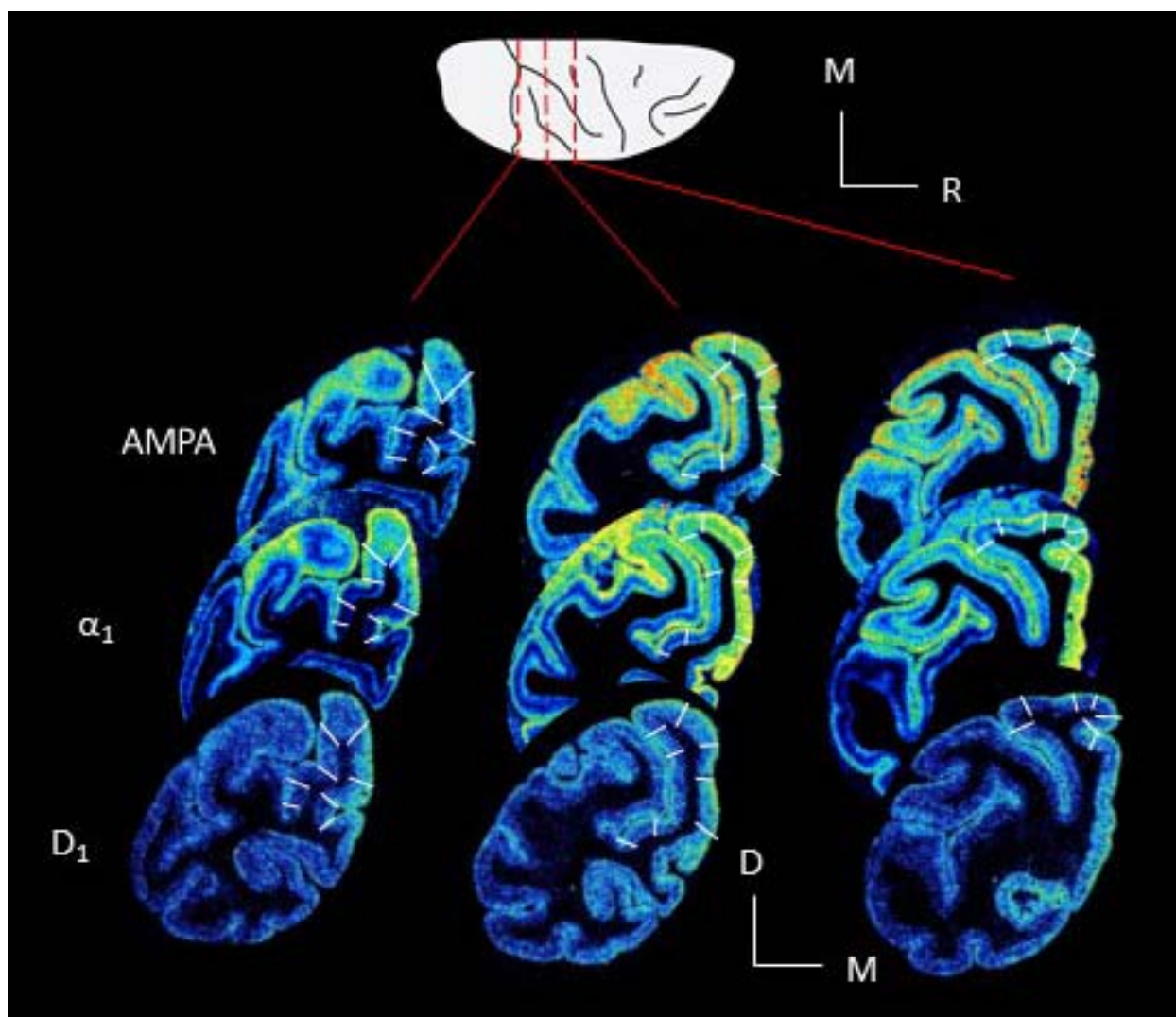


Figure 12. Coronal sections through three levels of a macaque hemisphere showing exemplary receptor distribution patterns in the SPL. Note the contrast between the relatively homogeneous expression of D₁ receptors in the cerebral cortex and the heterogeneous distribution patterns of the AMPA and α_1 receptors. White lines on each section represent the borders of SPL areas. Top: silhouette of a macaque brain showing the levels from which the sections presented below were obtained. D: dorsal; M: mesial; R: rostral.

The borders detected with the receptor autoradiography method were compared with the GLI method, analysing cyto-architectural material. In the following paragraph, the results obtained performing this analysis will be described.

Cyto-architecture of SPL areas

Figure 13 shows the results obtained from the quantitative cyto-architectonic analysis carried out on all SPL areas. The profiles shown in Fig. 13 represent the variations in the volume fraction of cell bodies as GLI (%) when moving from the pial surface to the border between layer VIb and the white matter. The congruity between the curve representing the mean GLI (thick line) and those indicating the standard deviation values (the thin lines localized one above and one below the thick line) highlights the ideal plane of sectioning of the site selected for GLI measurement.

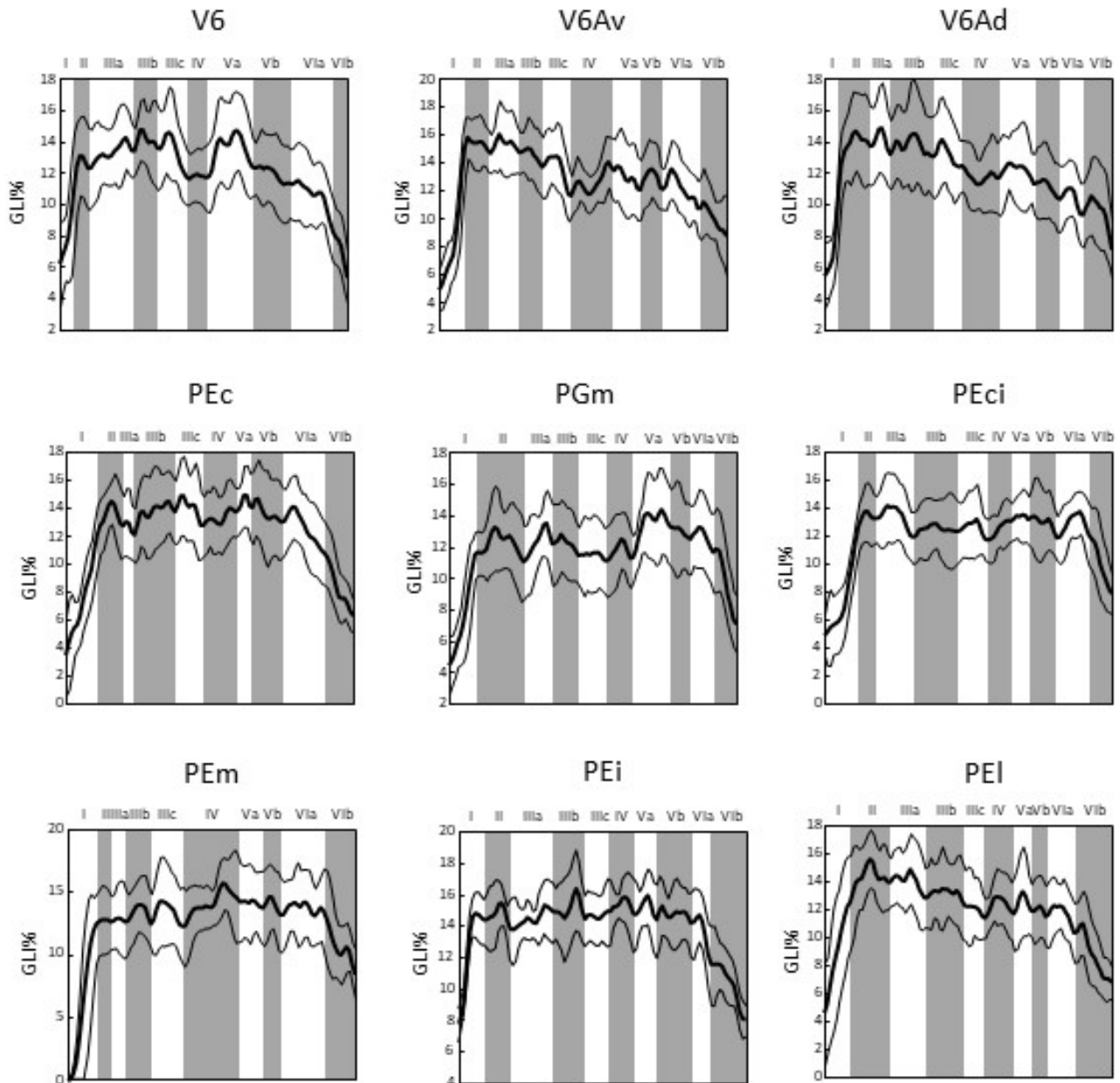


Figure 13. Grey Level Index (GLI) profiles quantifying the cyto-architecture of SPL areas. They depict the mean (thick line) \pm s.d. (thin lines) changes in the volume fraction of cell bodies (y axis) when moving from the pial surface to the layer VI/white matter border (x axis).

For all areas, a subdivision of layers III (a, b, c), V (a, b), and VI (a, b) was detected. As expected, the GLI value is low at the level of layer I, is highest between layers II and V, and then becomes low again in layer VI, particularly in layer VIb. The proportion of the thickness of each layer and sublayer changes between all the areas. As an example, area V6 shows a thinner layer IV and thicker layers IIIa and Vb in respect to the adjoining area V6Av.

It is worthwhile to note that differences in the cyto-architecture (Figure 14), as well as in the laminar distribution patterns of some of the examined receptors (though not in the mean densities; see below), enabled the subdivision of cyto-architectonic area PE into three portions. The proposed nomenclature of these three subdivisions reflects their locations on the exposed surface of the hemisphere if seen in coronal section. So that, area PE can be subdivided in a medial part (PEm), a lateral part (PEl), and an intermediate part (PEi) posed between the two.

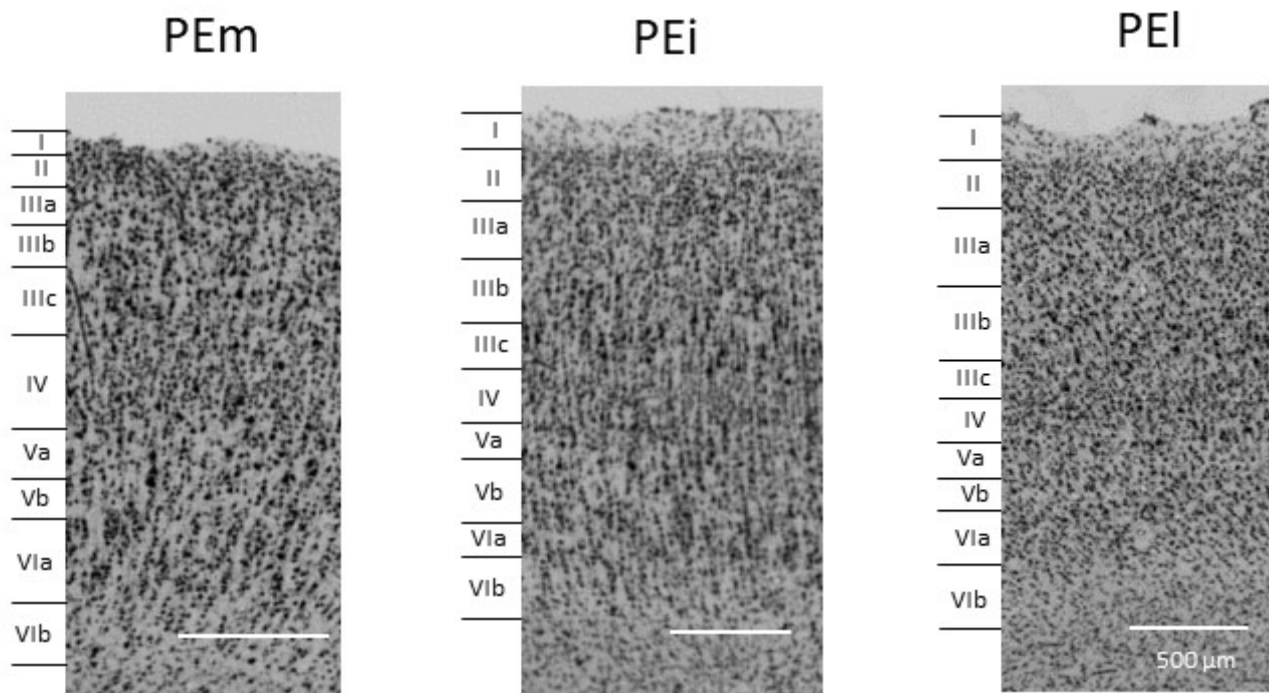


Figure 14. Cyto-architectonic pattern of areas PEm, PEi, and PEI. High magnification views of Nissl-stained segment of the three parts of area PE are shown.

In fact, areas PEm and PEi have a clearly visible columnar organization that is absent in area PEI. About layer thickness, the three areas have a very well developed layer III; on the contrary, layer IV differs between areas: area PEm shows a thick granular layer, which becomes thinner in areas PEi and PEI. Another difference is about the border with white matter, which is clearly distinct only in area PEi. About the cell population, area PEm shows well stained cell bodies, with few numbers of large pyramidal cells in layer V. Area PEi, on the contrary, shows a clear strip of large pyramids in layer III, in particular in sublayer IIIc. Granular cells are mainly localized in layer V. Area PEI shows a strip of well-impregnated pyramidal neurons in correspondence of layers III.

The qualitative observations from each of the examined SPL areas were confirmed by computing the Mahalanobis distances (Mahalanobis 1936) between the layer-specific GLI values extracted, as shown in Fig. 15. The highest degree of dissimilarity was found for area PEci (which presents more cyto-architectural dissimilarities with areas PEc and PEi), area V6Ad (more cyto-architectural dissimilarities with PEci and PGm), area V6Av (dissimilarity with PEm), and area V6 (dissimilarities with PEm and PEci).

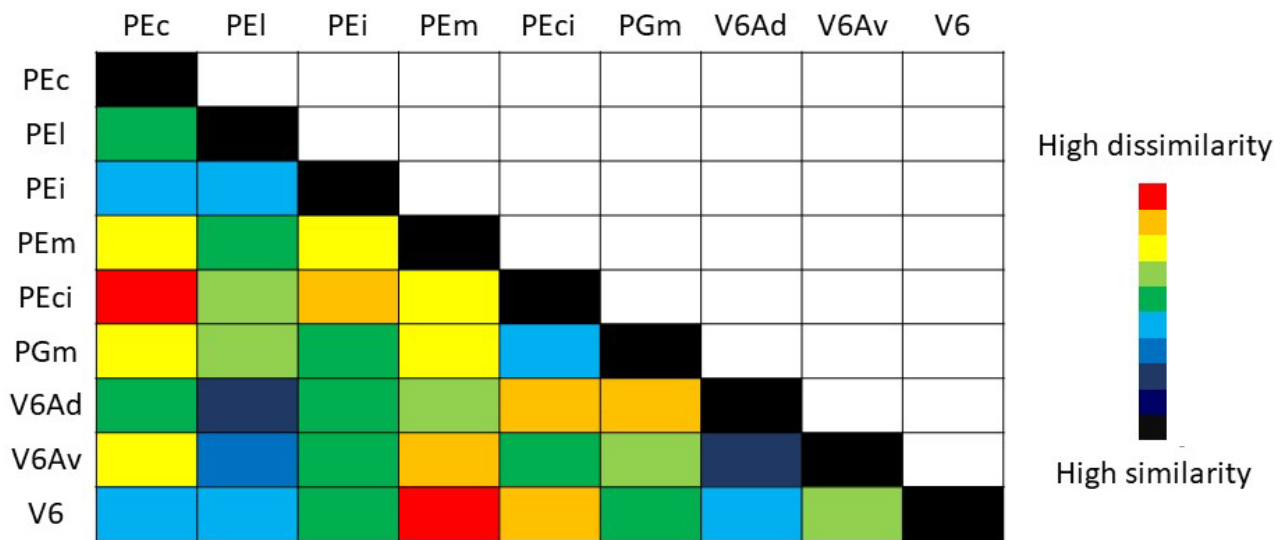


Figure 15. Mahalanobis distance analysis based on mean GLI%. A colour code was used to identify (dis)similarities between areas.

Both MDS and hierarchical cluster analyses (Figure 16A and 16B) show that the areas of the SPL object of this work belong mainly to two different cyto-architectonic patterns. The first one comprises areas V6, V6Av, V6Ad and PEI (negative values of the Dimension 1 axis; Cluster A). The second one (positive values of the Dimension 1 axis; Cluster B) is in turn divided in two branches, one formed by PEm, PEi, and PEc, and the other one by PGm and PEci (with positive and negative values of Dimension 2, respectively).

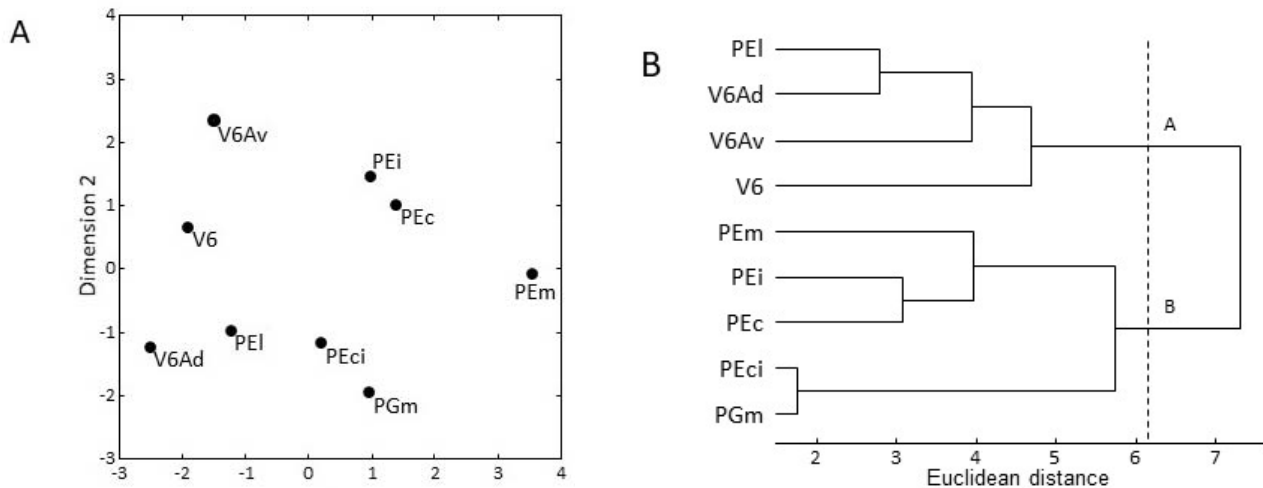


Figure 16. Multivariate analyses of GLI (%) values extracted from the layers of SPL areas. A: Multi-Dimensional Scaling (MDS) analysis. B: Hierarchical cluster analysis. Dashed line indicates the number of stable clusters as identified by the k-means analysis and the elbow method.

Receptor-architecture of SPL areas

Colour Tables 1 to 9 (pages 60 to 68) show the laminar distribution of the fifteen receptors analysed in each cortical area of the SPL. At first sight, it is clear that the highest expression level of most receptor types and subtypes is located in the supra-granular layers of all areas, although the absolute values reached by each receptor in a specific layer can vary between areas.

The areas of the SPL will be discussed in groups based on the anatomical location: areas located at the level of pos; areas located on the exposed surface of the SPL; areas located on the mesial surface of the hemisphere.

Areas located at the level of the parieto-occipital sulcus (pos)

As shown in Fig. 3, three areas are located in the proximity of the pos: areas V6, V6Av and V6Ad.

In area V6 (Colour Table 1) all receptors reach their maximum expression levels in layers II and/or III. In the glutamatergic family, AMPA and NMDA receptors present the highest densities in layers II and III, whilst the receptors for kainate present a local maximum restricted to layer II. GABAergic GABA_A receptors and GABA_A/BZ binding sites show a similar laminar distribution, with highest densities in all the supra-granular layers, whereas GABA_B receptors are more selective

for layer II. Muscarinic M₁, M₂, and M₃ receptors present comparable distribution patterns, since they all reach their maximum expression levels in layers II and III, although the M₂ density is lower than that of M₁ and M₃ receptors. The α -adrenergic receptor of type 1 presents a more restricted distribution compared to the α_2 receptor, since the former is confined in layers II and IIIa, and the latter is present at considerably higher densities in all supra-granular layers than in layers IV-VI. The serotonergic receptors present a differential distribution pattern, where high 5-HT_{1A} receptor densities are confined only to layers I-IIIa, while highest 5-HT₂ receptor densities are reached in layer III (in particular sublayers IIIb and IIIc). The D₁ receptor is present at a very low density throughout the cortex, but there is a higher density in the supra- than in the infra-granular layers. The purinergic receptor for adenosine of type 1 shows a different distribution in respect of all the other receptors analysed, because highest concentrations reach from layer III (in particular layers IIIb and IIIc) into layer IV.

Area V6Av (Colour Table 2) shows a laminar receptor density pattern similar to area V6, although several important differences are evident. At first, the absolute density of most receptors is higher than in area V6. Furthermore, highest A₁ receptor densities are mainly located in the infra-granular layers, and the α_2 receptor presents a more homogeneous distribution throughout all cortical layers.

In area V6Ad, dorsal to V6Av and close to the exposed surface of the SPL (Colour Table 3), the absolute receptor density continues to increase compared to V6Av and V6. There are several similarities with area V6Av, but also differences exist, the most prominent of which are that highest kainate and A₁ densities are mainly located in the infra-granular layers of V6Ad. Furthermore, M₂ receptor density is very low, and homogeneously distributed throughout all layers of V6Ad, whereas the α_2 receptor presents a conspicuous maximum in layer I.

Areas located on the exposed surface of the SPL

Two cyto-architectonic areas, PEc and PE, lie on the exposed surface of the superior parietal lobule (Figure 3).

The laminar distribution patterns in area PEc (Colour Table 4) clearly differ from those of areas located at the level of the pos. Differences are mainly due to higher densities, particularly of AMPA, Kainate, and M₂ receptors, in the infra-granular layers of PEc with respect to those in V6Ad. The M₂ receptor presents a local maximum in layer V, and kainate receptors present higher densities in the infra- than in the supra-granular layers of PEc. AMPA receptors are homogeneously distributed throughout PEc.

Because of chemoreceptor distribution, area PE could be divided into three regions: PEm, PEI and PEi. These three subdivisions of area PE present similarities, but also important differences (Colour Tables 5 to 7). Although most receptors are present in higher concentrations in the supra-granular than in the infra-granular layers of all three subdivisions of PE, differences are observed looking at kainate, M₂, α_1 , and A₁ receptors. AMPA receptors show a bilaminar distribution pattern in all three subdivisions of PE, whereas in PEm and PEi densities in the supra-granular layers are clearly higher than those in the infra-granular layers, whereas in PEI the supra-granular layers present only slightly higher densities than the infra-granular ones. The NMDA receptor clearly reveals the border between the medial and lateral subdivisions of PE. Whereas PEI and PEi present higher densities in the supra-granular than in the infra-granular layers, PEm shows a second local maximum in layer VI. The α_1 receptor enables the delineation of PEI from PEi and PEm, since it does not contain the local minimum over layers IIIc-IV that is clearly visible in the two latter areas. Finally, the A₁ receptor has a different laminar pattern in each of the subdivisions: in area PEI highest densities extend between layers IIIb and VI, area PEi shows a relatively homogeneous distribution, and in area PEm two local maxima are visible, one involving layers I and II, the other layers V and VIa.

Areas located on the mesial surface

Two areas lie on the mesial surface of the hemisphere: area PGm, located in the precuneate cortex, and area PEci, within the cingulate sulcus (Figure 3).

Area PEci (Colour Table 8) more closely resembles to be similar to a subdivision of area PE, and in particular PEi. The main difference between areas PEci and PEi is in their absolute receptor densities (see below), although there are also differences in the laminar distribution pattern of the A₁ receptor, which in area PEci is present in high concentrations only in the infra-granular layers, whilst it is homogeneously distributed throughout area PEi.

Area PGm (Colour Table 9) shows a laminar receptor pattern very similar to that of area PEc. Major differences are visible comparing the laminar distribution pattern of the AMPA receptor density, which is widespread in area PEc but mainly concentrated in the supra-granular layers in area PGm. Another difference regards the α_2 receptor, with highest densities confined to layer III in area PGm, whilst in area PEc it presents a bilaminar distribution. An additional difference is visible for the D₁ receptor, which is almost homogeneously distributed throughout area PEc, while presents a clear local maximum in layers II-IIIa of area PGm.

Receptor fingerprints and insights into functional organization of SPL areas

The mean densities (averaged over all cortical layers) of all examined receptors were extracted from each area and presented simultaneously in a polar coordinate plot. This plot represents the “receptor fingerprint” of an area. Figure 17 shows the “receptor fingerprints” for all the SPL areas taken into account in this study. The receptor fingerprints show that in all areas highest densities were measured for the GABAergic and NMDA receptors, followed by the M₁, M₃, and A₁ receptors. The other receptors are present at considerably lower densities. Lowest values were obtained for the D₁ receptor. The overall size of receptor fingerprints is indicative of the mean densities of receptors in a given area. Area V6 has the smallest receptor fingerprint, thus highlighting the fact that it contains the lowest mean densities measured within the areas of the SPL. Areas PEc and PGm have the largest receptor fingerprints, hence contain the highest mean receptor density measured in the SPL.

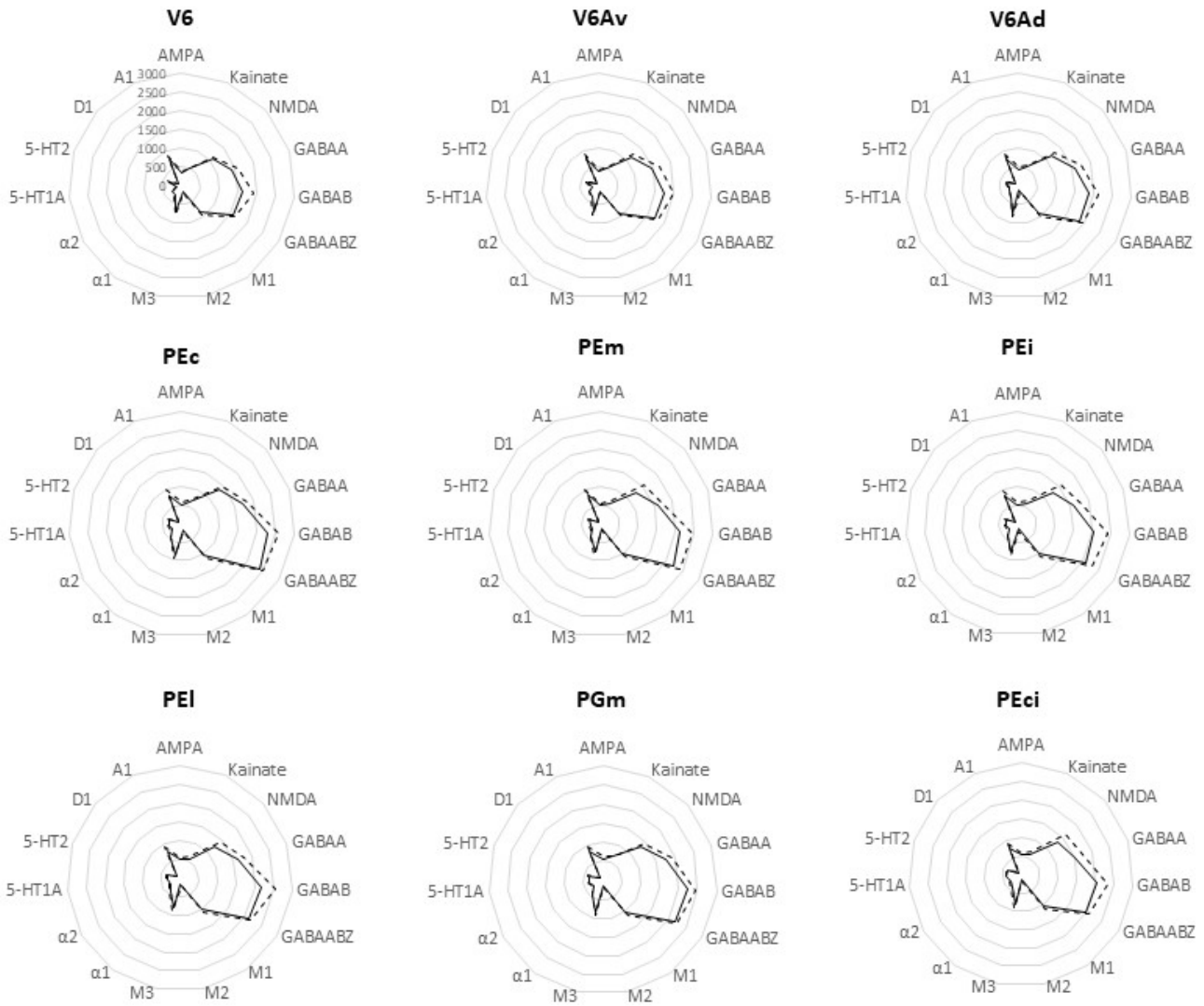


Figure 17. Receptor fingerprints of SPL areas. The data are expressed in fmol/mg.

Fig. 17 shows that there is an increase in absolute densities when moving from V6 through the nearby areas V6Av and V6Ad, as demonstrated by an increase in the size of their respective fingerprints. Notice that there were also small differences in mean receptor densities, though not in laminar distribution patterns, between the medial and lateral parts in both areas V6Av and V6Ad (Figure 18), with receptor densities slightly higher in the medial than in the lateral part.

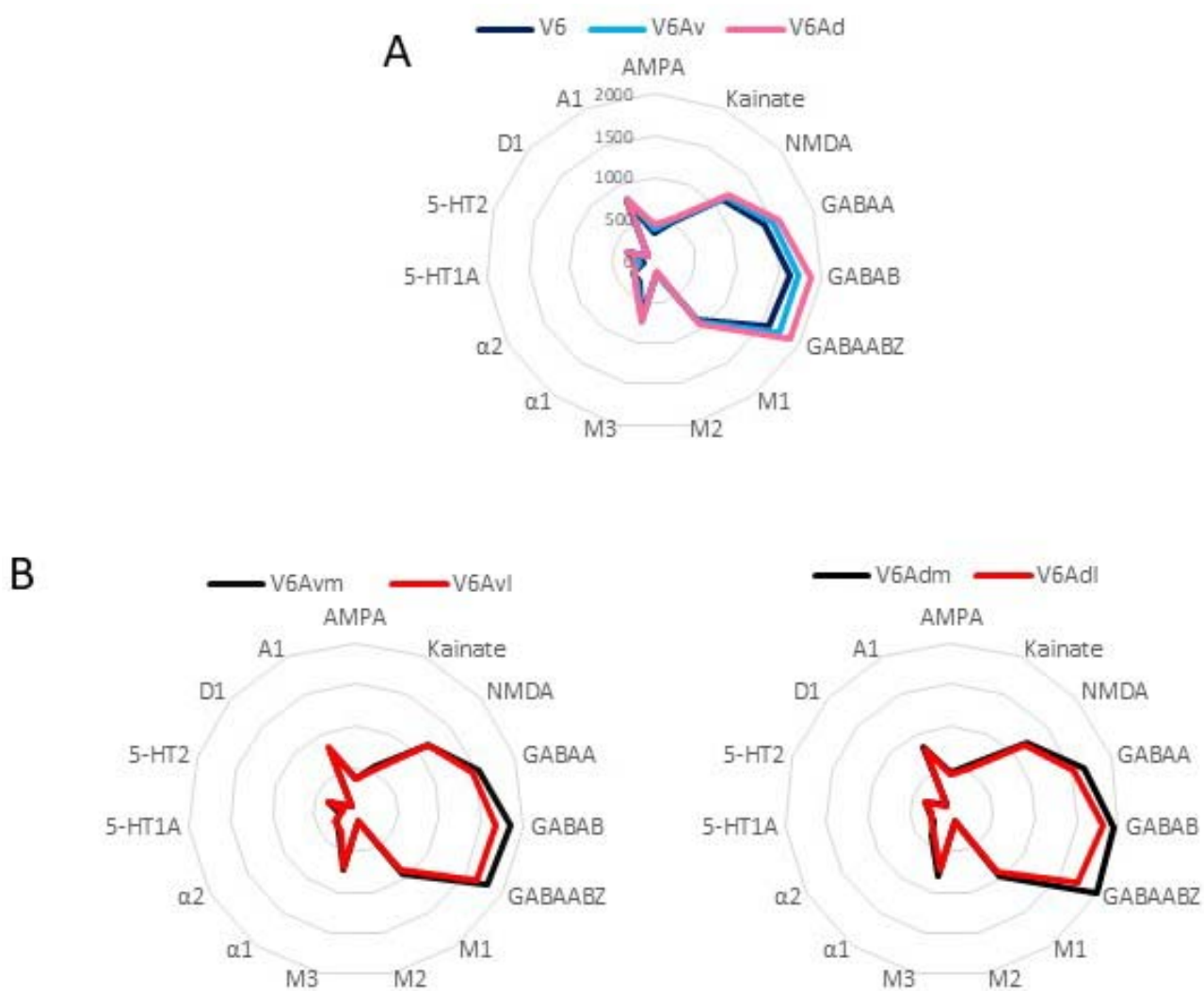


Figure 18. Comparison between areas of the pos. A: Receptor fingerprints of the areas of the pos. B: Differences in receptor density between medial and lateral parts of V6Av and V6Ad areas. The data are expressed in fmol/mg.

Multivariate analyses were carried out to assess the degree of (dis)similarity of the receptor fingerprints of areas of the SPL, as well as the (dis)similarity of SPL areas with areas located in other parts of the cerebral cortex and belonging to different functional systems.

Multi-Dimensional Scaling analysis (Figure 19A) shows that the areas taken in exam in this study can be divided in two groups based on the position in correspondence of the Dimension 1 axis. The first group is composed by areas PGm, PEc, PEci, and PE (negative values on the Dimension 1 axis); the second group by areas V6Ad, V6Av, and V6 (positive values of the Dimension 1 axis). The hierarchical cluster analysis (Figure 19B) confirms the subdivisions

suggested by the MDS analysis. In fact, SPL areas cluster in two different branches. The first branch is composed by areas V6, V6Av and V6Ad. Notice that in this first branch, areas V6 and V6Av strictly cluster together. The second branch comprises areas PEc, PGm, PE, and PEci. Notice that in this second branch areas PEc and PGm strictly cluster together.

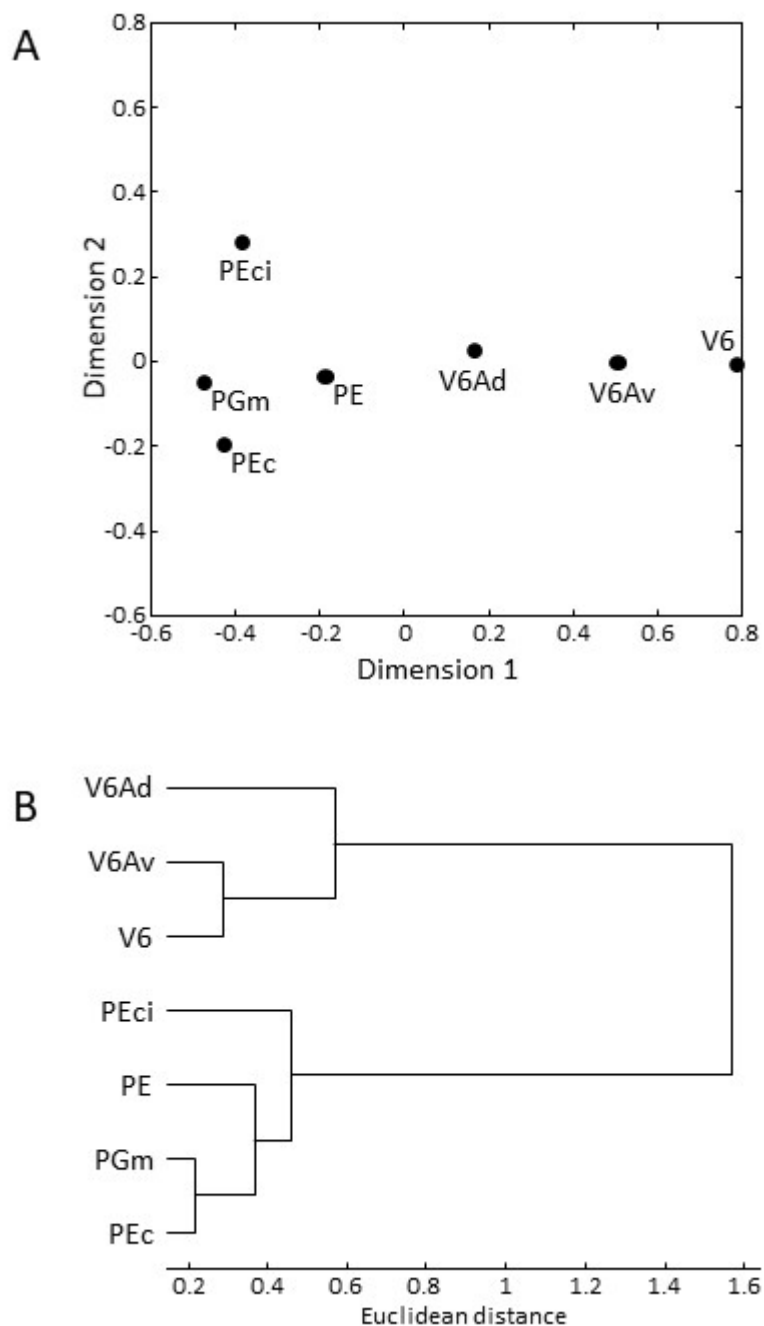


Figure 19. Multivariate analyses on mean receptor density. A: Multi-Dimensional Scaling (MDS) analysis obtained comparing mean receptor density for each SPL area. B: Hierarchical cluster analysis based on MDS and showing the correlation between SPL areas from a receptor-architectural point of view. Other details as in Fig. 16.

Figure 20 shows the results of the hierarchical cluster analysis done comparing the areas of the SPL with other cortical areas located in all the cerebral lobes.

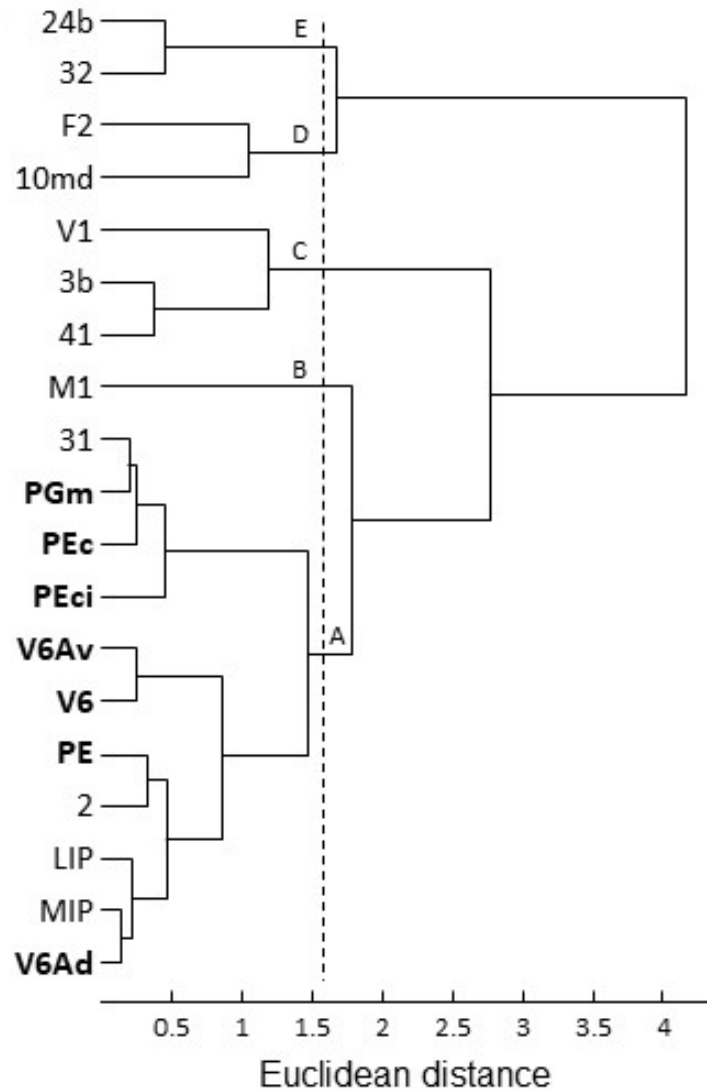


Figure 20. Comparative hierarchical cluster analysis with other brain areas. A comparison based on mean receptor density between SPL areas and other brain areas is shown to better characterize and differentiate the areas object of this study. Other details as in Figure 16.

Two main groups compose the dendrogram. The first group is in turn subdivided in two parts, one formed by cingulate areas 24b and 32, and the other by frontal area F2 and the medio-dorsal part of orbitofrontal area 10 (or 10md). The second group shows more heterogeneity. A first subgroup is composed by primary visual (V1), primary somato-sensory (3b), and primary auditory (41) areas, with the latter clustering together. Primary motor area (M1) clusters with the other

primary areas, but forming a branch alone. More, area M1 clusters with all the areas of the SPL, and those areas adjoining them. In particular, two subgroups contain SPL areas: the first one is composed by area PEci, clustering with area PEc, and in turn with area PGm and the cingulate area 31, which form a cluster together. The second subgroup is further divided in two branches. V6 and V6Av constitute the first branch, while the second branch is in turn subdivided in two groups, one composed by areas PE and the somatosensory area 2, and the other by intraparietal area LIP, which clusters with both area V6Ad and intraparietal area MIP.

5. DISCUSSION

The present study constitutes a multimodal analysis of areas located in the SPL, encompassing both their cyto-architecture and multi-receptor expression patterns. This approach enabled the definition of hitherto undescribed borders within the SPL, and thus resulted in a partial modification of the classic parcellation scheme for the SPL, as summarized in Fig. 21.

The first observation resulting from the analysis of receptor density is that receptors for GABA and glutamate are the predominant receptor types in all the areas of the SPL. This finding highlights the role that both neurotransmitters play, together with modulatory neurotransmitters, in maintaining the balance between excitation and inhibition essential for a correct functioning of the brain (Rao et al. 2000; Wehr and Zador 2003; Markram et al. 2004; Xu et al. 2011; Wu and Sun 2015). This finding is also in line with observations in other macaque brain regions such as the primary sensory (Zilles and Palomero-Gallagher 2017) and cingulate (Bozkurt et al. 2005; Palomero-Gallagher et al. 2013) cortices, as well as with analyses of homologue regions in the human brain (Eickhoff et al. 2007; Zilles and Palomero-Gallagher 2017; Palomero-Gallagher et al. 2009; Scheperjans et al. 2005a,b).

Parcellation schemes of the SPL

The parietal cortex has been object of several cyto-architectonic studies, some of which have provided maps of the entire SPL (Brodmann 1909; Pandya and Seltzer 1982; Lewis and Van Essen 2000; Morecraft et al. 2004), whereas others have focussed on specific parts of it such as the cortex located within the anterior wall of the pos (Colby et al. 1988; Luppino et al. 2005) or the precuneus (Passarelli et al. 2018). The multivariate analysis shown here confirms the parcellation scheme proposed by Luppino et al. (2005) for the anterior bank of the pos, and the existence of an area PGm on the precuneus as described by Pandya and Seltzer (1982). The delineations of Morecraft and colleagues (2004) on the convexity of the SPL and within the cingulate sulcus is largely confirmed, but previously undetected subdivisions within area PE were described.

The qualitative and quantitative assessment of the regional and laminar distribution patterns of multiple receptor types confirmed the subdivision of area V6A into dorsal and ventral components, as well as the location and extent of area PGm on the precuneus. In both areas V6Av and V6Ad, it was found that the medial part presented a higher receptor density pattern compared to the lateral part. It may be that the medial parts of both areas are involved in further, or different, processes with respect to the lateral ones. Because the precuneate cortex anterior to V6A codify for complex actions related to spatial navigation, scene perception, and spatial working memory (Sato et al. 2006, 2010; Baumann and Mattingley 2010; Kravitz et al. 2011; Hutchison et al. 2015), it can be suggested that the higher receptor density found in the medial part of areas V6Av and V6Ad could be necessary to encode complex aspect of the visuo-motor integration.

The distribution of receptor density and GLI profiles also confirms the existence of area PEci within the depth of the caudal tip of the cingulate sulcus, as previously described by Morecraft and colleagues (2004), and of area PE on the dorsal exposed surface of SPL, as described by Pandya and Seltzer (1982). Differences in the shape of GLI profiles, as well as in the laminar distribution patterns of multiple receptors, also enabled the definition of three subdivisions within area PE (see Fig. 21): area PEI, that forms a thin strip on the rim of the intraparietal sulcus; area PEi, that forms another long strip located between area PEI and area 2; area PEm, a cortical region located in the medial part of the dorsal exposed surface of SPL, which involves also the dorsal part of the mesial cortex. Pandya and Seltzer (1982) originally defined area PE as a cyto-architectonic homogeneous entity, but recent studies based on connectional data have suggested possible subdivisions within this area (see, for instance, Bakola et al. 2013; Gamberini et al. 2017; Impieri et al. 2018). Moreover, it is widely accepted that in area PE there are separate somatotopic sectors (see, for example, Seelke et al. 2012), but, until now, any match between the somatotopic maps and the connectional, cyto-architectonic, and neurochemical heterogeneity of area PE has been proved. Further studies are necessary to determine such a kind of relationships, if any.

In view of the present results, it may be interesting to reconsider the nomenclature used for area PEc. The pivotal work of Pandya and Seltzer (1982) was the first to define areas within SPL and IPL based on architectonic and connectional patterns. They assumed that Brodmann's area 5 corresponded to the SPL and Brodmann's area 7 to the IPL. Since they found cyto-architectonic heterogeneity in both SPL and IPL, they used a different nomenclature with respect to Brodmann. In SPL, they reported the presence of area PE and of other areas adjoining PE named using the same prefix, as areas PEa, PEc, and PEci. In the IPL, they described three main areas, i.e. PF, PFG, and PG. Since the cyto-architecture of precuneate cortex showed strong similarities with area PG, they termed this region as medial PG, or PGm.

In summary, IPL should be dominated by Brodmann's area 7 while SPL by Brodmann's area 5 dorsally and laterally, and by a variance of Brodmann's area 7 medially, in the precuneate cortex. However, a careful inspection of Brodmann's (1909) map of the guenon (Old World monkey) shows that the area 7 in this species is not restricted to the IPL, but it is also present in the posterior and medial aspects of the SPL as a thin strip of cortex delimiting the caudal aspect of area 5. Thus, according to Brodmann, the cortex corresponding to macaque area PEc in the caudal aspect of SPL is part of area 7, and not of area 5 as reported by Pandya and Seltzer (1982). The data shown in this work are in complete agreement with this view. In fact, both hierarchical cluster and MDS analyses reveal a tight neurochemical relationship between areas PGm and PEc, which is indicative of a neurochemical family of cortical areas with similar function (Zilles et al. 2002a; Palomero-Gallagher and Zilles 2018), strongly supporting the view that PEc is part of Brodmann's area 7 (Galletti and Gamberini 2018). For these reasons, it may be legitimate to rename area PEc as area PGc, being "PG" the term used by Pandya and Seltzer for Brodmann's area 7.

totality of neurons are activated by somatosensory stimulation (Mountcastle et al. 1975). No detailed description of cellular properties are available for areas PEci and PGm. From the available studies (Murray and Coulter 1981 for area PEci; Olson et al. 1996; Thier and Andersen 1998; Leichnetz 2001; Passarelli et al. 2018 for area PGm), it is possible to assume that area PEci contains only somatosensory neurons, while in area PGm neurons responding to both visual and somatosensory stimuli are present. Viewed as a whole, these findings suggest that two functional trends are present in the SPL: a visual one, whose incidence decreases going from the fundus of the pos to the exposed surface of the SPL, and a somatosensory one, whose incidence decreases in the opposite direction. In the light of this evidence, the gradual increase in receptor density that was observed moving caudo-rostrally in the SPL could be associated to the progressive increase in the incidence of somatosensory cells, a type of cells necessary to encode the somatosensory stimulations that underlie the movements of the limbs during reaching and grasping activity. However, according to this view, the highest receptor density should be achieved in area PE, the SPL area that hosts the major number of somatosensory cells, but this is not the case. Actually, it is area PEc that shows the highest receptor density pattern in the SPL. PEc is a cortical region where the visual and somatosensory streams mentioned before overlapped. Hence, it could be that the high receptor density in this area is needed for the integration of visual and somatosensory stimuli that occurs during reaching and grasping. This integration is made possible by specific balances of excitatory, inhibitory, and modulatory neurotransmission, hence it requires an high density of modulating membrane receptors. Of course, these are at present pure speculations, whose validity needs to be supported by further experimental data.

Hierarchical cluster and MDS analyses were carried out not only on the areas of the SPL, but also on other regions of the brain like the primary visual (V1), primary somatosensory (3b), primary auditory (41), and primary motor (M1) cortices, somatosensory area 2, intraparietal areas LIP and MIP, dorsal premotor area F2, fronto-polar area 10md, and cingulate areas 24b, 32, and 31.

By comparing the SPL areas with the areas of other regions of the brain a number of interesting considerations came out (see Figure 20).

Areas V6 and V6Av cluster together, whereas V6Ad clusters with intraparietal areas MIP and LIP. The separation of V6Av from V6Ad, and its strict relation with V6, likely reflects the higher amount of visual cells of area V6Av with respect to V6Ad (Gamberini et al. 2011, 2015). The mean receptor densities of areas V6Ad and MIP are more similar to each other than to that of LIP. Accordingly, both areas V6A and MIP are involved in the encoding of reaching activity in peri-personal space (Colby and Duhamel 1991; Snyder et al. 1997; Fattori et al. 2001; Andersen et al. 2014), whereas area LIP is mainly involved in the control of visual-oculomotor activity and in modulating spatial attention (Chen et al. 2016; Levichkina et al. 2017; Zhou et al. 2017). Posterior cingulate area 31 clusters with SPL areas PGm, PEc and PEci, and not with the anterior cingulate areas 24b and 32. In agreement with this observation, areas on the mesial surface of the SPL in both humans and monkeys have been associated with the default mode network (Greicius et al. 2003; Raichle et al. 2001; Arsenault et al. 2018), whereas the anterior cingulate cortex is implicated in motor control, arousal/drive state, and high order cognitive functions (Paus 2001; Palomero-Gallagher et al. 2013). Also, area PE and somatosensory area 2 are very similar from the neurochemical point of view, reflecting their common somatosensory characteristics (Padberg et al. 2007; Krubitzer and Disbrow 2008). As a final consideration, the three primary sensory areas were found in a single cluster, reflecting the situation also found in humans (Zilles et al. 2015) and highlighting their special position in the hierarchical organization of cortical areas. Finally, the primary motor cortex (M1) is not found to cluster with the other primary cortices, but is located in a cluster by itself, suggesting that area M1 should not be classified as a classical primary cortex, but as a part of the brain also implicated in associative brain functions. Further studies will be needed to corroborate this mere suggestion.

In conclusion, the position of the SPL areas in this extended cluster corroborates the vision that they are associative areas implicated in the encoding of various types of stimuli, in particular

visual and somatosensory ones, useful to the execution of reaching and grasping movements in peri-personal space.

Comparison with the human SPL

The cyto-architectonic and quantitative receptor autoradiographic techniques used here were also used to study the human SPL (Scheperjans, Grefkes, et al. 2005a; Scheperjans, Palomero-Gallagher, et al. 2005b; Scheperjans, Eickhoff, et al. 2008; Scheperjans, Hermann, et al. 2008). Results showed that human Brodmann's area 5 is composed of three subdivisions: 5L, 5M, and 5Ci. Area 5Ci corresponds to macaque area PEci, while areas 5L and 5M together to macaque area PE (Scheperjans, Grefkes, et al. 2005a; Scheperjans, Palomero-Gallagher, et al. 2005b). In the light of the present results, it can be suggested that macaque area PEi is the homologous of human area 5L, and macaque PEm of human 5M. It seems that area PEi found in the macaque does not have a homologue area in the human brain.

Human Brodmann's area 7 in the SPL is divided into 3 parts (areas 7A, 7P, and 7M; Scheperjans, Grefkes, et al. 2005a; Scheperjans, Palomero-Gallagher, et al. 2005b). In the macaque, only two SPL regions with the characteristics of area 7 (area PEc and PGm) were observed. Human area 7M is thought to be the homologous of macaque area PGm, while areas 7A and 7P together of area PEc of the macaque. These homologies are also corroborated by several functional studies (for a review, see Caminiti et al. 2015).

For the areas of the pos, studies in humans that used autoradiographic techniques have not yet reached the same degree of accuracy as in the macaque. So far, several ventral and dorsal parts have been identified within Brodmann's area 19 (e.g., hOc3d, hOc3v, hOc4d, hOc4v; Kujovic et al. 2013; Rottschy et al. 2007), showing respectively a more visual and somatosensory receptor-architectonic pattern (Scheperjans et al. 2005b). By the way, functional studies performed in human Brodmann's areas 18 and 19 that used the "wide-field retinotopy" technique allowed to recognize the homologues of macaque areas V6, V6Av, and V6Ad (Pitzalis, Galletti, Huang, et al. 2006; Pitzalis, Sereno, Committeri, et al. 2013; Pitzalis, Fattori, Galletti 2015). Human area V6 (part of

Brodmann's area 18) has the same anatomical and functional characteristics of its macaque homologous, in particular the presence of an organized retinotopy of the contralateral visual field, with an emphasis for the periphery (Pitzalis et al. 2006). Like area V6, also areas V6Av and V6Ad (parts of Brodmann's area 19) have been recently recognized in the human brain (Pitzalis, Sereno, Committeri, et al. 2013; Pitzalis, Fattori, Galletti 2015). Human V6Av presents almost the same anatomical and functional properties of the macaque counterpart, being considered a visual area representing the periphery of the contralateral lower visual field (Pitzalis, Sereno, Committeri, et al. 2013; Pitzalis, Fattori, Galletti 2015). Human area V6Ad was harder to characterize, because of its lack of retinotopy, which instead was the basic criterion for the identification of human areas V6 and V6Av (Pitzalis et al. 2015). Hence, a human brain region with no retinotopic maps, and located just dorsal to human area V6Av, was recently identified as the human area V6Ad (Pitzalis et al. 2015). These evidences are in agreement with the functional characteristics found in the pos of the macaque, in which the flow of visual information decreases going from area V6, located at the fundus of the pos, to area V6Ad, at the border with the exposed surface (Gamberini et al. 2011, 2015).

Concluding remarks

The present multimodal analysis largely confirms previous studies on the anatomical and functional characteristics of the areas located in the SPL of the macaque monkey (Mountcastle et al. 1975; Galletti et al. 2001; Leichnetz 2001; Morecraft et al. 2004; Luppino et al. 2005; Gamberini et al. 2009, 2011, 2015, 2018, Bakola et al. 2010, 2013, Passarelli et al. 2011, 2018; Seelke et al. 2012; Hutchison et al. 2015). However, a subdivision of area PE was proposed for the first time, based on differences in cyto-architecture and laminar receptor distribution patterns, and was remarked that the medial and lateral portions of areas V6Ad and V6Av differed in their mean receptor densities, suggesting possible differences in functional roles. Multivariate analyses of receptor fingerprints confirm the associative role of SPL areas in the encoding of visual and somatosensory stimuli necessary to execute reaching and grasping movements.

The data reported here also support a certain degree of homology between macaque and human SPL. Hopefully, future analyses will elucidate whether the ensuing novel parcellation scheme of the SPL has reliable functional counterparts, as suggested here.

REFERENCES

- Andersen RA, Andersen KN, Hwang EJ, Hauschild M. 2014. Optic ataxia: from Balint's syndrome to the parietal reach region. *Neuron*. 81:967–983.
- Arsenault JT, Caspari N, Vandenberghe R, Vanduffel W. 2018. Attention shifts recruit the monkey default mode network. *J Neurosci*. 38(5):1202-1217.
- Bakola S, Gamberini M, Passarelli L, Fattori P, Galletti C. 2010. Cortical connections of parietal field PEc in the macaque: Linking vision and somatic sensation for the control of limb action. *Cereb Cortex*. 20:2592–2604.
- Bakola S, Passarelli L, Gamberini M, Fattori P, Galletti C. 2013. Cortical connectivity suggests a role in limb coordination for macaque area PE of the superior parietal cortex. *J Neurosci*. 33:6648–6658.
- Battaglia-Mayer A, Ferraina S, Genovesio A, Marconi B, Squatrito S, Molinari M, Lacquaniti F, Caminiti R. 2001. Eye-Hand Coordination during Reaching. II. An Analysis of the Relationships between Visuomanual Signals in Parietal Cortex and Parieto-frontal Association Projections. *Cereb Cortex*. 11:528–544.
- Baumann O, Mattingley JB. 2010. Medial Parietal Cortex Encodes Perceived Heading Direction in Humans. *J Neurosci*. 30:12897–12901.
- Bhattacharyya R, Musallam S, Andersen RA. 2009. Parietal Reach Region Encodes Reach Depth Using Retinal Disparity and Vergence Angle Signals. *J Neurophysiol*. 102:805–816.
- Boussaoud D, Jouffrais C, Bremmer F. 1998. Eye position effects on the neuronal activity of dorsal premotor cortex in the macaque monkey. *J Neurophysiol*. 80:1132–1150.
- Bremner LR, Andersen RA. 2012. Coding of the reach vector in parietal area 5d. *Neuron*. 75:342–351.
- Breveglieri R, Galletti C, Gamberini M, Passarelli L, Fattori P. 2006. Somatosensory Cells in Area PEc of Macaque Posterior Parietal Cortex. *J Neurosci*. 26:3679–3684.
- Breveglieri R, Galletti C, Monaco S, Fattori P. 2008. Visual, somatosensory, and bimodal activities

- in the macaque parietal area P_{Ec}. *Cereb Cortex*. 18:806–816.
- Breveglieri R, Kutz D, Fattori P, Gamberini M, Galletti C. 2002. Somatosensory cells in the parieto-occipital area V6A of the macaque. *Neuroreport*. 13:2113–2116.
- Brodman K. 1909. *Vergleichende Lokalisationslehre der Großhirnrinde in ihren Prinzipien dargestellt auf Grund des Zellenbaues*.
- Burbaud P, Doegle C, Gross C, Bioulac B. 1991. A quantitative study of neuronal discharge in areas 5, 2, and 4 of the monkey during fast arm movements. *J Neurophysiol*. 66:429–443.
- Caminiti R, Innocenti GM, Battaglia-Mayer A. 2015. Organization and evolution of parieto-frontal processing streams in macaque monkeys and humans. *Neurosci Biobehav Rev*. 56:73–96.
- Cavada C, Goldman-Rakic PS. 1989. Posterior parietal cortex in rhesus monkey: I. Parcellation of areas based on distinctive limbic and sensory corticocortical connections. *J Comp Neurol*. 287:393–421.
- Chen J, Reitzen SD, Kohlenstein JB, Gardner EP. 2009. Neural representation of hand kinematics during prehension in posterior parietal cortex of the macaque monkey. *J Neurophysiol*. 102:3310–3328.
- Chen M, Li B, Guang J, Wei L, Wu S, Liu Y, Zhang M. 2016. Two subdivisions of macaque LIP process visual-oculomotor information differently. *Proc Natl Acad Sci*. 113:E6263–E6270.
- Colby CL, Duhamel JR. 1991. Heterogeneity of extrastriate visual areas and multiple parietal areas in the macaque monkey. *Neuropsychologia*. 29:517–537.
- Colby CL, Gattass R, Olson CR, Gross CG. 1988. Topographical organization of cortical afferents to extrastriate visual area PO in the macaque: a dual tracer study. *J Comp Neurol*. 269:392–413.
- Duffy FH, Burchfiel JL. 1971. Somatosensory system: organizational hierarchy from single units in monkey area 5. *Science*. 172:273–275.
- Fattori P, Breveglieri R, Amoroso K, Galletti C. 2004. Evidence for both reaching and grasping activity in the medial parieto-occipital cortex of the macaque. *Eur J Neurosci*. 20:2457–2466.

- Fattori P, Breveglieri R, Bosco A, Gamberini M, Galletti C. 2017. Vision for Prehension in the Medial Parietal Cortex. *Cereb Cortex*. 27:1149–1163.
- Fattori P, Breveglieri R, Marzocchi N, Filippini D, Bosco A, Galletti C. 2009. Hand orientation during reach-to-grasp movements modulates neuronal activity in the medial posterior parietal area V6A. *J Neurosci*. 29:1928–1936.
- Fattori P, Gamberini M, Kutz DF, Galletti C. 2001. “Arm-reaching” neurons in the parietal area V6A of the macaque monkey. *Eur J Neurosci*. 13:2309–2313.
- Fattori P, Kutz DF, Breveglieri R, Marzocchi N, Galletti C. 2005. Spatial tuning of reaching activity in the medial parieto-occipital cortex (area V6A) of macaque monkey. *Eur J Neurosci*. 22:956–972.
- Fattori P, Raos V, Breveglieri R, Bosco A, Marzocchi N, Galletti C. 2010. The dorsomedial pathway is not just for reaching: grasping neurons in the medial parieto-occipital cortex of the macaque monkey. *J Neurosci*. 30:342–349.
- Ferraina S, Battaglia-Mayer a, Genovesio a, Marconi B, Onorati P, Caminiti R. 2001. Early coding of visuomanual coordination during reaching in parietal area PEc. *J Neurophysiol*. 85:462–467.
- Ferraina S, Bianchi L. 1994. Posterior parietal cortex: functional properties of neurons in area 5 during an instructed-delay reaching task within different parts of space. *Exp brain Res*. 99:175–178.
- Ferraina S, Brunamonti E, Giusti MA, Costa S, Genovesio A, Caminiti R. 2009. Reaching in Depth: Hand Position Dominates over Binocular Eye Position in the Rostral Superior Parietal Lobule. *J Neurosci*. 29:11461–11470.
- Ferraina S, Garasto MR, Battaglia-Mayer A, Ferraresi P, Johnson PB, Lacquaniti F, Carniniti R. 1997. Visual Control of Hand-reaching Movement: Activity in Parietal Area 7m. *Eur J Neurosci*. 9:1090–1095.
- Ferraina S, Johnson PB, Garasto MR, Battaglia-Mayer A, Ercolani L, Bianchi L, Lacquaniti F,

- Caminiti R. 1997. Combination of hand and gaze signals during reaching: activity in parietal area 7 m of the monkey. *J Neurophysiol.* 77:1034–1038.
- Galletti C, Battaglini PP, Fattori P. 1993. Parietal neurons encoding spatial locations in craniotopic coordinates. *Exp Brain Res.* 96:221–229.
- Galletti C, Battaglini PP, Fattori P. 1995. Eye position influence on the parieto-occipital area PO (V6) of the macaque monkey. *Eur J Neurosci.* 7:2486–2501.
- Galletti C, Fattori P. 2003. Neuronal mechanisms for detection of motion in the field of view. *Neuropsychologia.* 41:1717–1727.
- Galletti C, Fattori P. 2017. The dorsal visual stream revisited: Stable circuits or dynamic pathways? *Cortex.* 1–15.
- Galletti C, Fattori P, Battaglini PP, Shipp S, Zeki S. 1996. Functional Demarcation of a Border Between Areas V6 and V6A in the Superior Parietal Gyrus of the Macaque Monkey. *Eur J Neurosci.* 8:30–52.
- Galletti C, Fattori P, Gamberini M, Kutz DF. 1999. The cortical visual area V6: brain location and visual topography. *Eur J Neurosci.* 11:3922–3936.
- Galletti C, Fattori P, Kutz DF, Battaglini PP. 1997. Arm Movement-related Neurons in the Visual Area V6A of the Macaque Superior Parietal Lobule. *Eur J Neurosci.* 9:410–413.
- Galletti C, Fattori P, Kutz DF, Gamberini M. 1999. Brain location and visual topography of cortical area V6A in the macaque monkey. *Eur J Neurosci.* 11:575–582.
- Galletti C, Gamberini M. 2018. Superior Parietal Lobule (SPL). *Encycl Anim Cogn Behav.*
- Galletti C, Gamberini M, Kutz DF, Fattori P, Luppino G, Matelli M. 2001. The cortical connections of area V6: an occipito-parietal network processing visual information. *Eur J Neurosci.* 13:1572–1588.
- Gallyas F. 1979. Silver staining of myelin by means of physical development. *Neurol Res.* 1:203–209.
- Gamberini M, Bakola S, Passarelli L, Burman KJ, Rosa MGP, Fattori P, Galletti C. 2016. Thalamic

projections to visual and visuomotor areas (V6 and V6A) in the Rostral Bank of the parieto-occipital sulcus of the Macaque. *Brain Struct Funct.* 221:1573–1589.

Gamberini M, Dal Bò G, Breveglieri R, Briganti S, Passarelli L, Fattori P, Galletti C. 2018. Sensory properties of the caudal aspect of the macaque's superior parietal lobule. *Brain Struct Funct.* 223:1863–1879.

Gamberini M, Fattori P, Galletti C. 2015. The medial parietal occipital areas in the macaque monkey. *Vis Neurosci.* 32:E013.

Gamberini M, Galletti C, Bosco A, Breveglieri R, Fattori P. 2011. Is the Medial Posterior Parietal Area V6A a Single Functional Area? *J Neurosci.* 31:5145–5157.

Gamberini M, Passarelli L, Bakola S, Impieri D, Fattori P, Rosa MGP, Galletti C. 2017. Claustral afferents of superior parietal areas PEc and PE in the macaque. *J Comp Neurol.* 525:1475–1488.

Gamberini M, Passarelli L, Fattori P, Zucchelli M, Bakola S, Luppino G, Galletti C. 2009. Cortical connections of the visuomotor parietooccipital area V6Ad of the macaque monkey. *J Comp Neurol.* 513:622–642.

Goodale MA, Milner AD. 1992. Separate visual pathways for perception and action. *Trends Neurosci.* 15:20–25.

Gregoriou GG, Luppino G, Matelli M, Savaki HE. 2005. Frontal cortical areas of the monkey brain engaged in reaching behavior: A 14C-deoxyglucose imaging study. *Neuroimage.* 27:442–464.

Grieve KL, Acuña C, Cudeiro J. 2000. The primate pulvinar nuclei: Vision and action. *Trends Neurosci.* 23:35–39.

Hadjidimitrakis K, Dal Bo' G, Breveglieri R, Galletti C, Fattori P. 2015. Overlapping representations for reach depth and direction in caudal superior parietal lobule of macaques. *J Neurophysiol.* 114:2340–2352.

Hutchison RM, Culham JC, Flanagan JR, Everling S, Gallivan JP. 2015. Functional subdivisions of medial parieto-occipital cortex in humans and nonhuman primates using resting-state fMRI.

Neuroimage. 116:10–29.

- Ilinsky IA, Kultas-Ilinsky K. 1987. Sagittal cytoarchitectonic maps of the *Macaca mulatta* thalamus with a revised nomenclature of the motor-related nuclei validated by observations on their connectivity. *J Comp Neurol.* 262:331–364.
- Impieri D, Gamberini M, Passarelli L, Rosa MGP, Galletti C. 2018. Thalamo-cortical projections to the macaque superior parietal lobule areas PEc and PE. *J Comp Neurol.* 526:1041–1056.
- Jones EG. 2007. *The Thalamus.* Cambridge: Cambridge Univ. Press.
- Kaas JH, Lyon DC. 2007. Pulvinar Contributions to the Dorsal and Ventral Streams of Visual Processing in Primates. *Brain Res Rev.* 55:285–296.
- Kalaska JF. 1996. Parietal cortex area 5 and visuomotor behavior. *Can J Physiol Pharmacol.* 74:483–498.
- Kobayashi Y, Amaral DG. 2003. Macaque monkey retrosplenial cortex: II. Cortical afferents. *J Comp Neurol.* 466:48–79.
- Kravitz DJ, Saleem KS, Baker CI, Mishkin M. 2011. A new neural framework for visuospatial processing. *Nat Rev Neurosci.* 12:217–230.
- Krubitzer L, Disbrow E. 2008. The evolution of parietal areas involved in hand use in primates. In: *The senses: a comprehensive reference* (Kaas J, Gardner E, eds). Elsevier. ed. London. p. 183–214.
- Lacquaniti F, Guigon E, Bianchi L, Ferraina S, Caminiti R. 1995. Representing spatial information for limb movement: role of area 5 in the monkey. *Cereb Cortex.* 5:391–409.
- Leichnetz GR. 2001. Connections of the medial posterior parietal cortex (area 7m) in the monkey. *Anat Rec.* 263:215–236.
- Levichkina E, Saalman YB, Vidyasagar TR. 2017. Coding of spatial attention priorities and object features in the macaque lateral intraparietal cortex. *Physiol Rep.* 5:1–17.
- Lewis JW, Van Essen DC. 2000. Mapping of architectonic subdivisions in the macaque monkey, with emphasis on parieto-occipital cortex. *J Comp Neurol.* 428:79–111.

- Luppino G, Ben Hamed S, Gamberini M, Matelli M, Galletti C. 2005. Occipital (V6) and parietal (V6A) areas in the anterior wall of the parieto-occipital sulcus of the macaque: A cytoarchitectonic study. *Eur J Neurosci.* 21:3056–3076.
- Mahalanobis PC. 1936. On the generalized distance in statistics. *Proc Natl Inst Sci India.* 2:49–55.
- Maimon G, Assad JA. 2006. Parietal Area 5 and the Initiation of Self-Timed Movements versus Simple Reactions. *J Neurosci.* 26:2487–2498.
- Markram H, Toledo-Rodriguez M, Wang Y, Gupta A, Silberberg G, Wu C. 2004. Interneurons of the neocortical inhibitory system. *Nat Rev Neurosci.* 5:793–807.
- Matelli M, Govoni P, Galletti C, Kutz DF, Luppino G. 1998. Superior area 6 afferents from the superior parietal lobule in the macaque monkey. *J Comp Neurol.* 402:327–352.
- Merker B. 1983. Silver staining of cell bodies by means of physical development. *J Neurosci Methods.* 9:235–241.
- Morecraft RJ, Cipolloni PB, Stilwell-Morecraft KS, Gedney MT, Pandya DN. 2004. Cytoarchitecture and Cortical Connections of the Posterior Cingulate and Adjacent Somatosensory Fields in the Rhesus Monkey. *J Comp Neurol.* 469:37–69.
- Mountcastle VB, Lynch JC, Georgopoulos a, Sakata H, Acuna C. 1975. Posterior parietal association cortex of the monkey: command functions for operations within extrapersonal space. *J Neurophysiol.* 38:871–908.
- Murray EA, Coulter JD. 1981. Supplementary sensory area. The medial parietal cortex in the monkey. In: Woolsey CN, editor. *Cortical sensory organization.* Clifton (NJ): Humana. p. 167–195.
- Olson CR, Musil SY, Goldberg ME. 1996. Single neurons in posterior cingulate cortex of behaving macaque: eye movement signals. *J Neurophysiol.* 76:3285–3300.
- Padberg J, Franca JG, Cooke DF, Soares JGM, Rosa MGP, Fiorani M, Gattass R, Krubitzer L. 2007. Parallel Evolution of Cortical Areas Involved in Skilled Hand Use. *J Neurosci.* 27:10106–10115.

- Palomero-Gallagher N, Zilles K, Schleicher A, Vogt BA. 2013. Cyto- and receptor architecture of area 32 in human and macaque brains. *J Comp Neurol.* 521:3272–3286.
- Palomero-Gallagher N, Zilles K. 2018. Cyto- and receptor architectonic mapping of the human brain. *Handb Clin Neurol.* 150:355-387.
- Pandya DN, Seltzer B. 1982. Intrinsic connections and architectonics of posterior parietal cortex in the rhesus monkey. *J Comp Neurol.* 204:196–210.
- Passarelli L, Rosa MGP, Bakola S, Gamberini M, Worthy KH, Fattori P, Galletti C. 2018. Uniformity and Diversity of Cortical Projections to Precuneate Areas in the Macaque Monkey: What Defines Area PGm? *Cereb Cortex.* 28:1700–1717.
- Passarelli L, Rosa MGP, Gamberini M, Bakola S, Burman KJ, Fattori P, Galletti C. 2011. Cortical Connections of Area V6Av in the Macaque: A Visual-Input Node to the Eye/Hand Coordination System. *J Neurosci.* 31:1790–1801.
- Paus T. 2001. Primate Anterior Cingulate Cortex : Where Motor Control , Drive and Cognition Interface. *Nat Rev Neurosci.* 2:417–424.
- Piserchia V, Breveglieri R, Hadjidimitrakis K, Bertozzi F, Galletti C, Fattori P. 2017. Mixed Body/Hand Reference Frame for Reaching in 3D Space in Macaque Parietal Area PEc. *Cereb Cortex.* 27:1976–1990.
- Pitzalis S, Fattori P, Galletti C. 2015. The human cortical areas V6 and V6A. 2015. *Vis Neurosci.* 32:e007.
- Pitzalis S, Sereno M I, Committeri G, Fattori P, Galati G, Tosoni A, Galletti C. 2013. The human homologue of area V6A. *NeuroImage.* 82:517-530.
- Pitzalis S, Galletti C, Huang R-S, Patria F, Committeri G, Galati G, Fattori P, Sereno M I. 2006. Wide-field retinotopy defines human cortical visual area V6. *J Neurosci.* 26(30):7962-7973.
- Raffi M, Squatrito S, Maioli MG. 2002. Neuronal Responses to Optic Flow in the Monkey Parietal Area PEc. *Cereb Cortex.* 639–646.
- Rao SG, Williams G V, Goldman-Rakic PS. 2000. Destruction and creation of spatial tuning by

- disinhibition: GABA(A) blockade of prefrontal cortical neurons engaged by working memory. *J Neurosci.* 20:485–494.
- Raos V, Franchi G, Gallese V, Fogassi L. 2003. Somatotopic organization of the lateral part of area F2 (dorsal premotor cortex) of the macaque monkey. *J Neurophysiol.* 89:1503–1518.
- Raos V, Umiltà MA, Gallese V, Fogassi L. 2004. Functional Properties of Grasping-Related Neurons in the Ventral Premotor Area F2 of the Macaque Monkey. *J Neurophysiol.* 92:1990–2002.
- Rizzolatti G, Matelli M. 2003. Two different streams form the dorsal visual system: anatomy and functions. *Exp Brain Res.* 153:146–157.
- Sakata H, Takaoka Y, Kawarasaki A, Shibutani H. 1973. Somatosensory properties of neurons in the superior parietal cortex (area 5) of the rhesus monkey. *Brain Res.* 64:85–102.
- Sato N, Sakata H, Tanaka YL, Taira M. 2006. Navigation-associated medial parietal neurons in monkeys. *Proc Natl Acad Sci U S A.* 103:17001–17006.
- Sato N, Sakata H, Tanaka YL, Taira M. 2010. Context-dependent place-selective responses of the neurons in the medial parietal region of macaque monkeys. *Cereb Cortex.* 20:846–858.
- Scheperjans F, Eickhoff SB, Hömke L, Mohlberg H, Hermann K, Amunts K, Zilles K. 2008. Probabilistic maps, morphometry, and variability of cytoarchitectonic areas in the human superior parietal cortex. *Cereb Cortex.* 18:2141–2157.
- Scheperjans F, Grefkes C, Palomero-Gallagher N, Schleicher A, Zilles K. 2005. Subdivisions of human parietal area 5 revealed by quantitative receptor autoradiography: A parietal region between motor, somatosensory, and cingulate cortical areas. *Neuroimage.* 25:975–992.
- Scheperjans F, Hermann K, Eickhoff SB, Amunts K, Schleicher A, Zilles K. 2008. Observer-independent cytoarchitectonic mapping of the human superior parietal cortex. *Cereb Cortex.* 18:846–867.
- Scheperjans F, Palomero-Gallagher N, Grefkes C, Schleicher A, Zilles K. 2005. Transmitter receptors reveal segregation of cortical areas in the human superior parietal cortex: Relations

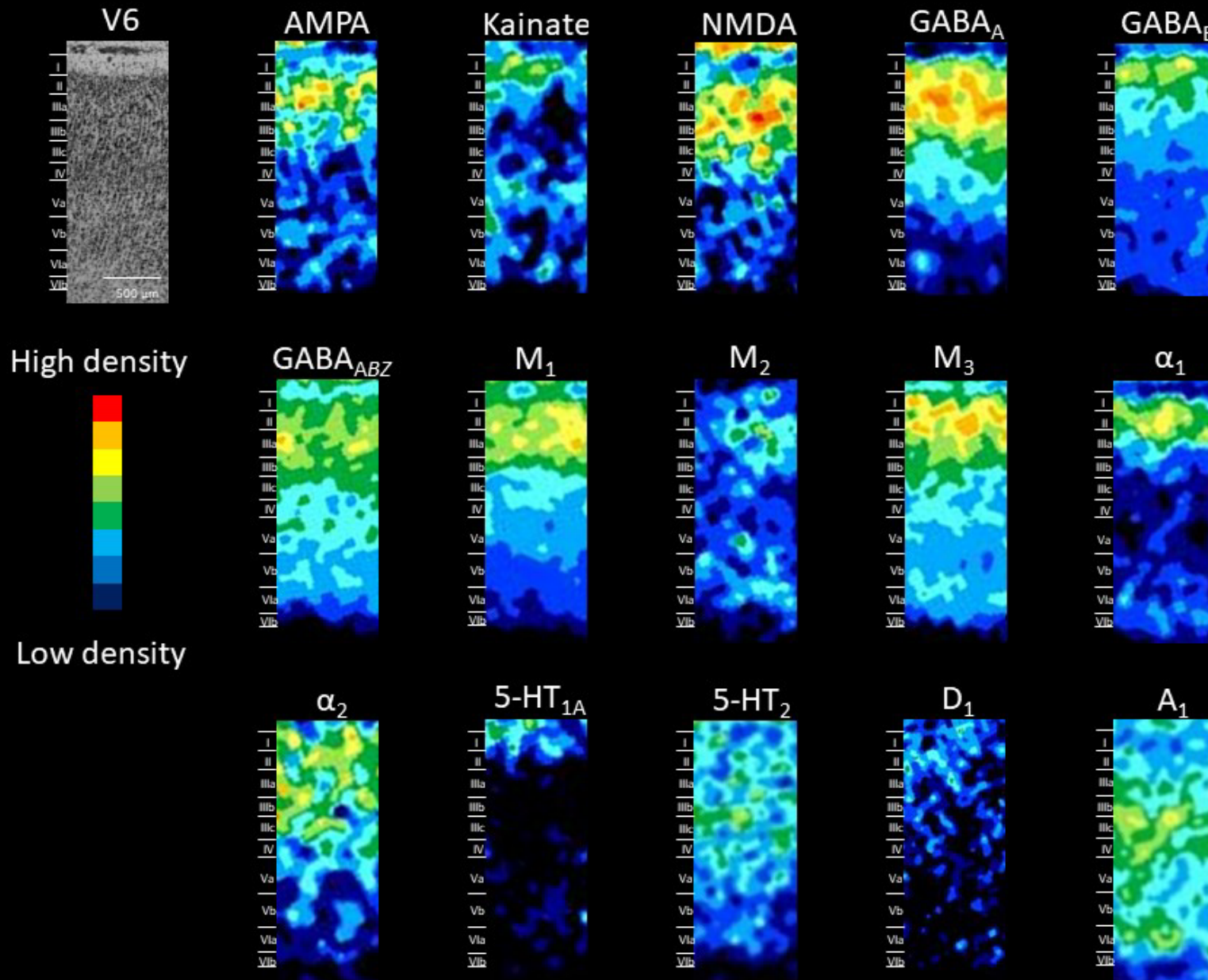
- to visual and somatosensory regions. *Neuroimage*. 28:362–379.
- Seelke AMH, Padberg JJ, Disbrow E, Purnell SM, Recanzone G, Krubitzer L. 2012. Topographic maps within brodmann's area 5 of macaque monkeys. *Cereb Cortex*. 22:1834–1850.
- Shi Y, Apker G, Buneo CA. 2013. Multimodal representation of limb endpoint position in the posterior parietal cortex. *J Neurophysiol*. 109:2097–2107.
- Snyder LH, Batista AP, Andersen RA. 1997. Coding of intention in the posterior parietal cortex. *Nature*. 386:167–170.
- Squatrito S, Raffi M, Maioli MG, Battaglia-Mayer A. 2001. Visual motion responses of neurons in the caudal area pe of macaque monkeys. *J Neurosci*. 21:RC130.
- Taoka M, Toda T, Iriki A, Tanaka M, Iwamura Y. 2000. Bilateral receptive field neurons in the hindlimb region of the postcentral somatosensory cortex in awake macaque monkeys. *Exp Brain Res*. 134:139–146.
- Taoka M, Toda T, Iwamura Y. 1998. Representation of the midline trunk, bilateral arms, and shoulders in the monkey postcentral somatosensory cortex. *Exp Brain Res*. 123:315–322.
- Thier P, Andersen R a. 1998. Electrical microstimulation distinguishes distinct saccade-related areas in the posterior parietal cortex. *J Neurophysiol*. 80:1713–1735.
- Watanabe Y, Funahashi S. 2004. Neuronal Activity Throughout the Primate Mediodorsal Nucleus of the Thalamus during Oculomotor Delayed-Responses.I. Cue-, Delay-, and Response-Period Activity. *J Neurophysiol*. 1756–1769.
- Wehr M, Zador AM. 2003. Balanced inhibition underlies tuning and sharpens spike timing in auditory cortex. *Nature*. 426:442–446.
- Wu C, Sun D. 2015. GABA receptors in brain development, function, and injury. *Metab Brain Dis*. 30:367–379.
- Xu G, Broadbelt KG, Haynes RL, Rebecca D, Volpe JJ, Kinney HC. 2011. Late Development of the GABAergic system in the Human Cerebral Cortex and White Matter. *J Neuropathol Exp Neurol*. 70:841–858.

- Zhou Y, Liu Y, Wu S, Zhang M. 2017. Neuronal Representation of the Saccadic Timing Signals in Macaque Lateral Intraparietal Area. *Cereb Cortex*. 1–14.
- Zilles K, Palomero-Gallagher N, Grefkes C, Scheperjans F, Boy C, Amunts K, Schleicher A. 2002a. Architectonics of the human cerebral cortex and transmitter receptor fingerprints: Reconciling functional neuroanatomy and neurochemistry. *Eur Neuropsychopharmacol*. 12:587–599.
- Zilles K, Qü MS, Köhling R, Speckmann EJ. 1999. Ionotropic glutamate and GABA receptors in human epileptic neocortical tissue: quantitative in vitro receptor autoradiography. *Neuroscience*. 94:1051–1061.
- Zilles K, Schleicher A. 1995. Correlative imaging of transmitter receptor distributions in human cortex. In: Stumpf WE,, Solomon HF, editors. *Autoradiography and Correlative Imaging*. San Diego: Academic Press. p. 277–307.
- Zilles K, Schleicher A, Palomero-Gallagher N, Amunts K. 2002b. Quantitative Analysis of Cyto- and Receptor Architecture of the Human Brain. In: *Brain Mapping: The Methods*. 2nd editio. ed. Elsevier Science (USA). p. 573–602.

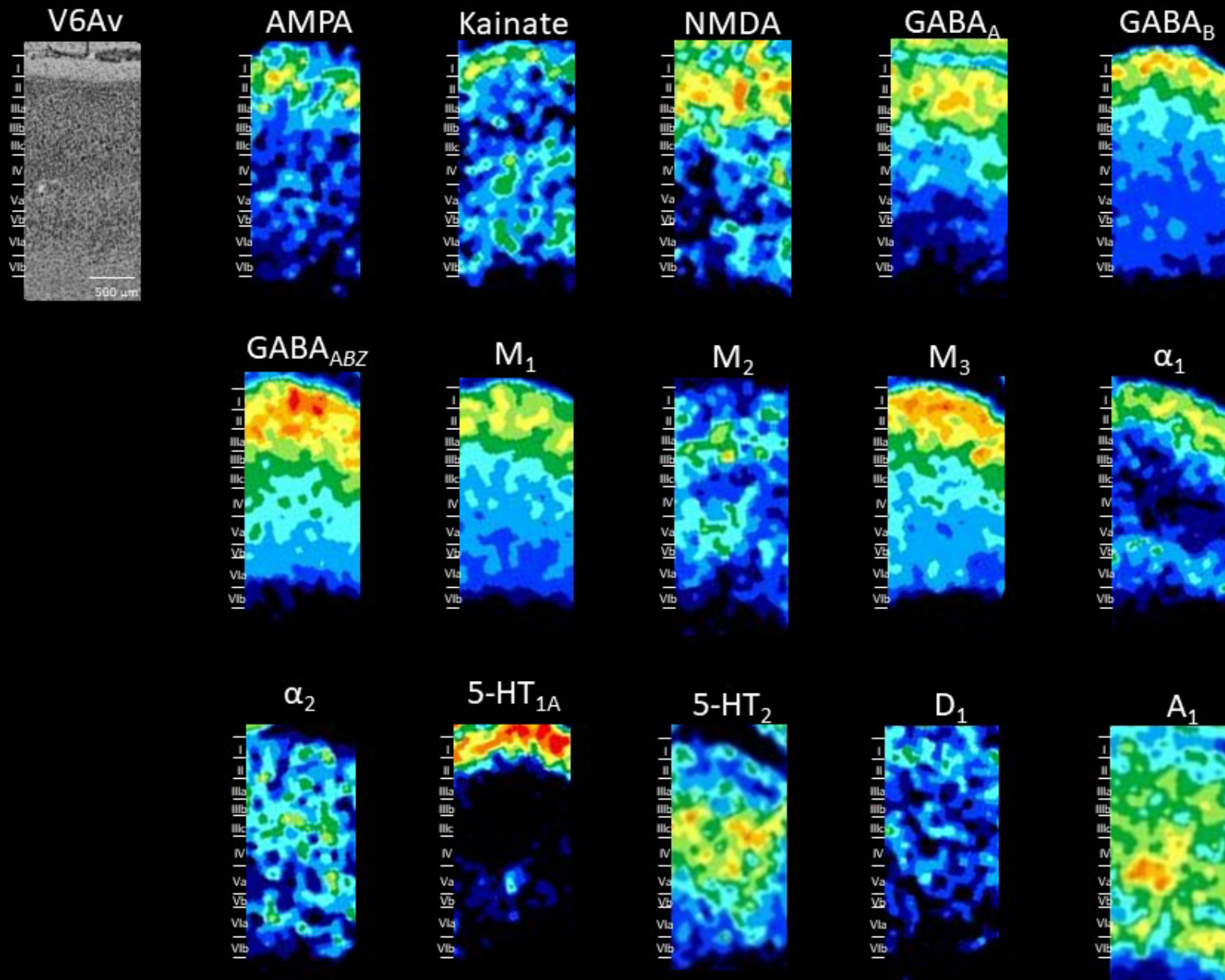
Books

- Mai JK, Paxinos G. 2012. *The human nervous system*. 3rd ed. Amsterdam: Academic Press.
- Kandel ER, Schwartz JH, Jessell TM. 2000. *Principles of Neural Science*. 4th ed. McGraw-Hill.
- Purves D, Augustine GJ, Fitzpatrick D, Hall WC, LaMantia A-S, White LE. 2018. *Neuroscience*. Oxford University Press.

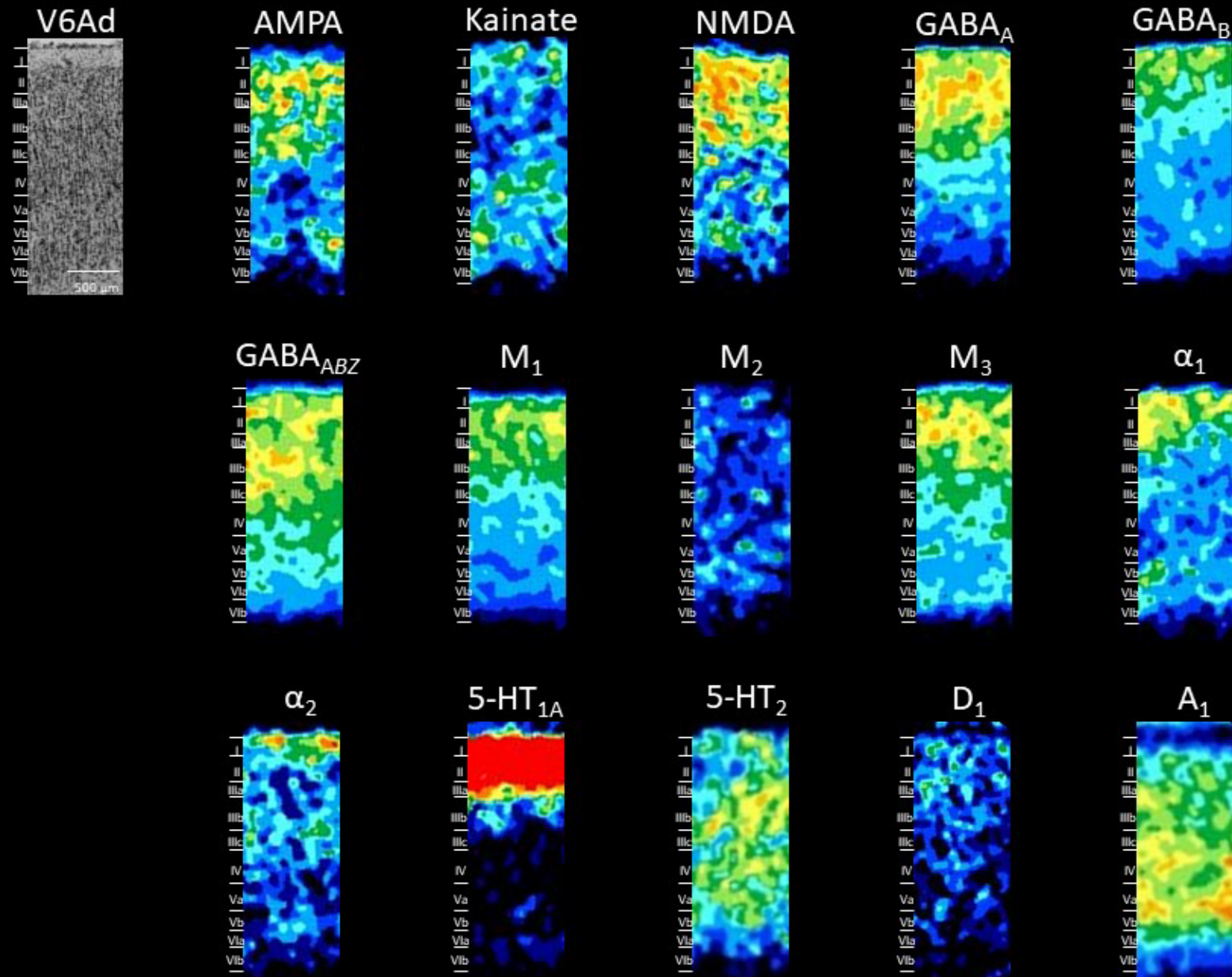
Colour Table 1. Laminar receptor distribution pattern of area V6. To the left, a Nissl stained segment of area V6 is shown. The same segment taken from the corresponding neighbouring autoradiographs is shown for all the fifteen receptors analysed. Colour scale codes for receptor densities.



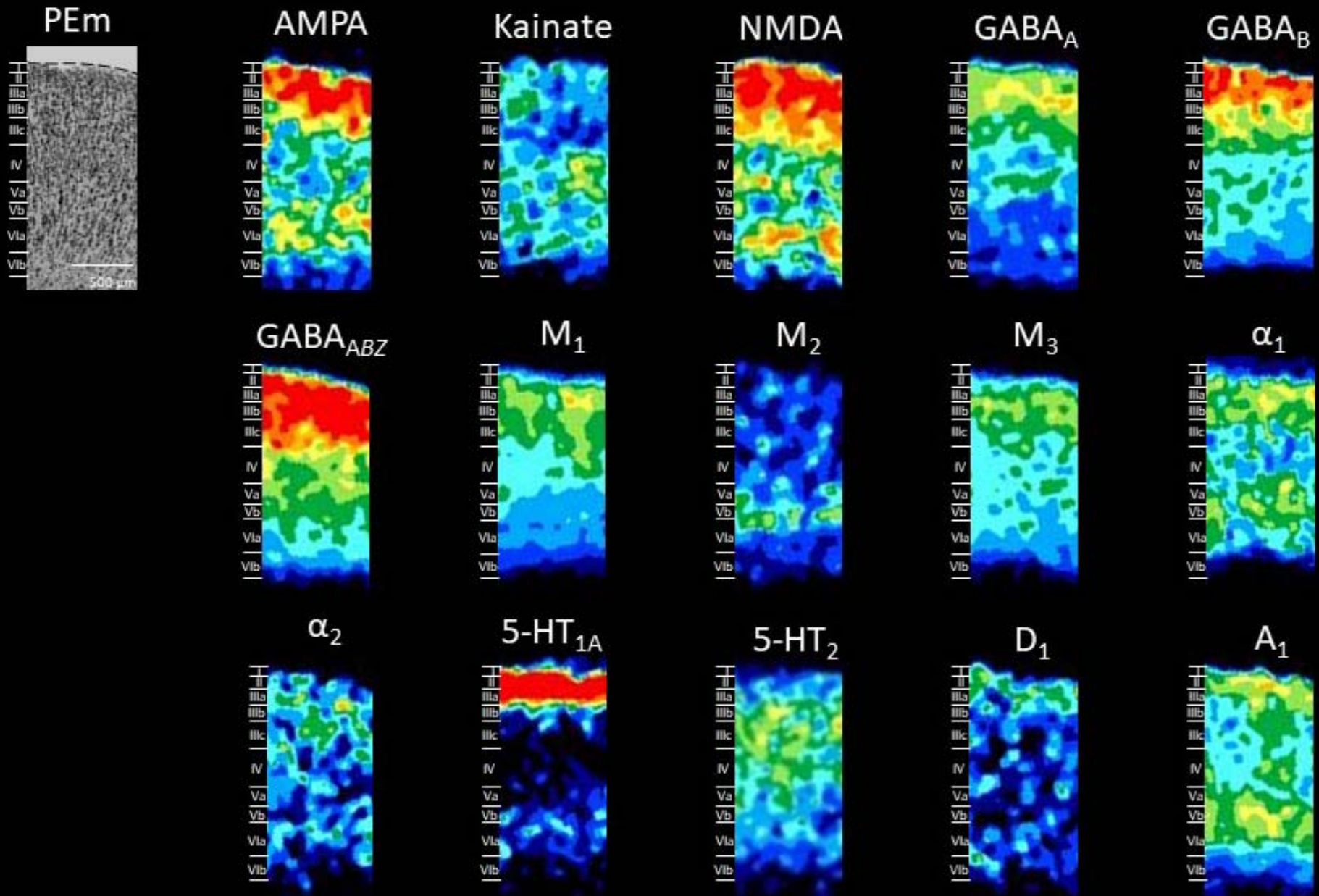
Colour Table 2. Laminar receptor distribution pattern of area V6Av. Other details in Colour Table 1.



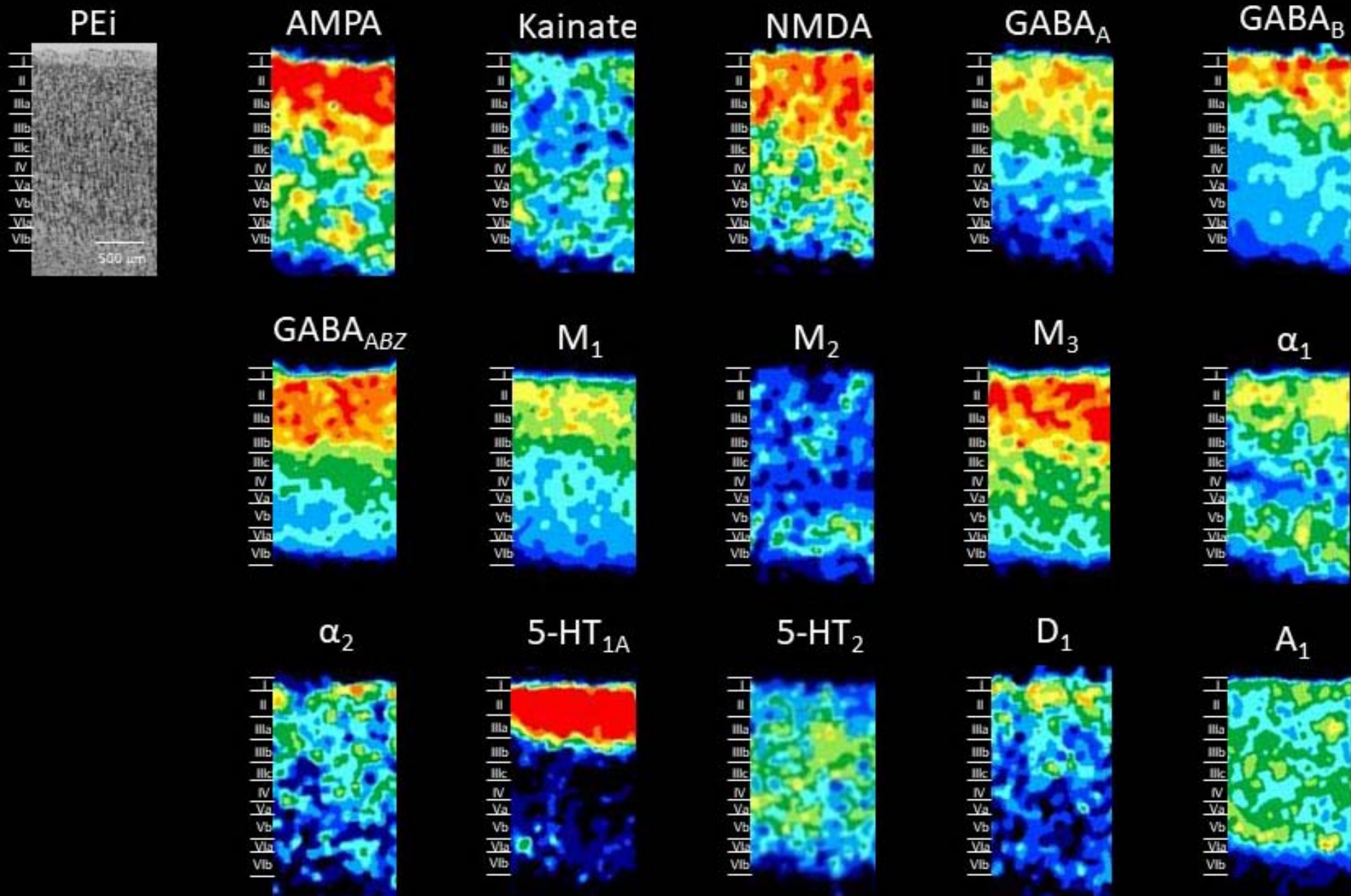
Colour Table 3. Laminar receptor distribution pattern of area V6Ad. Other details in Colour Table 1.



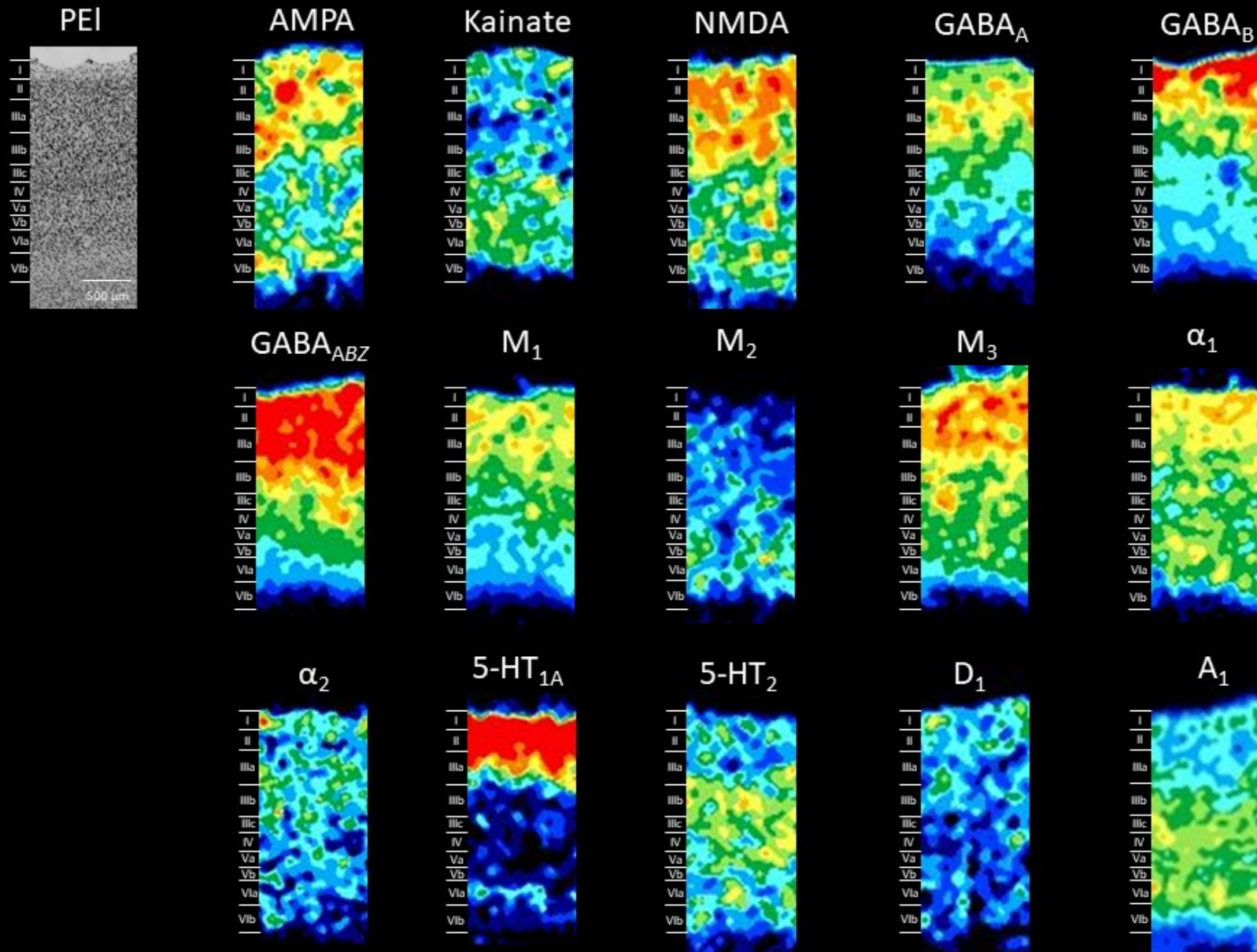
Colour Table 5. Laminar receptor distribution pattern of area PEm. Other details in Colour Table 1.



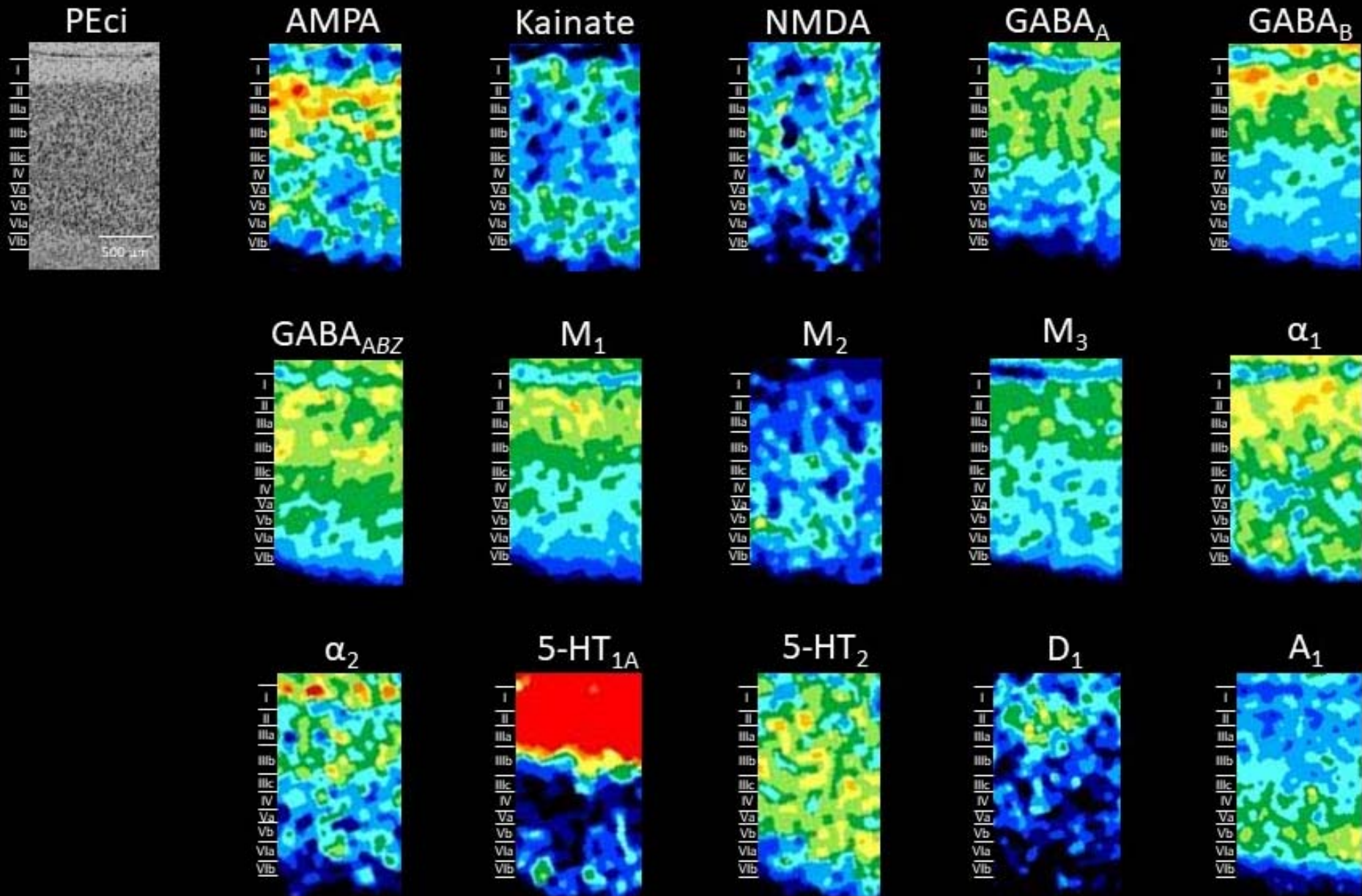
Colour Table 6. Laminar receptor distribution pattern of area PEi. Other details in Colour Table 1.



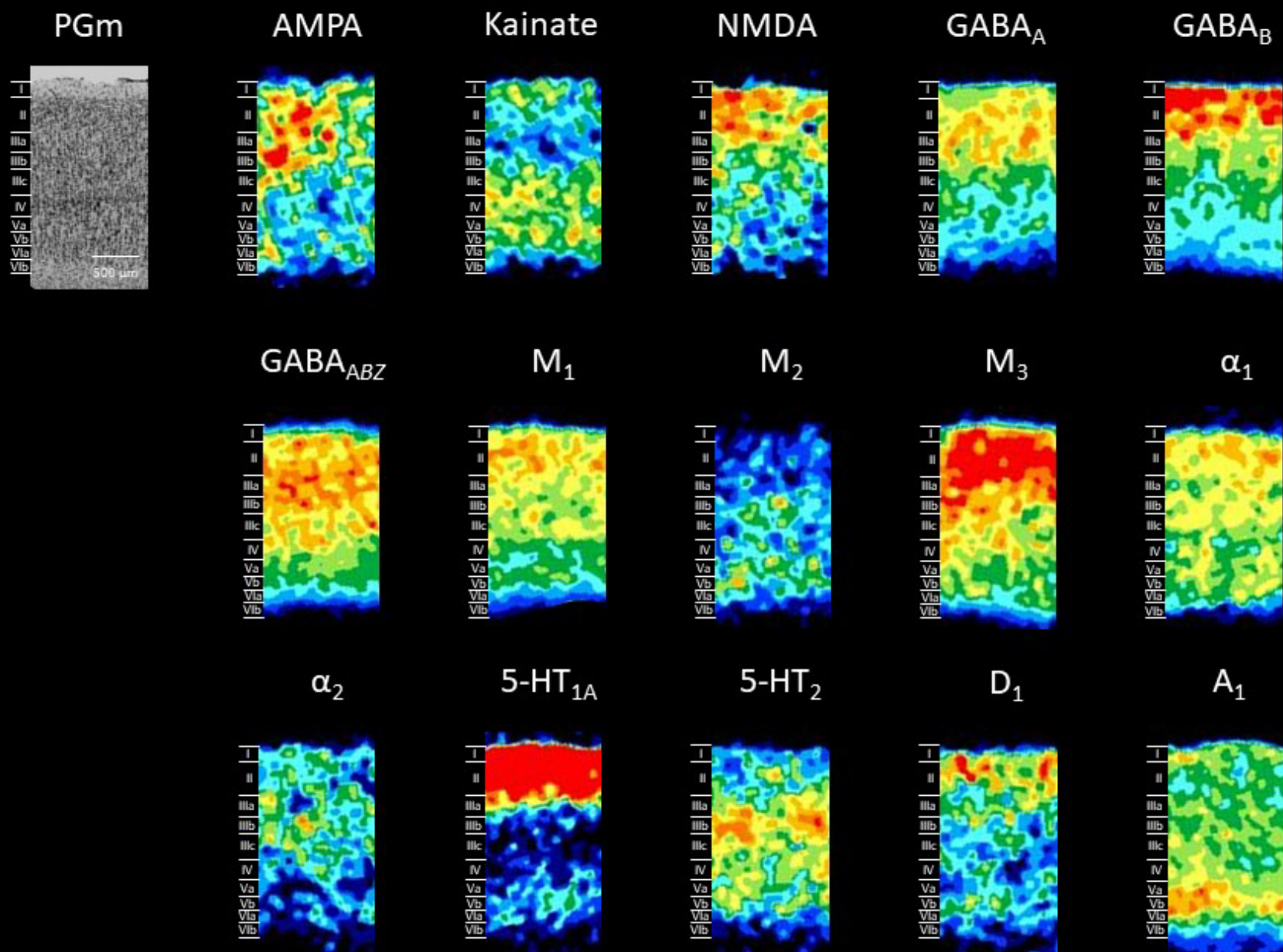
Colour Table 7. Lamina receptor distribution pattern of area PEI. Other details in Colour Table 1.



Colour Table 8. Laminar receptor distribution pattern of area PEci. Other details in Colour Table 1.



Colour Table 9. Laminar receptor distribution pattern of area PGm. Other details in Colour Table 1.



Claustral Afferents of Superior Parietal Areas PEc and PE in the Macaque

Michela Gamberini,¹ Laretta Passarelli,¹ Sophia Bakola,^{1,2,3} Daniele Impieri,¹ Patrizia Fattori,¹ Marcello G. P. Rosa,^{2,3†} and Claudio Galletti^{1†*}

¹Department of Pharmacy and Biotechnology, University of Bologna, 40126, Bologna, Italy

²Biomedicine Discovery Institute and Department of Physiology, Monash University, Clayton, Victoria, 3800, Australia

³Australian Research Council, Centre of Excellence for Integrative Brain Function, Monash University Node, Clayton, Victoria, 3800, Australia

ABSTRACT

The exposed surface of the primate superior parietal cortex includes two cytoarchitecturally defined areas, the PEc and PE. In the present study we describe the distribution of neurons projecting from the claustrum to these areas. Retrograde neuronal tracers were injected by direct visualization of regions of interest, and the location of injection sites was reconstructed relative to cytoarchitectural borders. For comparison, the patterns of claustral label that resulted from injections involving neighboring cytoarchitectonic areas were analyzed. We found that the claustral territories sending projections to areas PE and PEc partially overlapped zones previously shown to form projections to the posterior parietal, somatosensory, visual, and motor cortex. The projection zones to the PE and PEc overlapped extensively, and consisted of multiple patches separated by label-free zones. Most

of the labeled neurons were located in the posterior–ventral part of the claustrum. Area PE received additional inputs from a posterior–dorsal part of the claustrum, which has been previously reported to project to the somatosensory cortex, while the PEc receives additional input from an anterior–ventral region of the claustrum, which has been reported to project to the visual association cortex. These observations reflect the known functional properties of the PE and PEc, with the former containing neurons that are predominantly involved in somatosensory processing, and the latter including both somatosensory and visual neurons. The present results suggest that the claustrum projections may help coordinate the activity of an extensive neural circuit involved in sensory and motor processing for movement execution. *J. Comp. Neurol.* 525:1475–1488, 2017.

© 2016 Wiley Periodicals, Inc.

INDEXING TERMS: posterior parietal cortex; connectivity; primate; claustrum; superior parietal lobule; sensorimotor input

The claustrum forms a relatively thin, folded sheet of gray matter, inserted between the striatum and the insular cortex, which is surrounded by white matter (Crick and Koch, 2005). The claustrum has been classically considered as a component of the basal ganglia, but its direct projections to the cortex suggest a very different role. However, there are still relatively few data on which to build detailed hypotheses about its function (for comprehensive reviews, consult Smythies et al., 2012; Baizer et al., 2014; Mathur, 2014). Neuroanatomical studies in New and Old World monkeys have revealed widespread connections between the claustrum and neocortical regions in the frontal, occipital, and temporal lobes, as well as in the parietooccipital and posterior parietal regions, and somatosensory areas (Carman et al., 1964; Druga 1968, 1966; Kemp and Powell, 1970; Chadzypanagiotis

and Narkiewicz, 1971; Pearson et al., 1982; Baizer et al., 1993; Tanné-Gariepy et al., 2002; Burman et al., 2011; Reser et al., 2014; Milardi et al., 2015).

This article was published online on 16 June 2016. An error was subsequently identified. This notice is included in the online and print versions to indicate that both have been corrected 24 June 2016.

Marcello G.P. Rosa and Claudio Galletti contributed equally to this work.

Grant sponsor: European Union; Grant number: FP7-ICT 217077-EYE-SHOTS, FP7-PEOPLE-2011-IOF 300452 (to S.B.); Grant sponsor: Ministero dell'Università & della Ricerca and Fondazione del Monte di Bologna & Ravenna, Italy; Grant sponsor: Australian National Health and Medical Research Council; Grant numbers: 1020839 and 1082144.

*CORRESPONDENCE TO: Claudio Galletti, Department of Pharmacy and Biotechnology, Piazza di Porta S. Donato, 2, 40126 Bologna, Italy. E-mail: claudio.galletti@unibo.it

Received November 23, 2015; Revised April 12, 2016;

Accepted May 25, 2016.

DOI 10.1002/cne.24052

Published online June 16, 2016 in Wiley Online Library (wileyonlinelibrary.com)

© 2016 Wiley Periodicals, Inc.

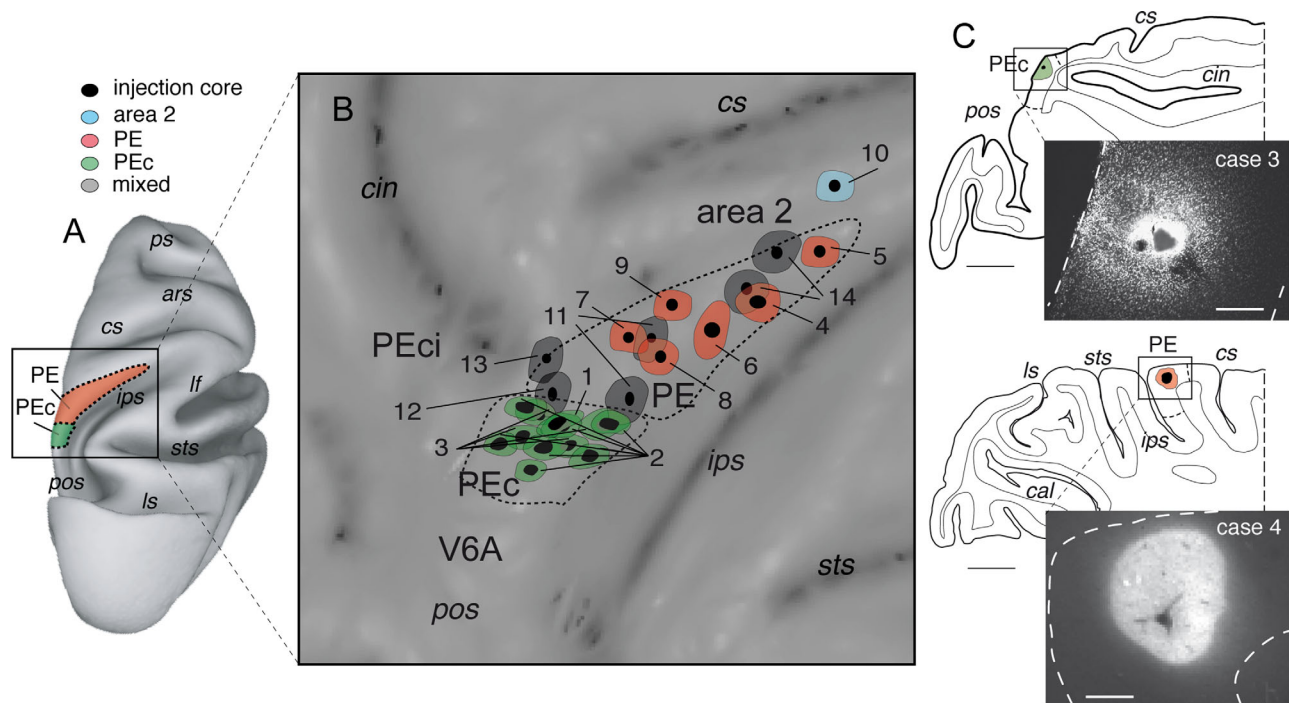


Figure 1. Summary of injection site locations. **A,B:** Injection sites in six animals are illustrated on a two-dimensional reconstruction (B) of the caudal superior parietal lobe of a reference monkey brain shown on the left (A). The dashed contours represent the average cytoarchitectonic borders of the PEc and PE, respectively. **C:** Examples of injection sites. Parasagittal sections taken at the level of injection sites in case 3 (DY injection in area PEc), and case 4 (CTB-green injection in area PE). Dashed lines within sections indicate the borders of areas PEc or PE. Abbreviations: ar, arcuate sulcus; cal, calcarine fissure; cin, cingulate sulcus; cs, central sulcus; ips, intraparietal sulcus; if, lateral fissure; ls, lunate sulcus; pos, parieto-occipital sulcus; ps, principal sulcus; sts, superior temporal sulcus. Scale bars in C = 5 mm for sections and 500 μ m for injection sites.

Here we investigated the claustral projections to cortical areas PEc and PE located on the exposed cortex of the superior parietal lobule. Area PEc contains visual, somatosensory, and bimodal neurons (Breviglieri et al., 2006, 2008), most of which are sensitive to the movement and position of hand and eye (Ferraina et al., 2001; Battaglia-Mayer et al., 2001). This area contains an incomplete representation of the body, mainly focused on upper and lower limbs, without an evident topographic organization (Breviglieri et al., 2006, 2008). It has been recently demonstrated that a large percentage of PEc neurons encodes both direction and depth information during arm reaching movements (Hadjidimitrakis et al., 2015), and contributes to hand-target transformations for reaching (Pisierchia et al., 2016). In contrast, area PE (which has been traditionally equated to Brodmann's area 5) contains an almost complete representation of the body, with a coarse topographic organization (Taoka et al., 1998, 2000; Padberg et al., 2007). The majority of its neurons respond to proprioceptive stimulation, while fewer cells are activated by tactile stimuli, and even fewer by visual stimuli (Duffy and Burchfiel, 1971; Sakata et al., 1973; Mountcastle et al., 1975).

Area PE is involved in the preparation of limb movements (Burbaud et al., 1991) and in the generation of different types of reference systems for encoding reaching movements (Ferraina and Bianchi, 1994; Lacquaniti et al., 1995; Kalaska, 1996; Batista et al., 1999; Bremner and Andersen, 2012).

Very few studies have investigated the claustrum in macaque monkeys in the context of sensorimotor integration. Neuronal activity recorded in the claustrum while macaques performed arm movements, either visually guided or triggered by memorized information, suggested that claustral neurons could play a role in arm movement execution (Shima et al., 1996). A comparison with neuronal activity in the primary motor cortex showed that neurons of the claustrum, in contrast to those of the motor cortex, showed little selectivity to the type of movement (Shima et al., 1996). Other studies have suggested that the claustrum integrates multi-sensory information from different sensory cortices (Ettlinger and Wilson, 1990). The present study defines the origin of projections from the claustrum to the PEc and PE, and links these results to previous observations on claustral projections to other nodes of the cortical

TABLE 1.
Injection Sites and Neuronal Tracers Employed in the Experiments

Case ¹	Cutting plane	Injected area	Tracer	Amount and concentration of tracer
1 ^a	Coronal	PEc	FB ²	1 crystal
2	Coronal	PEc	DY ³	7 crystals
3	Parasagittal	PEc	DY ³	4 crystals
4 ^b	Parasagittal	PE	CTB-green ⁴	1.7 μ l, 1% in PBS
5 ^b	Parasagittal	PE	CTB-red ⁴	1.7 μ l, 1% in PBS
6 ^c	Parasagittal	PE	FB ²	1 crystal
7 ^c	Parasagittal	PE	CTB-green ⁴	2 μ l, 1% in PBS
8 ^c	Parasagittal	PE	FR ⁴	0.3 μ l, 10% in saline
9	Parasagittal	PE	CTB-green ⁴	1.7 μ l, 1% in PBS
10 ^b	Parasagittal	2	FB ²	1 crystal
11 ^a	Coronal	PE/PEc	CTB-red ⁴	2 \times 1.6 μ l, 1% in PBS
12 ^a	Coronal	PEc/PE	CTB-green ⁴	1.7 μ l, 1% in PBS
13	Coronal	PE/PEci	DY ³	1 crystal
14	Parasagittal	PE/2	WGA-HRP ³	2 \times 0.12 μ l, 4% in distilled water

¹The letters a, b, and c correspond to the same hemisphere.

²Polysciences Europe, Germany.

³Sigma Aldrich.

⁴Molecular Probes.

Abbreviations: CTB, cholera toxin B; DY, Diamidino Yellow; FB, Fast Blue; FR, Fluoro-Ruby; PBS, phosphate-buffered saline; WGA-HRP, wheat germ agglutinin-horseradish peroxidase.

network of areas involved in movement planning and visuomotor integration.

MATERIALS AND METHODS

Experimental protocols were approved by the Bioethics Committee of the University of Bologna, in accordance with the guidelines of the European Directive 86/609/EEC, and the revised Directive 2010/63/EU for the Care and Use of Animals for Scientific Purposes. In total, 14 retrograde tracer injections were placed in eight hemispheres of six male adult monkeys (*Macaca fascicularis*, 3–7 kg). The injections were aimed at areas PEc and PE, located in the superior parietal lobule (Fig. 1A), based on sulcal morphology. The attribution of each injection site to specific areas was based on postmortem analysis of cyto- and myeloarchitectural material following previously defined criteria (Bakola et al., 2010, 2013; Luppino et al., 2005).

Figure 1B illustrates the extent and location of the injection sites relative to histological boundaries of cortical areas, projected onto a flat map reconstruction of a reference macaque brain obtained with the software CARET (Van Essen et al., 2001). For each injection, Figure 1B and C shows both the core of the injection (black spot) and the halo zone (colored region around the core). Three of the injections were within the limits of area PEc, and six were within area PE. In other cases, as shown in Figure 1B, the injection sites crossed the boundary between the PE and PEc (two injections), or the boundary between one of these and an adjacent area (two injections). Finally, one of the injection sites was entirely confined within rostral parie-

tal area 2. Table 1 presents details of individual injections.

Full details of the surgical procedures have been described previously (Bakola et al., 2010, 2013; Galletti et al., 2001). Briefly, in all animals the target region was visualized during surgery under aseptic conditions. The animals were pretreated with atropine (0.05 mg/kg, i.m.) and anesthetized with ketamine hydrochloride (12 mg/kg, i.m.) followed, after 30 minutes, with sodium thiopental (8 mg/kg, i.v. with supplemental doses as required). To avoid edema, mannitol was administered intravenously (1 g/kg). The animals were secured to a stereotaxic frame and, after craniotomy, the superior parietal lobule was exposed and the dura mater retracted. Neuronal tracers were injected through a Hamilton microsyringe that had been fitted with a glass micropipette attached to the needle. The tracers Fast Blue (FB) and Diamidino Yellow (DY) were directly applied as crystals by visual inspection of the exposed cortex (Rosa and Tweedale, 2005). At the end of the surgery, the exposed cortex was covered with surgical foam. The bone was replaced, and the dura mater and the wound were sutured. Analgesics (Ketorolac, 1 mg/kg, i.m., for 2–3 consecutive days) and antibiotics (erythromycin, 1–1.5 ml/10 kg) were administered postoperatively. In all cases, the veterinary staff of the University of Bologna monitored physiological parameters during surgery, as well as the animal's recovery in subsequent days.

Histological procedures

After a variable survival period (14 days for fluorescent tracers, and 2 days for wheat germ agglutinin-

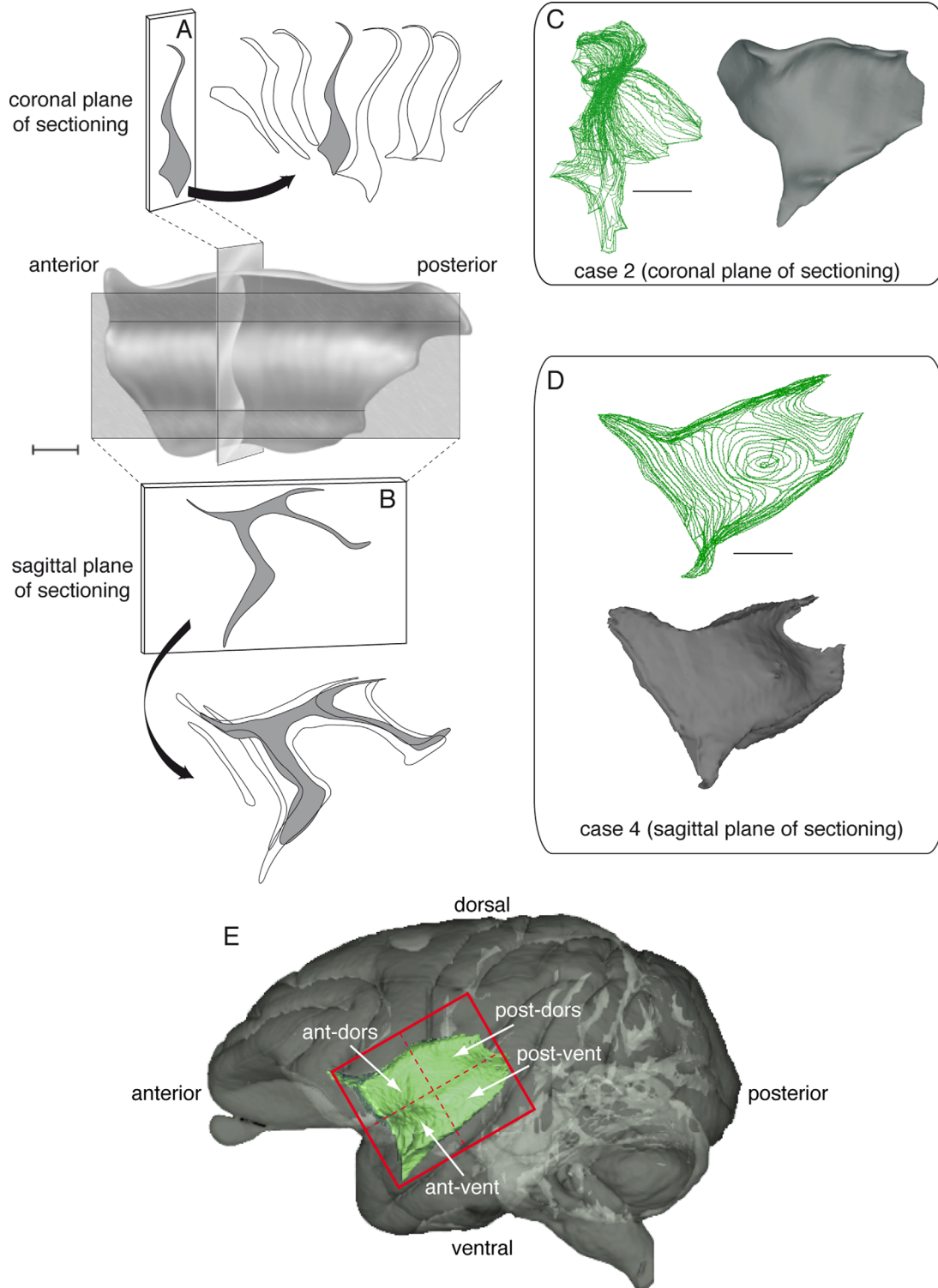


Figure 2. Anatomy of the claustrum. **A,B:** Illustration of the sheet-like structure of the claustrum of a young squirrel monkey (modified from Fig. 1 of Crick and Koch, 2005). The insets show single coronal (A) and sagittal (B) sections. **C,D:** Green outlines: claustrum contours in a case sectioned in the coronal plane and another sectioned in the parasagittal plane, respectively. The gray volumes represent 3D reconstructions of the lateral surface of the claustrum, prepared using the software CARET. **E:** Lateral view of the left hemisphere of a macaque brain showing (in green) the approximate anatomical location and shape of the claustrum (from BrainInfo: <http://braininfo.rprc.washington.edu/TemplateNeuroMaps.aspx>). The red rectangle illustrates the anatomical quadrants used for the present analysis. Abbreviations: ant-dors: anterior-dorsal; ant-vent: anterior-ventral; post-dors: posterior-dorsal; post-vent: posterior-ventral. Scale bar = 1.2 mm in A; 5 mm in C,D.

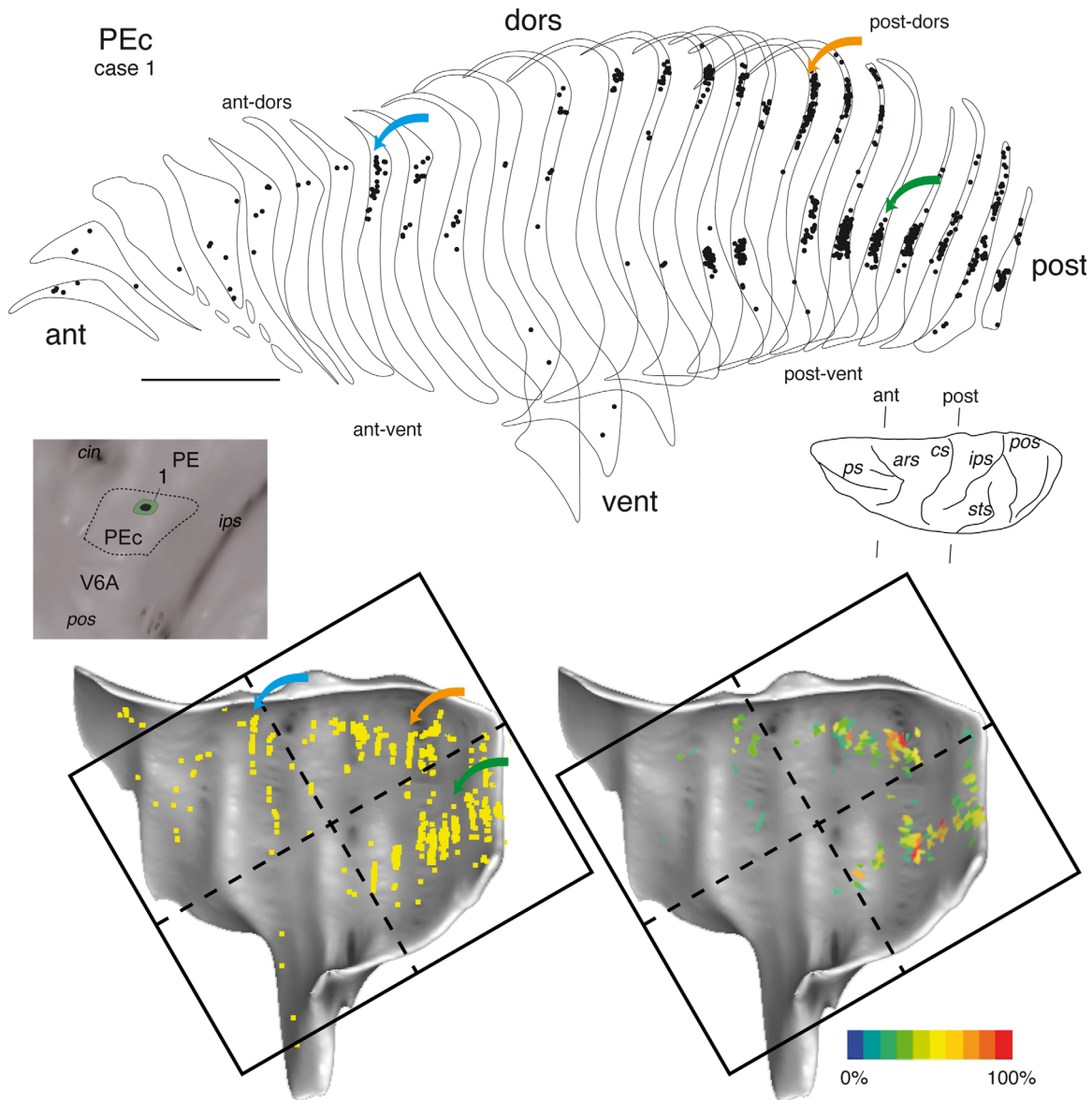


Figure 3. Distribution of retrogradely labeled cells after injection in area PEc (case 1). **Top:** Outlines of the claustrum in this brain, which was sectioned in the coronal plane. Locations of single-labeled neurons are shown as black circles, and colored arrows point to patches in the sections. Corresponding places are shown in the 3D reconstruction (blue in the ant-dors quadrant, orange in the post-dors quadrant, and green in the post-vent quadrant). The insert on the left shows the location of the injection site. **Bottom:** Lateral views of 3D reconstructions of the claustrum, illustrating the distribution (left) and density (right) of labeled cells. Color scale indicates the relative density of labeled cells, counted within $300 \times 300 \mu\text{m}$ units, as a percentage of the maximum value. In this and other figures the claustrum is represented with the anterior end at the left, irrespective of the hemisphere injected, to facilitate comparisons. Abbreviations: ant-, anterior; dors-, dorsal; post-, posterior; vent-, ventral. Other details and abbreviations as in Figure 1. Scale bar = 5 mm at top.

horseradish peroxidase [WGA-HRP]), the animals were treated with ketamine hydrochloride (15 mg/kg, i.m.). Following loss of consciousness, they received a lethal dose of sodium thiopental (i.v.), and, upon cardiac arrest, were perfused with 3 liters of normal saline solution, followed by 5 liters of 4% paraformaldehyde in 0.1 M phosphate buffer at pH 7.4 (3.5% in the case of the WGA-HRP injection), and 4 liters of 5% glycerol in the same buffer. The brains were removed from the skulls,

photographed from all views, and cryoprotected by immersion in 0.1 M phosphate buffer solutions containing glycerol (10% and 20%; all cases). The brains were then snap-frozen and stored at -80°C . Sections ($60 \mu\text{m}$) were obtained using a freezing microtome. In most cases the brain was sectioned in parasagittal plane. The preference for the sagittal plane was dictated by the need to determine the histological boundaries of the PEc, the PE, and area 2, which are best visualized

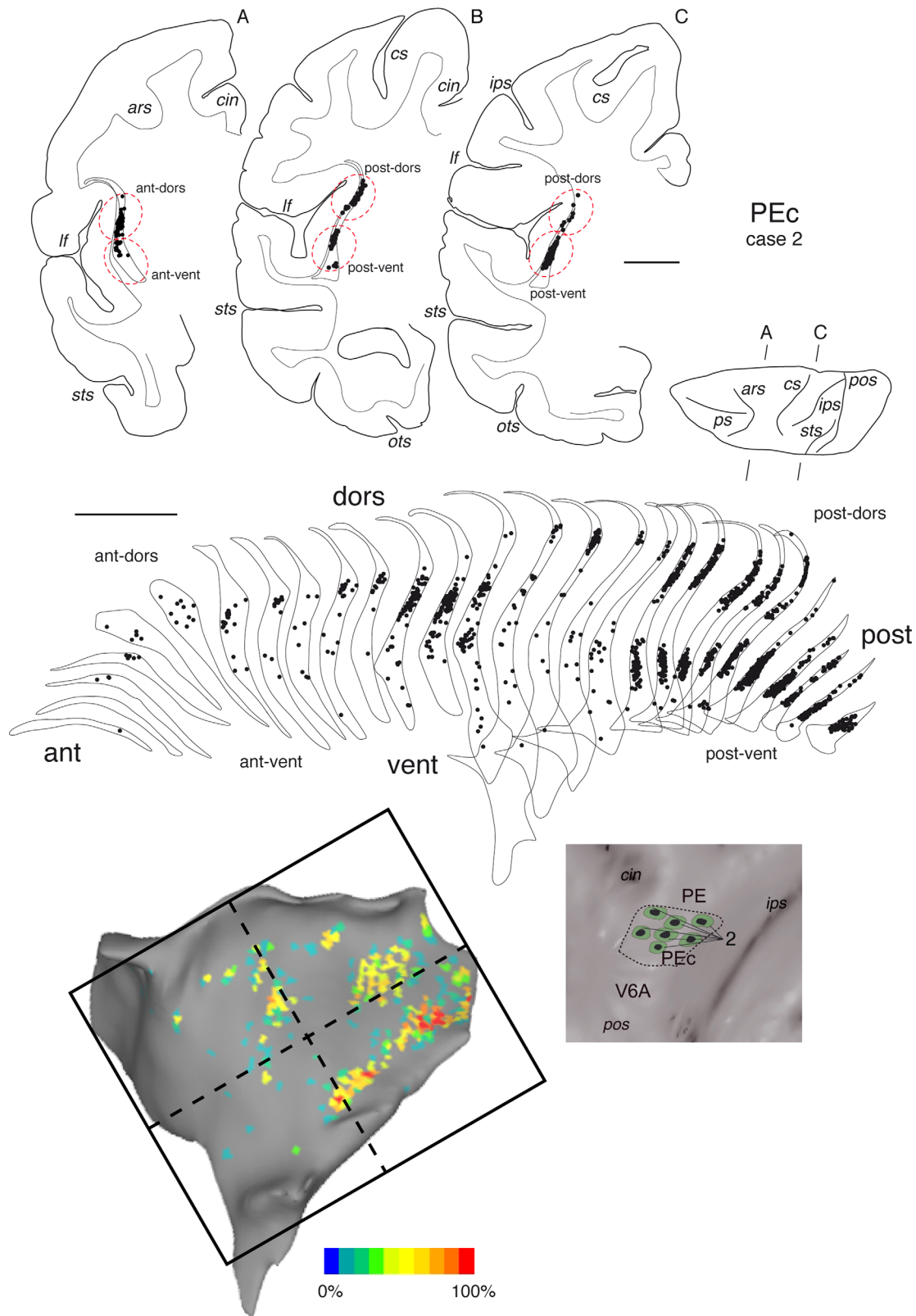


Figure 4. Distribution of retrogradely labeled cells after injection in area PEc (case 2). **Top:** Coronal sections at the levels indicated on a dorsal view of the brain. Labeled cells are represented as black dots. Dashed red ovals indicate labeled cells attributed to different claustral quadrants. **Center:** Set of claustrum contours. **Bottom:** 3D reconstruction illustrating the density of labeled neurons (left) and the location of injection sites (right). Abbreviation: ots, occipitotemporal sulcus. Other details and abbreviations as in Figures 1–3. Scale bar = 5 mm at top.

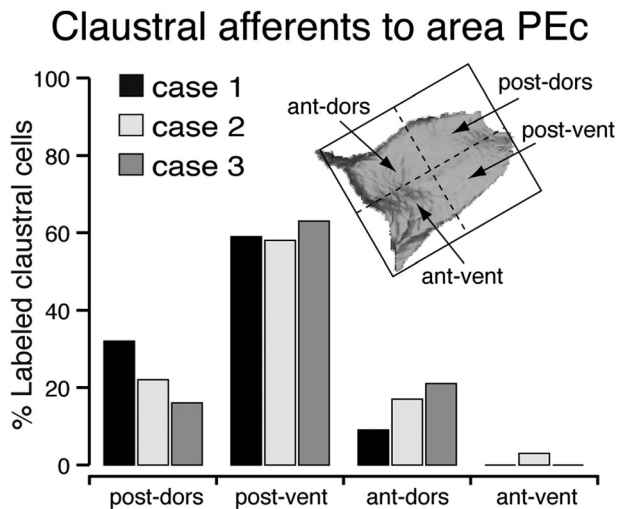


Figure 5. Percentage of labeled cells in the four quadrants of the claustrum after injections confined within the cytoarchitectonic limits of area PEc.

in this plane of section. Five series of sections were obtained, one of which was always stained for Nissl substance and another for myelin (Gallyas, 1979). The other series were left unstained for fluorescence observation, or processed to reveal WGA–HRP using the tetramethylbenzidine method (Mesulam and Rosene, 1979). All sections were coverslipped with DPX after quick steps of dehydration in 100% ethanol, and cleared with xylene.

Data analysis

The sections were examined for labeled neurons using a microscope (Zeiss Axioscope) equipped with 10× and 20× objectives. In each case, the entire hemisphere ipsilateral to the injection site was examined for retrograde label. Although anterograde label from some of the injections was visualized, only the retrograde label has been quantified for the purposes of the present report. The section outlines and location of labeled neurons were plotted at 600 μm intervals, using a computerized system linked to X/Y transducers mounted on the microscope stage.

The histological criteria used for the definition of the boundaries of areas around the injection sites have been fully described in previous studies (Bakola et al., 2010, 2013; Galletti et al., 2001; Luppino et al., 2005). The present report focuses on injections that were found to be confined to a single architectonic area, although data from injections that crossed areal boundaries have been used as comparison and/or confirmation of particular aspects of the data, as detailed in the Results section.

The limits of the claustrum were plotted together with the external (pial) and internal (gray/white matter boundaries) contours of each histological section stained with the Nissl protocol at 300 μm intervals. To define the labeled region of the claustrum, a camera lucida attachment was used to bring stained histological sections into register with the corresponding drawings.

Figure 2 shows examples of 3D reconstructions of the claustrum in cases cut in coronal (A and C) or sagittal (B and D) planes. The 3D reconstructions of the claustrum shown in Figures 2C and D were obtained from section contours with CARET software (Van Essen et al., 2001), according to the procedures described previously (Galletti et al., 2005; Gamberini et al., 2009). We used the midthickness contours of the cortical gray matter to align brain sections, to reconstruct the brain shape in each case. Adjustments were applied to the contours of the claustrum only in specific cases, to improve local alignment. CARET tools allowed us to display individual labeled neurons in the claustrum reconstructions (Galletti et al., 2005), or to prepare labeled neuron density maps (Bakola et al., 2010; Passarelli et al., 2011) in 300 × 300 μm area units superimposed on a lateral view of the claustrum. The area unit that contained the highest number of labeled neurons was considered as reference, and the density of neurons was expressed as a percentage of this maximum unit value (Rosa et al., 2009). To facilitate the comparison between cases, claustral representations will always be represented as the left hemisphere observed from the lateral surface (Fig. 2E).

For regional analysis of the location of labeled cells, we followed a subdivision similar to that proposed by Pearson and colleagues (1982). The shape of the reconstructed claustrum was fitted into a rectangle tilted 30° counterclockwise from horizontal when aligned according to stereotaxic coordinates (see red rectangle in Fig. 2E). This rectangle was subdivided into four quadrants of equal size (dashed red lines in Fig. 2E). The exact aspect ratio of the rectangle was adjusted according to the shape of the reconstructed claustrum in different cases. Analysis of the location of labeled neurons was then performed with reference to the posterior–ventral (post-vent), posterior–dorsal (post-dors), anterior–ventral (ant-vent), and anterior–dorsal (ant-dors) quadrants.

RESULTS

Here we report the results of tracer injections in areas PEc and PE in eight hemispheres of six animals, together with one injection in area 2 (details in Table 1). Data from an injection that involved both area PE

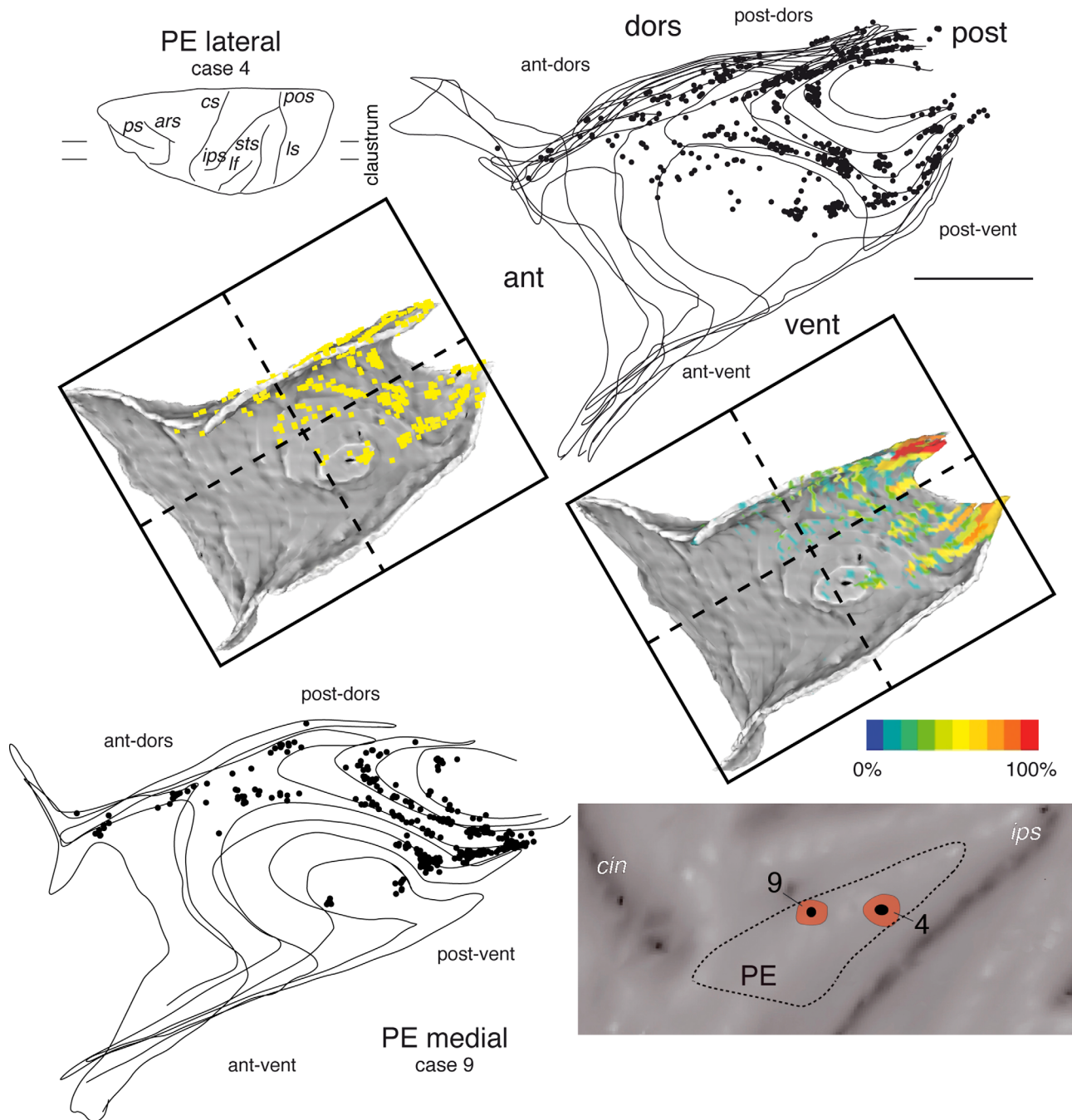


Figure 6. Distribution of retrogradely labeled cells after two injections in area PE (two cases within the cytoarchitectonic limits of area PE). **Top:** Case 4. **Bottom left:** Case 9. For both cases a set of superimposed claustrum contours in parasagittal sections is illustrated, as well as the locations of labeled neurons (black circles). **Center:** 3D reconstructions of the distribution and density of labeled cells in the claustrum. **Bottom right:** The location of the injection sites. Other details and abbreviations as in Figures 1–3. Scale bar = 5 mm at top right.

and area 2 will be discussed only briefly. In all cases, we found that neurons in the claustrum represented only a small fraction of the total number of those labeled by the tracer across the brain (PEc, mean = $5.0 \pm 3.3\%$; PE, mean = $4.1 \pm 4.1\%$; area 2, 6.2%).

Claustral afferents of areas PEc and PE

Figures 3 and 4 show two cases of claustral projections to area PEc. In case 1 (Fig. 3), the retrograde tracer FB was injected at a single site, in the anterior part of the PEc (see inset at the left part of Fig. 3, case

1). In case 2 (Fig. 4), the tracer DY was injected in multiple sites, which collectively encompassed nearly the entire extent of area PEc (see inset at the bottom right part of Fig. 4). Despite the difference in the extent of injection sites, the distribution of labeled neurons in the claustrum was similar in both cases.

In case 1, visual inspection of coronal sections (Fig. 3, top) revealed that the majority of label in the claustrum formed three patches, two located posteriorly (in the ventral and dorsal parts of the claustrum), and one at an anterior–dorsal location. The 3D reconstruction and density map, generated by the software CARET (Fig. 3, bottom), confirmed the wide distribution of labeled cells, mainly in the posterior half of the claustrum. In case 2 (Fig. 4) the same three patches of labeled cells were clearly evident in coronal sections (top), with the densest label being located in the posterior–ventral part of the structure (see density map, Fig. 4 bottom). Data from a third case with one injection in the PEc (not illustrated) reproduced the above findings. Figure 5 summarizes the quantitative analysis of the three cases in which tracer deposits were entirely confined within the cytoarchitectural limits of area PEc.

Figure 6 shows the claustral afferents in two cases with injections within area PE (locations shown in Fig. 6, bottom right). One injection was in the lateral part of area PE (case 4, Fig. 6, top), and one in the medial part of the area (case 9, Fig. 6, bottom left). Although the topographic organization of projection neurons was similar to that seen in the projection to area PEc, patches were not as clear as in PEc injection cases, perhaps due to the use of parasagittal sections. The distribution of label, in terms of quadrants of the claustrum, was quite similar to that observed after PEc injections (compare Figs. 5 and 7).

Figure 2A, together with the 3D reconstructions in Figures 3 and 4, shows that the typical sheet of gray matter that forms the claustrum curves laterally for few millimeters in the most dorsal part of the structure, to follow the curvature of the dorsal insular cortex. This very dorsal region of the claustrum was free of labeling after PEc injections (Figs. 3 and 4), but was labeled after PE injections, particularly in its posterior half (Fig. 6).

Claustal afferents of area 2

One of our injections was placed in area 2. Figure 8 shows the location of labeled neurons in the claustrum after this injection (case 10). The comparison of the patterns of claustrum afferents after area 2 and PE injections is facilitated by the fact that the same hemisphere received one injection in area PE (case 4, Fig. 6) and one injection in area 2 (case 10).

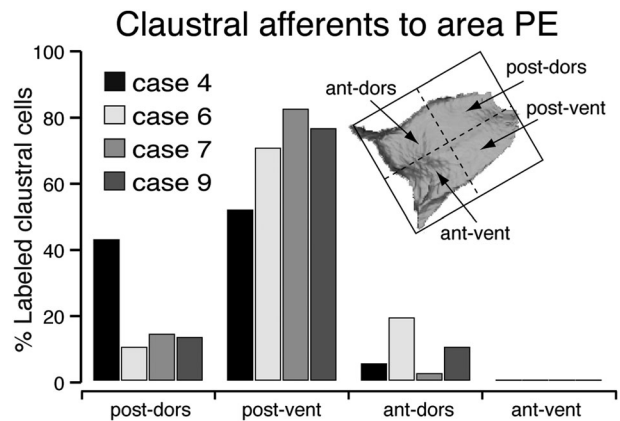


Figure 7. Percentage of labeled cells in the four quadrants of the claustrum after injections confined within the cytoarchitectonic limits of area PE.

The distribution of projection neurons was different from those observed following injections in areas PEc and PE, with concentrations of label in the posterior–dorsal and anterior–dorsal quadrants of the claustrum, and fewer labeled neurons in the posterior–ventral quadrant (compare Figs. 7 and 8). Indeed, the dorsal part of the claustrum was fully labeled, in both the posterior and anterior portions of this structure (see reconstruction in the bottom left panels of Fig. 8). The part of the dorsal claustrum that bends laterally to follow the dorsal bank of the lateral fissure was heavily labeled throughout its extent (see parasagittal section shown in Fig. 8C, and the dorsal view of the 3D reconstruction). The strong involvement of this sector of the claustrum in projections to area 2 was confirmed in another case (case 14) in which the injection sites involved both area 2 and area PE (Fig. 9).

DISCUSSION

The aim of this study was to examine the distribution of claustral afferents to cortical areas of the caudal part of the superior parietal lobule, namely, areas PEc and PE. We found that the common territory of origin of projections to areas PE and PEc includes a large fraction of the claustrum, but essentially spares the anterior–ventral part of this structure. As summarized in Figure 10A, most claustral projections to areas PEc and PE originate in the posterior–ventral part of the structure (60–70% of labeled neurons), followed by the posterior–dorsal (~ 20%), and anterior–dorsal (10–20%) parts. The posterior part of the claustrum is known to be mainly concerned with sensory information (visual and somatic) (Olson and Graybiel, 1980; Pearson et al., 1982), while the anterior–dorsal part is known to be

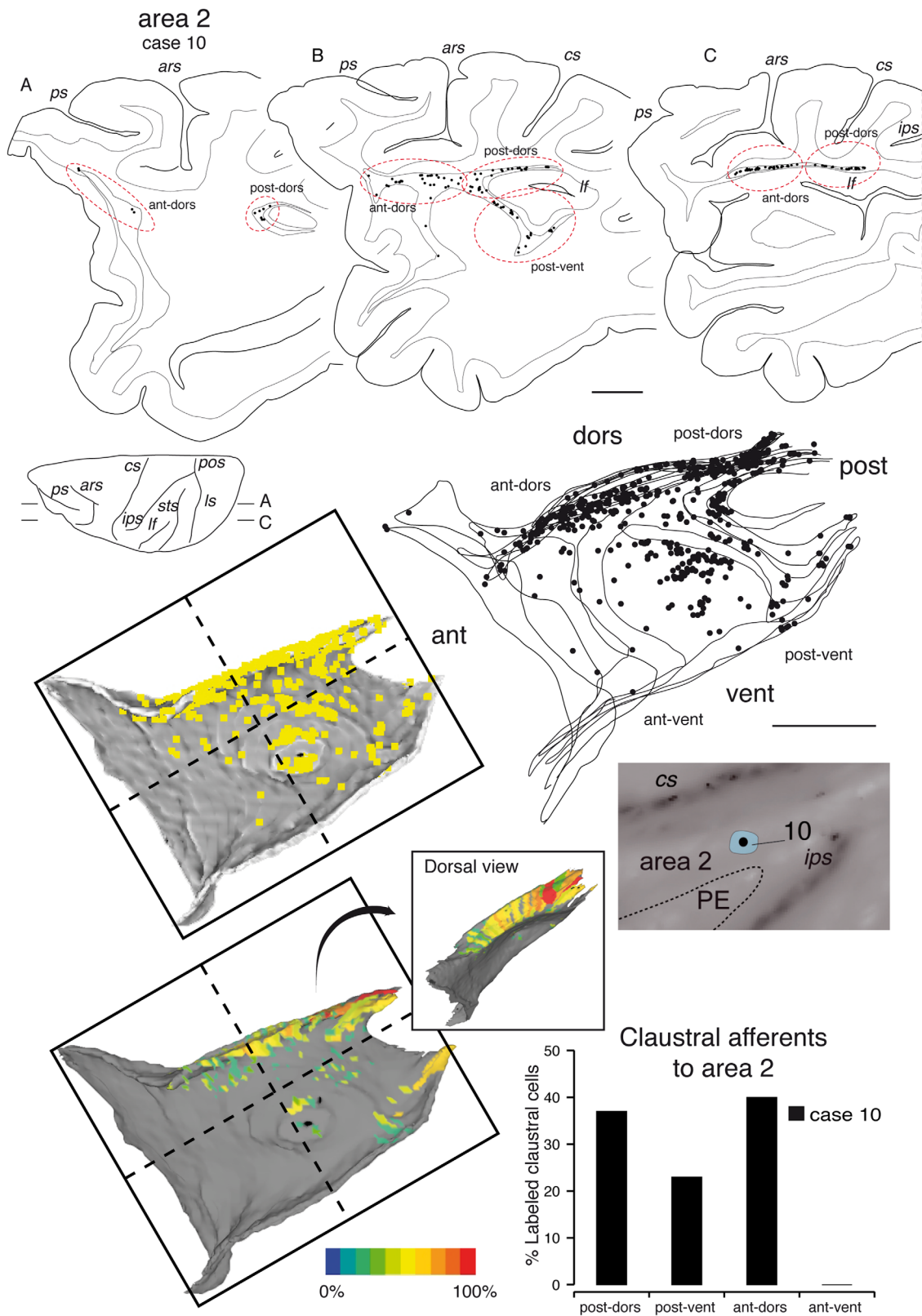
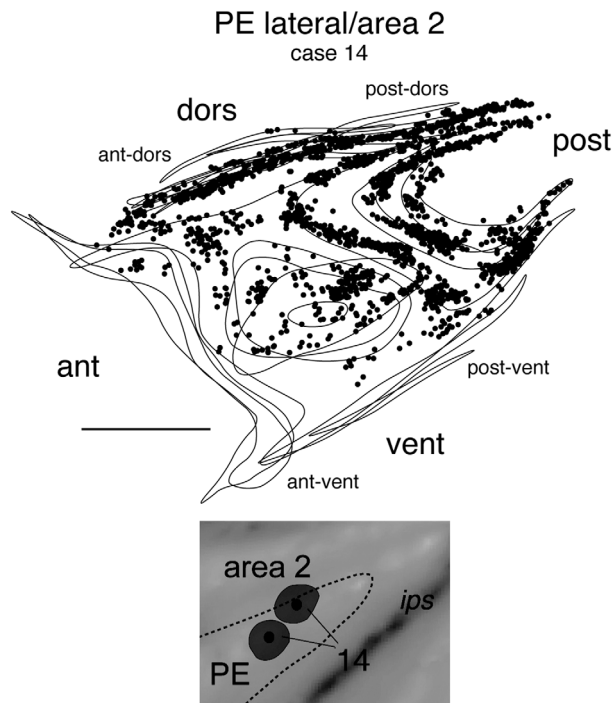


Figure 8. Distribution of retrogradely labeled cells after an injection in area 2 (case 10). **Top:** Parasagittal sections (A-C) at the levels indicated on a dorsal view of the brain. **Center right:** Set of claustrum contours with the locations of labeled neurons represented as black dots. **Bottom left:** 3D reconstruction illustrating the location and density of labeled neurons in lateral view, and dorsal view (insert). **Bottom right:** The location of the injection site and percentages of labeled neurons in different quadrants of the claustrum. Other details and abbreviations as in Figures 1-4. Scale bars = 5 mm at top.



Claustral afferents to PE & area 2

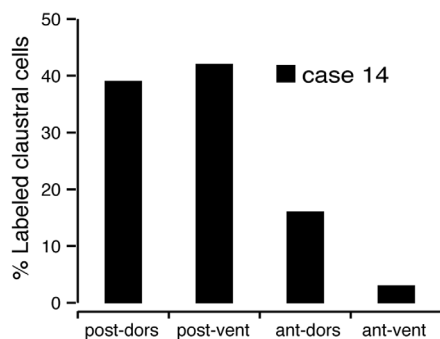


Figure 9. Claustral distribution of retrograde-labeled cells after a case in which tracer was injected at two adjacent sites, which collectively crossed the boundary between area PE and area 2 (case 14). For conventions, see Figure 8. Scale bar = 5 mm at top.

connected to the somatomotor cortex (present results; Pearson et al., 1982; Minciacchi et al., 1991; Mathur, 2014). By comparison, the anterior-ventral portion of the claustrum, which is not connected with any of the areas considered in the present study, has been reported to form strong connections with the granular prefrontal cortex (Reser et al., 2013).

The considerable overlap of claustral labeling after injections in different parietal areas (PEc, PE, area 2) is not surprising. Pearson and colleagues (1982) reported that a similar degree of overlap may be found after injections of two widely separated, but interconnected areas, referring to cortical areas located in parietal and

frontal lobes. Here we show that neighboring cytoarchitectural subdivisions of the parietal lobe, which are strongly and reciprocally interconnected (Bakola et al., 2010, 2013; Pons and Kaas, 1986) show a similar degree of overlap. This supports the idea that one cortical area may influence another, not only through the association cortical fibers, but also through the claustrum (Pearson et al., 1982).

As shown by comparison of panels C and D in Figure 10, our observations are in good agreement with those of Pearson et al. (1982) in other respects. Neurons forming projections to area 2 (part of the S1 complex) were concentrated along the entire dorsal limit of the claustrum, while those projecting to areas PE and PEc (parts of area 5; Pandya and Seltzer, 1982) were, on average, shifted caudally and ventrally. Furthermore, the claustral territories projecting to areas PE and PEc appear to partially overlap with those projecting to frontal motor and premotor areas (Tanné-Gariépy et al., 2002). Although the origins of claustral afferents to areas PEc and PE overlapped in the posterior-ventral quadrant of the claustrum, the strongest foci of label appear to occupy somewhat different regions. In particular, the origins of afferent projections to area PEc seem to extend further into the “visual” sector of the claustrum (i.e., regions that have been demonstrated to project to the extrastriate cortex; Maioli et al., 1983; Gattass et al., 2014; Fig. 10E,F), in comparison with those to area PE. These data agree well with a primarily somatosensory nature of area PE and a bimodal visual and somatosensory nature of area PEc (Breveglieri et al., 2006, 2008). On a historical note, based on cytoarchitecture, Brodmann (1909) originally considered the territory currently assigned to area PEc to be part of the area 7 complex, while the current area PE was assigned to area 5. The spatial shift in the origin of claustral projections to the PE and PEc shown in Figure 10C can be related to that described by Pearson et al. (1982), for the projections to areas 5 and 7, although modern visualization techniques allow a better appreciation of the patchy nature of the projections, and the gradual nature of the spatial shift.

According to Gattass et al. (2014), the claustrum can be subdivided into four sectors according to projections to the occipital, parietal, temporal, and frontal lobes (Fig. 10F, right). Our data do not agree with this summary, because many of the afferents to posterior parietal areas PE and PEc originate from a claustral region that has been assigned to the occipital lobe, rather than the parietal lobe (compare Figs. 10C and F). In fact, one way in which our data extend those of many previous studies is by emphasizing the complexity of the spatial distribution of projection neurons. Rather

Average percentage of labeled cells to areas PEc-PE-2

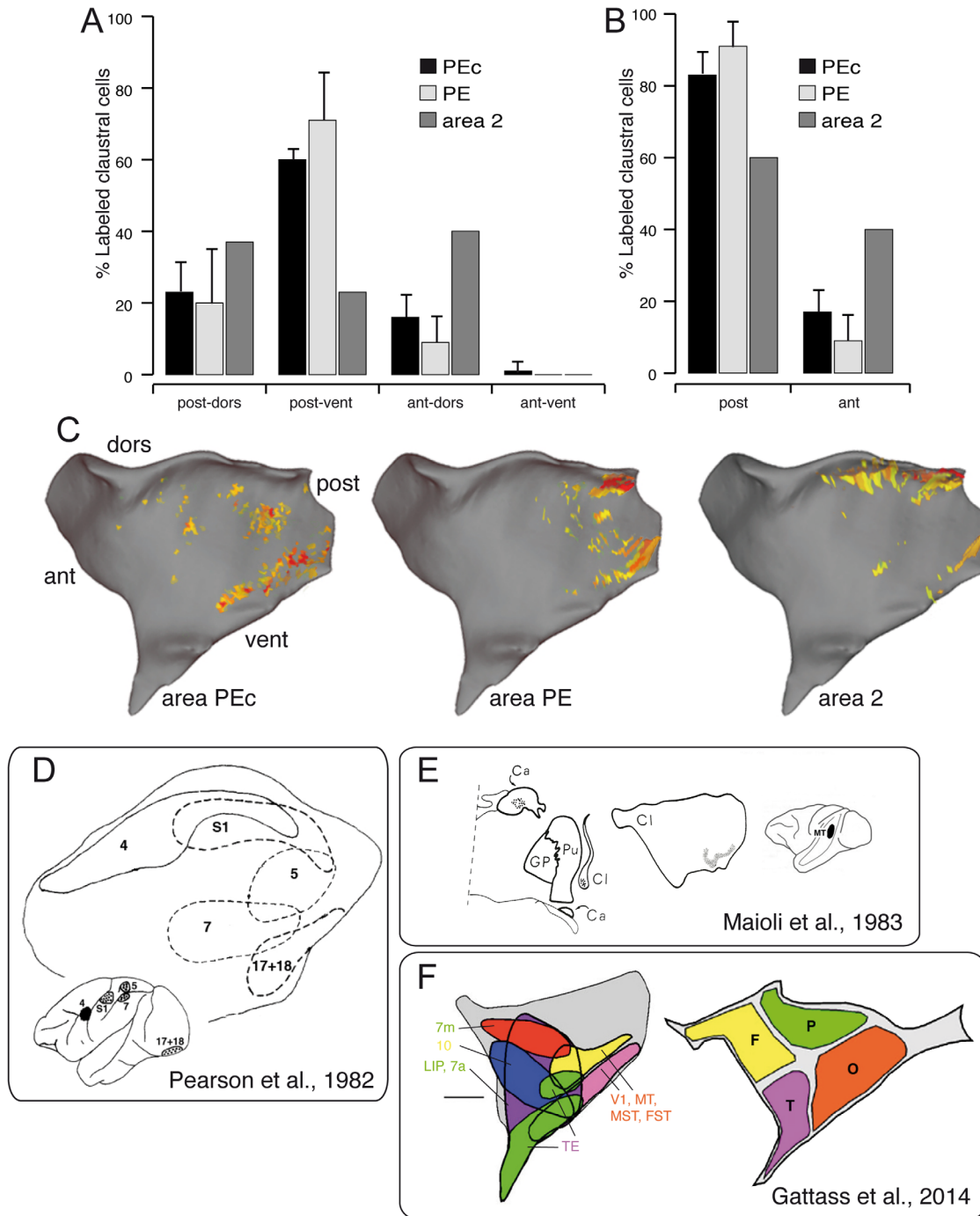


Figure 10. Summary and comparison with previous studies. **A:** Percentages of labeled cells in different quadrants of the claustrum after tracer injections in area PEc (three cases, mean \pm SD), PE (four cases, mean \pm SD), and area 2 (one case). **B:** Graph highlighting the predominance of label in the posterior part of the claustrum following injections in areas PE and PEc, and the more balanced distribution following injection in area 2. **C:** Average distributions of labeled cells following injections in the three areas, following morphing of individual reconstructions to a standard representation of the claustrum (based on case 2 of the present sample). Although there is wide overlap between the distributions of cells projecting to different targets, there is a gradual shift from ventral, to posterior, to dorsal locations as one considers the results of injections in areas PEc, PE and 2. **D–F:** Comparable lateral reconstructions of the claustrum modified from previous studies, shown in comparable orientation. Scale bar = 4 mm in F.

than conforming to some simple topographic rule, these neurons form multiple patches of origin separated by significant gaps, across relatively large territories of the claustrum.

Because the claustrum appears to be connected to the whole cortex, Crick and Koch (2005) hypothesized that it is the structure where sensory information is bound, functioning as a generator of the unified perception of a multitude of sensory stimuli. According to this view, the role of the claustrum would be important to rapidly integrate and bind information between neurons that are located across distinct cortical and thalamic regions. The present results appear to be compatible with this view. The spatially diffuse nature of the claustrorocortical projections also seems compatible with the proposal recently advanced by Reser and coworkers (2014) that the claustrum promotes the “switch” between different cortical networks, as the “default” resting state network and task-specific networks. In both these cases, specific cortical areas with distinct functional properties and architectural characteristics would need to receive afferents from large, overlapping portions of claustrum to allow recombination and redistribution of information according to behavioral demands.

ACKNOWLEDGMENTS

The authors thank M. Verdosci, F. Campisi, and G. Placenti for technical assistance.

CONFLICT OF INTEREST STATEMENT

The authors declare that they have no conflicts of interest.

ROLE OF AUTHORS

All authors had full access to all the data in the study and take responsibility for the integrity of the data and the accuracy of the data analysis. Study concept and design: MG, CG, PF. Acquisition of data: MG, LP, SB, DI, MR. Analysis and interpretation of data: MG, CG. Drafting of the manuscript: MG, CG, PF, MR. Critical revision of the manuscript for important intellectual content: MR, LP, SB. Obtained funding: CG, PF, SB, MR. Administrative, technical, and material support: LP, DI. Study supervision: MG, CG, PF.

LITERATURE CITED

Baizer JS, Desimone R, Ungerleider LG. 1993. Comparison of subcortical connections of inferior temporal and posterior parietal cortex in monkeys. *Vis Neurosci* 10:59–72.
Baizer JS, Sherwood CC, Noonan M, Hof PR. 2014. Comparative organization of the claustrum: what does structure tell us about function? *Front Syst Neurosci* 8:117.

Bakola S, Gamberini M, Passarelli L, Fattori P, Galletti C. 2010. Cortical connections of parietal field PEc in the macaque: linking vision and somatic sensation for the control of limb action. *Cereb Cortex* 20:2592–2604.
Bakola S, Passarelli L, Gamberini M, Fattori P, Galletti C. 2013. Cortical connectivity suggests a role in limb coordination for macaque area PE of the superior parietal cortex. *J Neurosci* 33:6648–6658.
Batista AP, Buneo CA, Snyder LH, Andersen RA. 1999. Reach plans in eye-centered coordinates. *Science* 285:257–260.
Battaglia-Mayer A, Ferraina S, Genovesio A, Marconi B, Squatrito S, Molinari M, Lacquaniti F, Caminiti R. 2001. Eye-hand coordination during reaching. II. An analysis of the relationships between visuomanual signals in parietal cortex and parieto-frontal association projections. *Cereb Cortex* 11:528–544.
Bremner LR, Andersen RA. 2012. Coding of the reach vector in parietal area 5d. *Neuron* 75:342–351.
Breveglieri R, Galletti C, Gamberini M, Passarelli L, Fattori P. 2006. Somatosensory cells in area PEc of macaque posterior parietal cortex. *J Neurosci* 26:3679–3684. Erratum in: *J Neurosci* 2006;26:4452.
Breveglieri R, Galletti C, Monaco S, Fattori P. 2008. Visual, somatosensory, and bimodal activities in the macaque parietal area PEc. *Cereb Cortex* 18:806–816.
Brodmann K. 1909. *Vergleichende Localisationslehre der Grosshirnrinde in Ihren Prinzipien Dargestellt auf Grund des Zellenbaues*. Leipzig: Barth JA.
Burbaud P, Doegle C, Gross C, Bioulac B. 1991. A quantitative study of neuronal discharge in areas 5, 2, and 4 of the monkey during fast arm movements. *J Neurophysiol* 66:429–443.
Burman KJ, Reser DH, Richardson KE, Gaulke H, Worthy KH, Rosa MGP. 2011. Subcortical projections to the frontal pole in the marmoset monkey. *Eur J Neurosci* 34:303–319.
Carman JB, Cowan WM, Powell TP. 1964. The cortical projection upon the claustrum. *J Neurol Neurosurg Psychiatry* 27:46–51.
Chadzypanagiotis D, Narkiewicz O. 1971. Connections of the visual cortex with the claustrum. *Acta Neurobiol Exp (Wars)* 31:291–311.
Crick FC, Koch C. 2005. What is the function of the claustrum? *Philos Trans R Soc Lond B Biol Sci* 360:1271–1279.
Druga R. 1968. Cortico-claustral connections. II. Connections from the parietal, temporal and occipital cortex to the claustrum. *Folia Morphol (Praha)* 16:142–149.
Duffy FH, Burchfiel JL. 1971. Somatosensory system: organizational hierarchy from single units in monkey area 5. *Science* 172:273–275.
Ettlinger G, Wilson WA. 1990. Cross-modal performance: behavioural processes, phylogenetic considerations and neural mechanisms. *Behav Brain Res* 40:169–192.
Ferraina S, Bianchi L. 1994. Posterior parietal cortex: functional properties of neurons in area 5 during an instructed-delay reaching task within different parts of space. *Exp Brain Res* 99:175–178.
Ferraina S, Battaglia-Mayer A, Genovesio A, Marconi B, Onorati P, Caminiti R. 2001. Early coding of visuomanual coordination during reaching in parietal area PEc. *J Neurophysiol* 85:462–467.
Galletti C, Gamberini M, Kutz DF, Fattori P, Luppino G, Matelli M. 2001. The cortical connections of area V6: an occipito-parietal network processing visual information. *Eur J Neurosci* 13:1572–1588.
Galletti C, Gamberini M, Kutz DF, Baldinotti I, Fattori P. 2005. The relationship between V6 and PO in macaque extrastriate cortex. *Eur J Neurosci* 21:959–970.

- Gallyas F. 1979. Silver staining of myelin by means of physical development. *Neurol Res* 1:203–209.
- Gamberini M, Passarelli L, Fattori P, Zucchelli M, Bakola S, Luppino G, Galletti C. 2009. Cortical connections of the visuomotor parietooccipital area V6Ad of the macaque monkey. *J Comp Neurol* 513:622–642.
- Gattass R, Soares JG, Desimone R, Ungerleider LG. 2014. Connectional subdivision of the claustrum: two visuotopic subdivisions in the macaque. *Front Syst Neurosci* 8:63.
- Hadjidimitrakis K, Dal Bo' G, Breveglieri R, Galletti C, Fattori P. 2015. Overlapping representations for reach depth and direction in caudal superior parietal lobule of macaques. *J Neurophysiol* 114:2340–2352.
- Kalaska JF. 1996. Parietal cortex area 5 and visuomotor behavior. *Can J Physiol Pharmacol* 74:483–498.
- Kemp JM, Powell TP. 1970. The cortico-striate projection in the monkey. *Brain* 93:525–546.
- Lacquaniti F, Guigon E, Bianchi L, Ferraina S, Caminiti R. 1995. Representing spatial information for limb movement: role of area 5 in the monkey. *Cereb Cortex* 5:391–409.
- Luppino G, Hamed SB, Gamberini M, Matelli M, Galletti C. 2005. Occipital (V6) and parietal (V6A) areas in the anterior wall of the parieto-occipital sulcus of the macaque: a cytoarchitectonic study. *Eur J Neurosci* 21:3056–3076.
- Maioli MG, Squatrito S, Battaglini PP, Rossi R, Galletti C. 1983. Projections from the visual cortical region of the superior temporal sulcus to the striatum and claustrum in the macaque monkey. *Arch Ital Biol* 121:259–266.
- Mathur BN. 2014. The claustrum in review. *Front Syst Neurosci* 8:48.
- Mesulam MM, Rosene DL. 1979. Sensitivity in horseradish peroxidase neurohistochemistry: a comparative and quantitative study of nine methods. *J Histochem Cytochem* 27:763–773.
- Milardi D, Bramanti P, Milazzo C, Finocchio G, Arrigo A, Santoro G, Trimarchi F, Quartarone A, Anastasi G, Gaeta M. 2015. Cortical and subcortical connections of the human claustrum revealed in vivo by constrained spherical deconvolution tractography. *Cereb Cortex* 25:406–414.
- Minciocchi D, Granato A, Barbaresi P. 1991. Organization of claustrum-cortical projections to the primary somatosensory area of primates. *Brain Res* 553:309–312.
- Mountcastle VB, Lynch JC, Georgopoulos A, Sakata H, Acuña C. 1975. Posterior parietal association cortex of the monkey: command function for operations within extrapersonal space. *J Neurophysiol* 38:871–908.
- Olson CR, Graybiel AM. 1980. Sensory maps in the claustrum of the cat. *Nature* 288:479–481.
- Padberg J, Franca JG, Cooke DF, Soares JG, Rosa MG, Fiorani Jr. M, Gattass R, Krubitzer L. 2007. Parallel evolution of cortical areas involved in skilled hand use. *J Neurosci* 27:10106–10115.
- Pandya DN, Seltzer B. 1982. Intrinsic connections and architectonics of posterior parietal cortex in the rhesus monkey. *J Comp Neurol* 204:196–210.
- Passarelli L, Rosa MG, Gamberini M, Bakola S, Burman KJ, Fattori P, Galletti C. 2011. Cortical connections of area V6Av in the macaque: a visual-input node to the eye/hand coordination system. *J Neurosci* 31:1790–17801.
- Pearson RC, Brodal P, Gatter KC, Powell TP. 1982. The organization of the connections between the cortex and the claustrum in the monkey. *Brain Res* 234:435–441.
- Piserchia V, Breveglieri R, Hadjidimitrakis K, Bertozzi F, Galletti C, Fattori P. 2016. Mixed body/hand reference frame for reaching in 3D space in macaque parietal area PEc. *Cereb Cortex*. Mar 3:p:ii: bhw039.
- Pons TP, Kaas JH. 1986. Corticocortical connections of area 2 of somatosensory cortex in macaque monkeys: a correlative anatomical and electrophysiological study. *J Comp Neurol* 248:313–335.
- Reser DH, Burman KJ, Yu HH, Chaplin TA, Richardson KE, Worthy KH, Rosa MG. 2013. Contrasting patterns of cortical input to architectural subdivisions of the area 8 complex: a retrograde tracing study in marmoset monkeys. *Cereb Cortex* 23:1901–1922.
- Reser DH, Richardson KE, Montibeller MO, Zhao S, Chan JM, Soares JG, Chaplin TA, Gattass R, Rosa MG. 2014. Claustrum projections to prefrontal cortex in the capuchin monkey (*Cebus apella*). *Front Syst Neurosci* 8:123.
- Rosa MG, Tweedale R. 2005. Brain maps, great and small: lessons from comparative studies of primate visual cortical organization. *Philos Trans R Soc Lond B Biol Sci* 360:665–691.
- Rosa MG, Palmer SM, Gamberini M, Burman KJ, Yu HH, Reser DH, Bourne JA, Tweedale R, Galletti C. 2009. Connections of the dorsomedial visual area: pathways for early integration of dorsal and ventral streams in extrastriate cortex. *J Neurosci* 29:4548–4563.
- Sakata H, Takaoka Y, Kawarasaki A, Shibutani H. 1973. Somatosensory properties of neurons in superior parietal cortex (area 5) of the rhesus monkey. *Brain Res* 64:85–102.
- Shima K, Hoshi E, Tanji J. 1996. Neuronal activity in the claustrum of the monkey during performance of multiple movements. *J Neurophysiol* 76:2115–2119.
- Smythies J, Edelman L, Ramachandran V. 2012. Hypotheses relating to the function of the claustrum. *Front Integr Neurosci*. 6:53.
- Tanné-Gariepy J, Boussaoud D, Rouiller EM. 2002. Projections of the claustrum to the primary motor, premotor, and prefrontal cortices in the macaque monkey. *J Comp Neurol* 454:140–157.
- Taoka M, Toda T, Iwamura Y. 1998. Representation of the midline trunk, bilateral arms, and shoulders in the monkey postcentral somatosensory cortex. *Exp Brain Res* 123:315–22.
- Taoka M, Toda T, Iriki A, Tanaka M, Iwamura Y. 2000. Bilateral receptive field neurons in the hindlimb region of the postcentral somatosensory cortex in awake macaque monkeys. *Exp Brain Res* 134:139–146.
- Van Essen DC, Drury HA, Dickson J, Harwell J, Hanlon D, Anderson CH. 2001. An integrated software suite for surface-based analyses of cerebral cortex. *J Am Med Inform Assoc* 8:443–459.

Thalamo-cortical projections to the macaque superior parietal lobule areas PEc and PE

Daniele Impieri¹ | Michela Gamberini^{1,2} | Laretta Passarelli¹ |
Marcello G. P. Rosa^{3,4} | Claudio Galletti^{1,2}

¹Department of Pharmacy and Biotechnology, University of Bologna, Bologna 40126, Italy

²Department of Biomedical and Neuromotor Sciences, University of Bologna, Bologna 40126, Italy

³Biomedicine Discovery Institute and Department of Physiology, Monash University, Clayton, Victoria 3800, Australia

⁴Australian Research Council, Centre of Excellence for Integrative Brain Function, Monash University Node, Clayton, Victoria 3800, Australia

Correspondence

Claudio Galletti, Department of Pharmacy and Biotechnology, Piazza di Porta San Donato, 2, 40126, Bologna, Italy.
Email: claudio.galletti@unibo.it

Funding information

European Union, Grant/Award number: FP7-ICT 217077-EYESHOTS; Ministero dell'Università & della Ricerca, Italy; Fondazione del Monte di Bologna & Ravenna, Italy; National Health and Medical Research Council, Australia, Grant/Award number: 1082144; Australian Research Council, Grant/Award number: CE14010007

Abstract

The exposed surface of the superior parietal lobule in macaque brain contains two architectonically defined areas named PEc and PE. The aim of the present study is the characterization of thalamic afferents of these two areas. For this purpose, retrograde neuronal tracers were injected, or placed in crystal form, in areas PEc and PE. We found that the two areas show a similar pattern of thalamic inputs, mainly originating from Lateral Posterior (LP), Pulvinar (Pul), Ventral Posterior Lateral (VPL), and Ventral Lateral (VL) nuclei, all structures known to be involved in visual, somatosensory, and/or sensorimotor processing. Minor afferents were observed from the Centromedian/Parafascicular complex (CM/PF), Central Lateral (CL), Ventral Anterior (VA), and Medial Dorsal (MD) nuclei. LP and VL were more strongly connected to PEc than to PE, while the other main thalamic inputs to the two areas showed slight differences in strength. The part of the Pul mostly connected with areas PEc and PE was the Medial Pul. No labeled cells were found in the retinotopically organized Lateral and Inferior Pul. In the somatotopically organized VPL and VL nuclei, labeled neurons were mainly found in regions likely to correspond to the trunk and limb representations (in particular the legs). These findings are in line with the sensory-motor nature of areas PEc and PE, and with their putative functional roles, being them suggested to be involved in the preparation and control of limb interaction with the environment, and in locomotion.

KEYWORDS

connectivity, macaque, sensory-motor input, somatosensory, superior parietal lobule, thalamus, RRID: SCR_006260

1 | INTRODUCTION

In macaques, the exposed surface of the superior parietal lobule contains two cyto-architectural areas, named PEc and PE (Pandya & Seltzer, 1982), which are functionally distinct. Here we describe the

thalamic sources of projections to these areas, using fluorescent tracer injections.

Area PEc, which overlaps with the most caudal and medial part of Brodmann's area 7 (Brodmann, 1909; Luppino, Ben Hamed, Gamberini, Matelli, & Galletti, 2005; Gamberini, Fattori, & Galletti, 2015), forms an

Abbreviations: AD, Anterior Dorsal; AM, Anterior Medial; AV, Anterior Ventral; bsc, brachium of superior colliculus; Cdc, Central denso-cellularis; CL, Central Lateral; Clc, Central latocellularis; CM/PF, Centromedian/Parafascicular; Cn.Md, Centromedian; eml, External medullary lamina; ITP, Inferior thalamic peduncle; LD, Lateral Dorsal; LG, Lateral Geniculate; LP, Lateral Posterior; MD, Medial Dorsal; MDdc, Medial Dorsal, pars denso-cellularis; MDmc, Medial Dorsal, pars magnocellularis; MDmc/pc, Medial Dorsal, pars magnocellularis/parvocellularis; MDmf, Medial Dorsal, pars multiformis; MDpc, Medial Dorsal, pars parvocellularis; MGmc, Medial Geniculate, pars magnocellularis; MGpc, Medial Geniculate, pars parvocellularis; ot, optic tract; Pa, Paraventricular; Pf/PF, Parafascicular; Pg, Pregeniculate; Pul, Pulvinar; Pul.i, Pulvinar, inferior subdivision; Pul.l, Pulvinar, lateral subdivision; Pul.m, Pulvinar, medial subdivision; Pul.o, Pulvinar, oral (anterior) subdivision; R, Reticular; Re, Reuniens; Sg, Supragenulate; VA, Ventral Anterior; VAdc, Ventral Anterior, pars denso-cellularis; VAmc, Ventral Anterior, pars magnocellularis; VApc/dc, Ventral Anterior, pars parvocellularis/denso-cellularis; VL, Ventral Lateral; VLc, Ventral Lateral, pars caudalis; VLo, Ventral Lateral, pars oralis; VLps, Ventral Lateral, pars postrema; VM, Ventral Medial; VPI, Ventral Posterior Inferior; VPL, Ventral Posterior Lateral; VPLc, Ventral Posterior Lateral, pars caudalis; VPLo, Ventral Posterior Lateral, pars oralis; VPM, Ventral Posterior Medial; VPMpc, Ventral Posterior Medial, pars parvocellularis.

incomplete map of the body, principally focused on the limbs, without any evident sign of topographical organization (Breveglieri, Galletti, Gamberini, Passarelli, & Fattori, 2006; Breviglieri, Galletti, Monaco, & Fattori, 2008). PEc neurons respond to visual and tactile stimuli, as well as to passive single-joint rotations (Squatrito, Raffi, Maioli, & Battaglia-Mayer, 2001; Raffi, Squatrito, & Maioli, 2002; Breviglieri et al., 2006, 2008), and some neurons are capable of bimodal responses (Breviglieri et al., 2008). PEc neurons are also known to show arm and eye movement-related activity (Battaglia-Mayer et al., 2001; Ferraina et al., 2001; Piserchia et al., 2017), including sensitivity to the direction and depth of movement (Bhattacharyya, Musallam, & Andersen, 2009; Hadjidimitrakakis, Dal Bo, Breviglieri, Galletti, & Fattori, 2015). In contrast, area PE, which overlaps with Brodmann's area 5 (Brodmann, 1909), contains a rough topographical representation of the body, with over-representation of the arms and hands (Taoka, Toda, & Iwamura, 1998; Taoka, Toda, Iriki, Tanaka, & Iwamura, 2000; Padberg et al., 2007; Krubitzer & Disbrow, 2008; Seelke et al., 2012). PE neurons are mainly activated by proprioceptive stimulation, although some respond to tactile stimulation (Duffy & Burchfiel, 1971; Sakata, Takaoka, Kawarasaki, & Shibutani, 1973; Mountcastle, Lynch, Georgopoulos, Sakata, & Acuña, 1975). PE neurons are involved in the preparation and control of limb movements (Burbaud, Doegle, Gross, & Bioulac, 1991; Ferraina & Bianchi, 1994; Lacquaniti, Guigon, Bianchi, Ferraina, & Caminiti, 1995; Kalaska, 1996; Ferraina et al., 2009; Bremner & Andersen, 2012), and become active during skilled actions (Maimon & Assad, 2006; Chen, Reitzen, Kohlenstein, & Gardner, 2009; Shi, Apker, & Buneo, 2013).

In summary, PEc is a bimodal area, albeit with predominantly somatosensory inputs, whereas PE is essentially a high-order somatosensory area. Both areas over-represent the limbs, whether according to a crude somatotopic map (PE), or non-topographically (area PEc), and their functional properties strongly suggest that both areas are involved in the control of limb movements. The cortico-cortical connections of these areas are well established (PEc: Pandya & Seltzer, 1982; Tanné, Boussaoud, Boyer-Zeller, & Rouiller, 1995; Matelli, Govoni, Galletti, Kutz, & Luppino, 1998; Marconi et al., 2001; Tanné-Gariépy, Rouiller, & Boussaoud, 2002; Bakola, Gamberini, Passarelli, Fattori, & Galletti, 2010; PE: Jones, Coulter, & Hendry, 1978; Johnson, Ferraina, Bianchi, & Caminiti, 1996; Matelli et al., 1998; Bakola, Passarelli, Gamberini, Fattori, & Galletti, 2013), but their subcortical connections have not been investigated with the same level of detail. Previous studies have shown that the main thalamic afferents to the exposed surface of the superior parietal lobule arise from the Lateral Posterior (LP), Pulvinar (Pul), Ventral Posterior Lateral (VPL), and Ventral Lateral (VL) nuclei (Yeterian & Pandya, 1985; Schmahmann & Pandya, 1990; Cappe, Morel, & Rouiller, 2007; Padberg et al., 2009), but it has remained unclear whether PE and PEc differ. Moreover, previous studies have been based mostly on the analysis of single or few injections, leaving unexplored the issue of possible variations in the pattern of connections, according to location of the injection sites. Here we describe in detail the thalamo-cortical projections to areas PEc and PE, based on the analysis of retrograde tracer injections that cover, together, almost the whole extent of the two areas.

2 | MATERIALS AND METHODS

Experimental protocols followed the guidelines of the European Directive 86/609/EEC and the revised Directive 2010/63/EU for the Care and Use of Animals for Scientific Purposes.

Retrograde neuronal tracers were released into the cortex of six hemispheres of five male adult monkeys (*Macaca fascicularis*, 2.0–5.3 kg). The tracer cholera toxin subunit B (CTB; conjugated with Alexa Fluor® 488 [CTB-green], 1.7–2.0 µl, 1% in phosphate buffer solution, or with Alexa Fluor® 594 [CTB-red], 1.7 µl, 1% in phosphate buffer solution; Molecular Probes, Inc., Eugene, OR, USA) was injected through Hamilton micro-syringes fitted with a glass micropipettes attached to the needles. Fast Blue (FB; C₂₀H₁₇N₅O · HCl; Polysciences, Europe GmbH, Eppelheim, Germany) and Diamidino Yellow (DY; Diamidino Yellow dihydrochloride; Sigma-Aldrich Logistik GmbH, Schnelldorf, Germany) were inserted into the cortex as crystals with the aid of a tungsten rod (Rosa et al., 2005; Palmer & Rosa, 2006). The injections were directed to the exposed surface of the superior parietal lobule based on visual inspection. The attribution of each injection site to a specific cortical area was based on *post mortem* analysis of cyto- and myelo-architectural material, according to criteria described by Luppino et al. (2005) and Bakola et al. (2010, 2013). This analysis indicated that 3 of the injections were within the limits of area PEc, and 5 within those of area PE. Table 1 presents the details of each injection, and Figure 1 shows the extent and location of injection sites relative to the histological boundaries of cortical areas, projected onto a flat map reconstruction of a reference macaque brain obtained with the software CARET (Computerized Anatomical Reconstruction and Editing Toolkit, RRID: SCR_006260; Van Essen et al., 2001). To appreciate the location of the injection sites into the cortical thickness, coronal (for cases 1 and 2) and parasagittal (for cases from 3 to 8) sections are shown. For each injection, the core (dark spot) and the halo zone (colored region around the core) are shown.

2.1 | Surgical procedures

A detailed description of the experimental procedures is available in previous publications. Briefly (for details see Bakola et al., 2010, 2013), the surgeries were performed under aseptic conditions and full anesthesia, with the animal's head held in a stereotaxic frame. The animals were pretreated with atropine (0.05 mg/kg, i.m.), pre-anesthetized with ketamine hydrochloride (12 mg/kg, i.m.) and, after 30 min, anesthetized with sodium thiopental (8 mg/kg, i.v. with supplemental doses as required). To avoid edema, mannitol was administered intravenously (1 g/kg). The injections were placed in the cortex following craniotomy and durotomy. At the end of the surgical procedures, the dura mater was sutured, and the surgical site covered with surgical foam; the bone flap was positioned back in place, and the wound sutured. Analgesics (Ketorolac, 1 mg/kg, i.m., for 2–3 subsequent days) and antibiotics (erythromycin, 1–1.5 ml/10 kg) were administered postoperatively. The veterinary staff of the University of Bologna assisted to the surgery, monitoring physiological parameters, as well as the animal's recovery in the subsequent days.

TABLE 1 Injection sites and neuronal tracers employed in the experiments

Case			Cutting plane	Injected area	Tracer	Amount and concentration of tracer	Number of cortical/thalamic labeled cells
Present study	Gamberini et al. (2017)	Bakola et al., (2010) and Bakola et al. (2013)					
1 ^a	1	A5L	Coronal	PE ^c	FB ^d	1 crystal	8,933/256
2 ^a	2	A5R	Coronal	PE ^c	DY ^e	7 crystals	36,899/725
3	3	A4R	Parasagittal	PE ^c	DY ^e	4 crystals	17,175/102
4 ^b	4	2	Parasagittal	PE	CTB-green ^f	1.7 μ l; 1% in PBS ⁱ	17,315/498
5 ^b	5		Parasagittal	PE	CTB-red ^g	1.7 μ l; 1% in PBS ⁱ	604/40
6 ^c	6	1	Parasagittal	PE	FB ^d	1 crystal	13,925/138
7 ^c	7	6	Parasagittal	PE	CTB-green ^f	2 μ l; 1% in PBS ⁱ	3,567/84
8	9	4	Parasagittal	PE	CTB-green ^f	1.7 μ l; 1% in PBS ⁱ	3,124/244

^aSame animal.

^{b,c}Same hemisphere.

^dFast Blue, Polysciences Europe.

^eDiamidino Yellow, Sigma Aldrich.

^fCholera Toxin subunit B-green, Molecular Probes.

^gCholera Toxin subunit B-red, Molecular Probes.

^hFluoro Ruby, Invitrogen – Molecular Probes.

ⁱPhosphate Buffered Saline solution.

2.2 | Histological procedures

Fourteen days after the tracer injections, the animals were treated with ketamine hydrochloride (15 mg/kg, i.m.). Following loss of consciousness, they received a lethal dose of sodium thiopental (i.v.) and, upon cardiac arrest, were perfused with 3 L of normal saline solution, followed by 5 L of 4% paraformaldehyde in 0.1 M phosphate buffer at pH 7.4, and 4 L of 5% glycerol in the same buffer. The brains were removed from the skulls, photographed from all views, and cryoprotected by immersion in 0.1 M phosphate buffer solutions containing glycerol (10% and 20% for all cases). The brains were then snap-frozen and stored at minus 80°C. Sections (60 μ m of thickness) were obtained using a freezing microtome. In most cases, the brain was sectioned in parasagittal plane. This choice was dictated by the need to determine the histological boundaries between areas PE^c and PE, which are better recognizable in this plane of section, as shown in Figure 1c. Five series of sections were obtained, one of which was always stained for Nissl substance and another for myelin (Gallyas, 1979). The other series were left unstained, and one of these was used for analysis of fluorescent tracers. All sections were cover-slipped with DPX after quick steps of dehydration in 100% ethanol, and cleared with xylene.

2.3 | Data analysis

The unstained sections were examined for labeled neurons using a Zeiss microscope (Axioscope 2 Plus) equipped with 10 \times and 20 \times objectives. In each case, the entire hemisphere ipsilateral to the

injection site was processed. Section outlines and locations of labeled neurons were plotted at 600 μ m intervals (1 in 10 sections) using a computerized system linked to X/Y transducers mounted on the microscope stage. Photomicrographs of labeled cells were obtained using a digital camera connected to the microscope (Axiovision software, version 4.4; Carl Zeiss). Figure 2 illustrates examples of labeled cells.

The assignment to each injection site to area PE^c or PE was made taking into account the architectonic subdivision of the exposed surface of the superior parietal lobule proposed by Pandya and Seltzer (1982). To identify the thalamic nuclei, the atlases of Olszewski (1952), for coronal sections, and Ilinsky and Kultas-Ilinsky (1987), for parasagittal sections, were used. To harmonize the names and abbreviations of thalamic nuclei across these atlases we took into account the conclusions of Mai and Forutan (2012), who reviewed previous studies of the primate thalamus in light of recent improvements made possible by neuroimaging technologies. With respect to the lateral region of the thalamus, these authors concluded that the most accurate nomenclature was the one proposed by Ilinsky and Kultas-Ilinsky (1987).

Table 2 shows the terminology adopted in the present work.

A camera lucida was used to bring into register the stained histological sections and locations of labeled cells. The borders of thalamic nuclei were reconstructed using sections stained with Nissl method. In some cases, the sections stained with Gallyas method were used to distinguish borders that were not well evident with Nissl method. In order to facilitate the identification of the thalamic nuclei, the cases in which parasagittal sections were obtained were resliced in coronal plane, using the software CARET. Figure 3 shows a comparison between

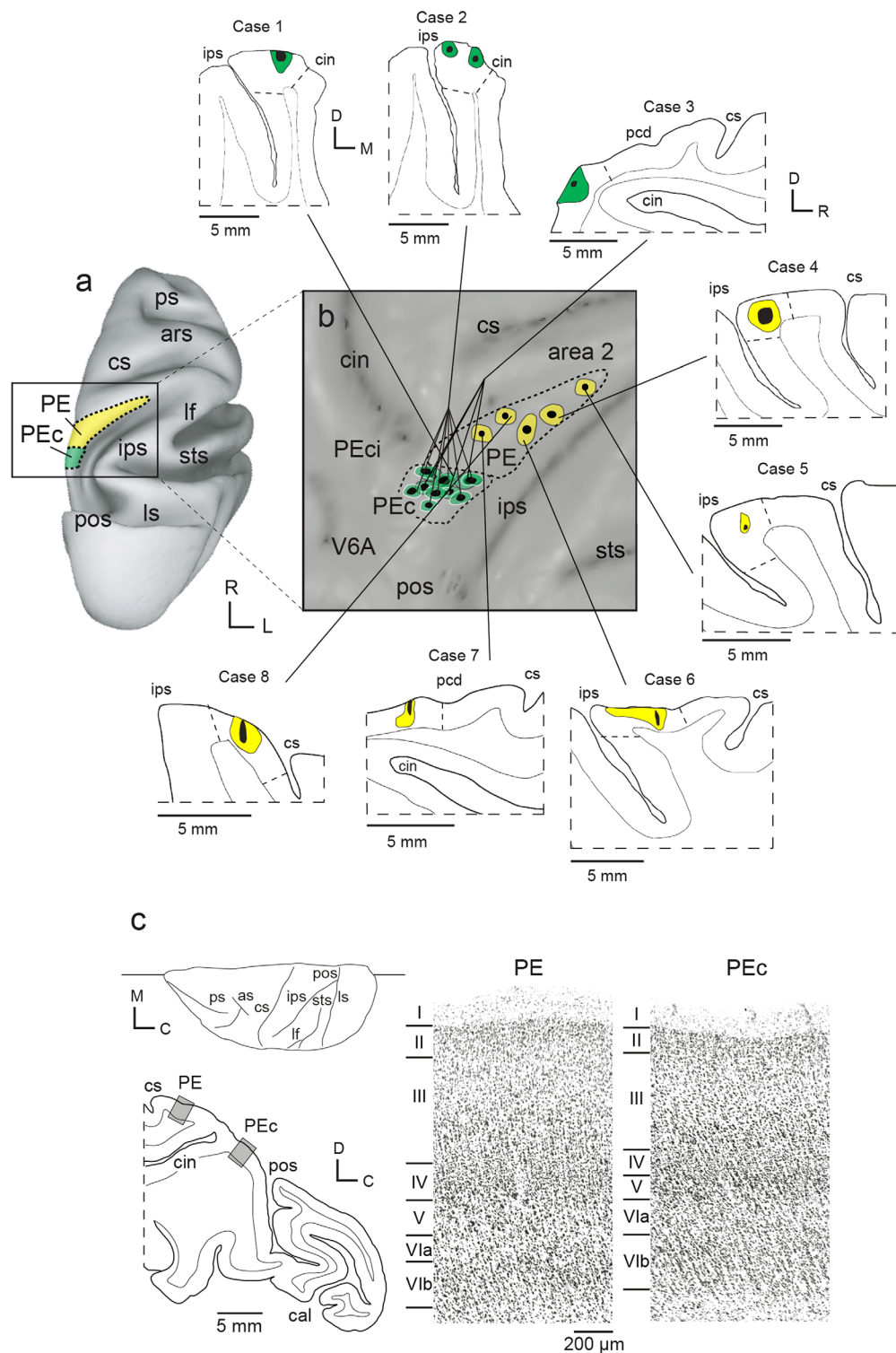


FIGURE 1 Summary of injection site locations. (a, b) Injection sites in five animals are illustrated on a two-dimensional reconstruction (b) of the caudal superior parietal lobule of the right hemisphere of a reference macaque brain shown on the left (a). For each injection, the core (dark spot) and the halo zone (colored region around the core) are shown. The dashed contours indicate the average cyto-architectonic border of areas PEc and PE. The location of the injection sites in the cortical thickness is shown on coronal (cases 1 and 2) and parasagittal (cases from 3 to 8) sections. (c) Drawing of a parasagittal section centered on the anterior wall of the parieto-occipital sulcus. The brain silhouette shows the level of the parasagittal section shown below. The grey boxes indicate the location of two high-magnification views shown in the panels on the right. Abbreviations: ars, arcuate sulcus; cal, calcarine sulcus; cin, cingulate sulcus; cs, central sulcus; ips, intraparietal sulcus; lf, lateral fissure; ls, lunate sulcus; pcd, post-central dimple; pos, parieto-occipital sulcus; ps, principal sulcus; sts, superior temporal sulcus; C, caudal; D, dorsal; L, lateral; M, medial; R, rostral. V6A, PEc, PE, PEci, area 2: areas V6A, PEc, PE, PEci, 2 [Color figure can be viewed at wileyonlinelibrary.com]

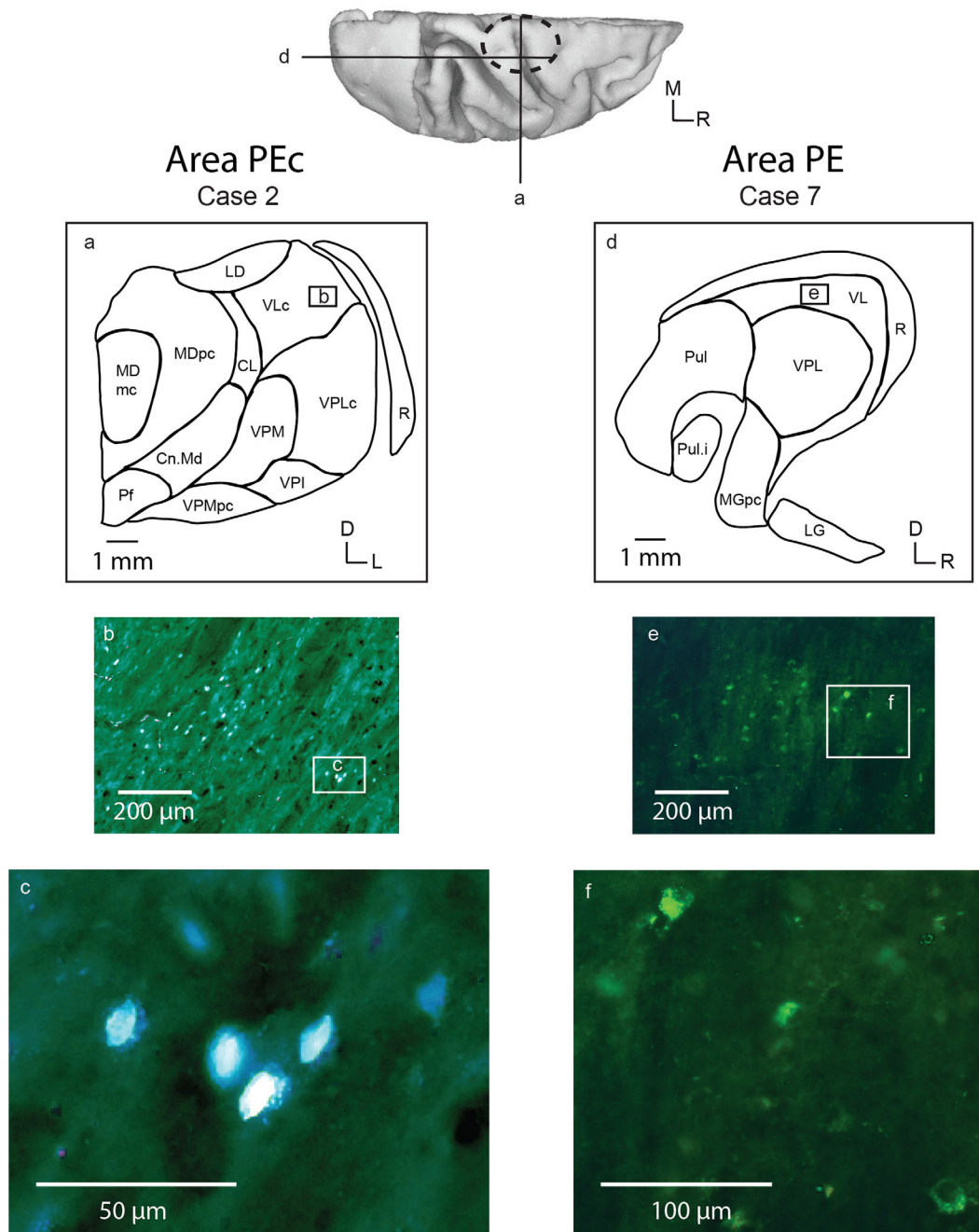


FIGURE 2 Examples of labeled cells in the thalamus. Top: dorsal view of a reference macaque brain; the dashed circle represents the approximate location and extent of the thalamus. (a) thalamic section of a PEc injection case. (b, c) medium- and high-power photomicrographs, respectively, of DY labeled cells taken at 10× and 20× magnifications. (d) Thalamic section of a PE case. (e, f) Medium- and high-power photomicrographs, respectively, of CTB-green labeled cells taken at 10× and 20× magnifications. For the nomenclature of thalamic nuclei, see the list of abbreviations. Other details and abbreviations as in Figure 1 [Color figure can be viewed at wileyonlinelibrary.com]

sections reported in Olszewski (1952) atlas (Figure 3a, b) and our reconstructions of thalamic nuclei obtained from coronal sections taken at similar levels (Figure 3e, f). There was a good correspondence between our observations (actual or digitally reconstructed) and the atlas. Similarly, there was a good fit between Ilinsky and Kultas-Ilinsky (1987) atlas (Figure 3c, d) and our observations in parasagittal sections (Figure 3g, h).

To obtain the overall maps of the distribution of labeled neurons in LP, Pul, VPL, and VL thalamic nuclei (Figure 8), we first reconstructed these nuclei in each animal by aligning the coronal sections according to the Olszewski (1952) atlas, as shown in Figure 3 for the whole thalamus. As mentioned above, if a case was sectioned in sagittal plane, coronal sections were obtained with the re-slicing tool of CARET. Then, we superimposed on a template obtained from the Olszewski (1952)

TABLE 2 Correspondence of nomenclature of the thalamic nuclei involved in this study

Thalamic regions	Olszewski (1952)	Ilinsky and Kultas-Ilinsky (1987)	Present study
Medial	MDdc	MDdc	MD
	MDmc/pc	MDmc/pc	MD
	MDmf	MDmf	MD
	MDpc	MDpc	MD
Lateral			
<i>Motor</i>	VA	VA	VA
	VAdc	VAdc	VA
	VAmc	VAmc	VA
	VApC/dc	VApC/dc	VA
	VLo	VAdc	VA
	VLc	VL	VL
	VLps	VL	VL
	VPLo	VL	VL
<i>Sensory</i>	VPLc	VPL	VPL
Intralaminar	CL	CL	CL
	Cn.Md	CM	CM
	Pf	PF	PF
Posterior	LP	LP	LP
	Pul.i	Pul.i	Pul
	Pul.l	Pul	Pul
	Pul.m	Pul	Pul
	Pul.o	Pul	Pul

For the extended nomenclature of the thalamic nuclei, see the list of abbreviations.

atlas the reconstructions of each nucleus of each case, and the labeled cells found within that nucleus (see left and central columns in Figure 8).

3 | RESULTS

It is well known that subcortical neurons represent a small fraction of the overall number of cells projecting to a cortical area (Markov et al., 2011), and our results confirm this general rule. The number of labeled neurons in cortex and thalamus differed between cases (see Table 1) likely because of the different type of tracer used, the different uptake of the tracer in different cases, and/or the different cortical layers involved by the injection site. On average, labeled cells after PEc tracer injections were $1.8\% \pm 0.8\%$ of the total labeled cells, and after PE injections they were $4.1\% \pm 2.6\%$.

3.1 | Thalamic afferents to area PEc

Figure 4 shows the results of a representative case of thalamic labeling after PEc injection (Case 3, see injection site in Figure 1). Four parasagittal sections through the thalamus are shown, together with a reconstruction of a medial view of the thalamus, which shows the most densely labeled thalamic nuclei (colored polygons) obtained by overlapping outlines deriving from all sections available. As visible in both

single sections and reconstruction, labeled cells were concentrated in the dorsal part of the thalamus, including the LP (green), Pul (blue), VPL (purple), and VL (red) nuclei. The proportions of thalamic afferents in different nuclei are shown in Figure 5a.

Minor afferents to PEc were found in two out of three cases (from 2.3% to 5.4% of the total label), and originated from Central Lateral (CL) nucleus in cases 1 and 2, and from the Medial Dorsal (MD), and Ventral Anterior (VA) nuclei, in case 2.

3.2 | Thalamic afferents to area PE

Figure 6 shows the thalamic labeling following one of the PE injections (Case 8, see injection site in Figure 1). Five parasagittal sections and a reconstruction of a medial view of the thalamus are illustrated. These illustrations show that labeled cells were, as for area PEc injections, mainly distributed in the dorsal part of the thalamus. However, the distribution of labeled cells was more widespread, particularly in the dorso-ventral dimension. Figure 5b shows that the thalamic nuclei that were strongly labeled in cases with PE injections were the same as those that were strongly labeled after PEc injection (see Figure 5a), that is, the LP, Pul, VPL, and VL nuclei. Minor afferents to area PE, observed only in some cases, originated from the MD and VA nuclei, and from the CM/PF complex.

3.3 | Comparison between thalamic connections to areas PEc and PE

Figure 7a shows the distribution of the thalamic afferents to areas PEc and PE according to the thalamic subdivision proposed by Mai and Forutan (2012). The superior and periventricular regions did not show any labeled cells. Only a low percentage of labeled cells were observed in the medial region (PEc: $1.1\% \pm 1.6\%$; PE: $1.8\% \pm 2.2\%$) and in the intralaminar formation (PEc: $2.8\% \pm 2.0\%$; PE: $5.6\% \pm 4.8\%$). The highest numbers of labeled cells were observed in the lateral (PEc: $52.7\% \pm 8.8\%$; PE: $43.0\% \pm 18.7\%$) and posterior (PEc: $42.5\% \pm 5.3\%$; PE: $49.3\% \pm 17.5\%$) nuclear groups of the thalamus. According to this analysis, differences between PEc and PE were not statistically significant (unpaired Student's t test).

Mai and Forutan (2012) suggested that the lateral region of the thalamus can be subdivided in two regions, which they named "motor" and "sensory" based on functional properties, and we analyzed the distribution of the labeled cells among these two subdivisions. According to Mai and Forutan (2012), the "motor" thalamus includes the VA and VL nuclei, while the "sensory" thalamus comprises the VM, VPI, VPL, and VPM nuclei. As shown in Figure 7b, the sensory thalamus projections were stronger than the motor projections to both cortical areas, with this trend being particularly clear following injections in area PE.

3.4 | Topographic distribution of labeled cells

As reported above, the main thalamic nuclei projecting to the cortical areas PEc and PE are LP, Pul, VPL, and VL. Figure 8 shows the spatial

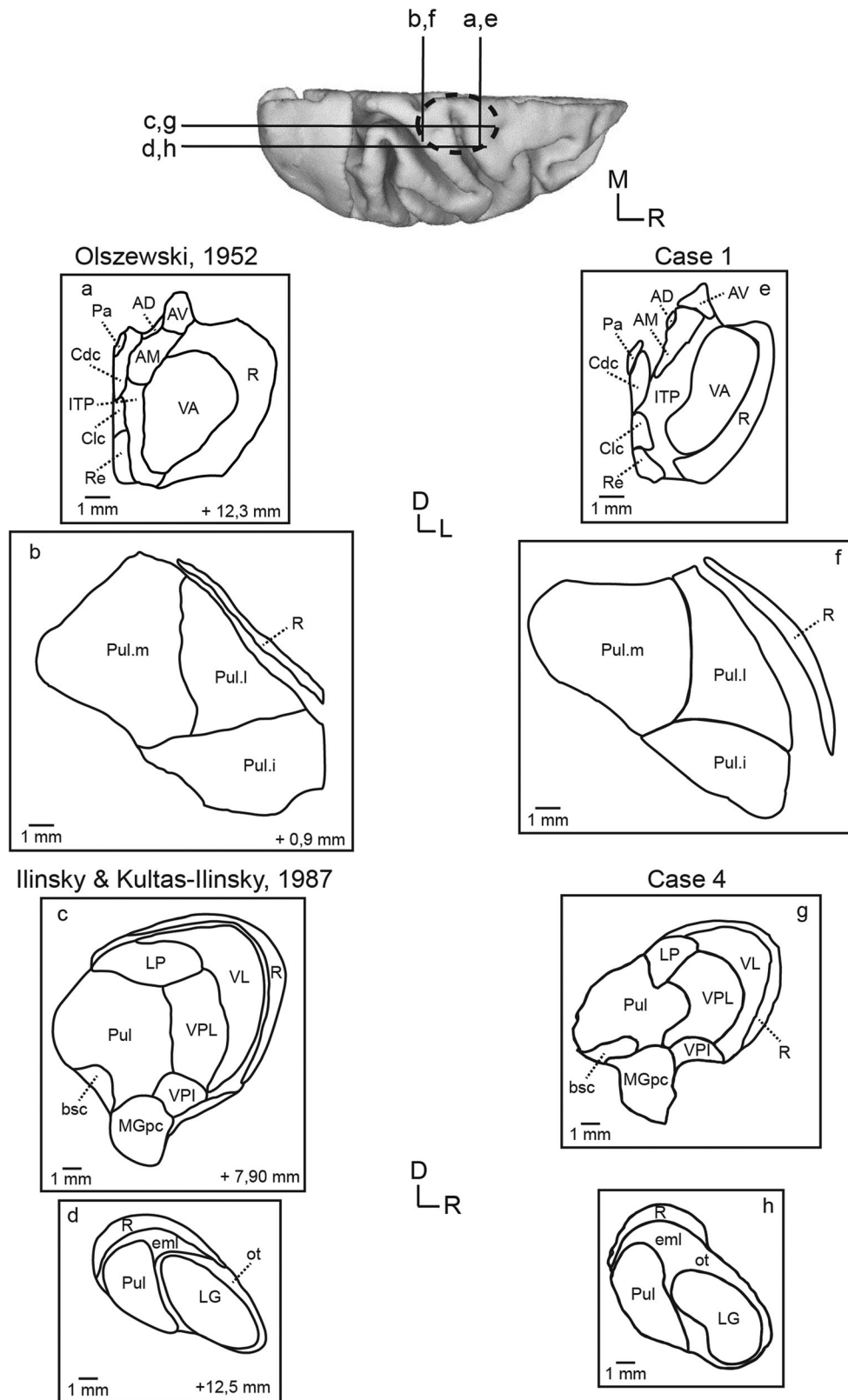


FIGURE 3 Thalamic nuclei. Top: dorsal view of a reference macaque brain; the dashed circle represents the location and extent of the thalamus. (a, b) Typical brain sections showing the thalamic nuclei, taken from Olszewski (1952) atlas. (e, f) Sections of Case 1 taken at the same approximate level of atlas sections (a, b). (c, d) Typical brain sections showing the thalamic nuclei, taken from the Ilinsky and Kultas-Ilinsky (1987) atlas. (g, h) Sections of Case 4 taken at the same approximate level of atlas sections (a–c). For the nomenclature of thalamic nuclei and tracts, see the list of abbreviations. Other details and abbreviations as in Figures 1 and 2

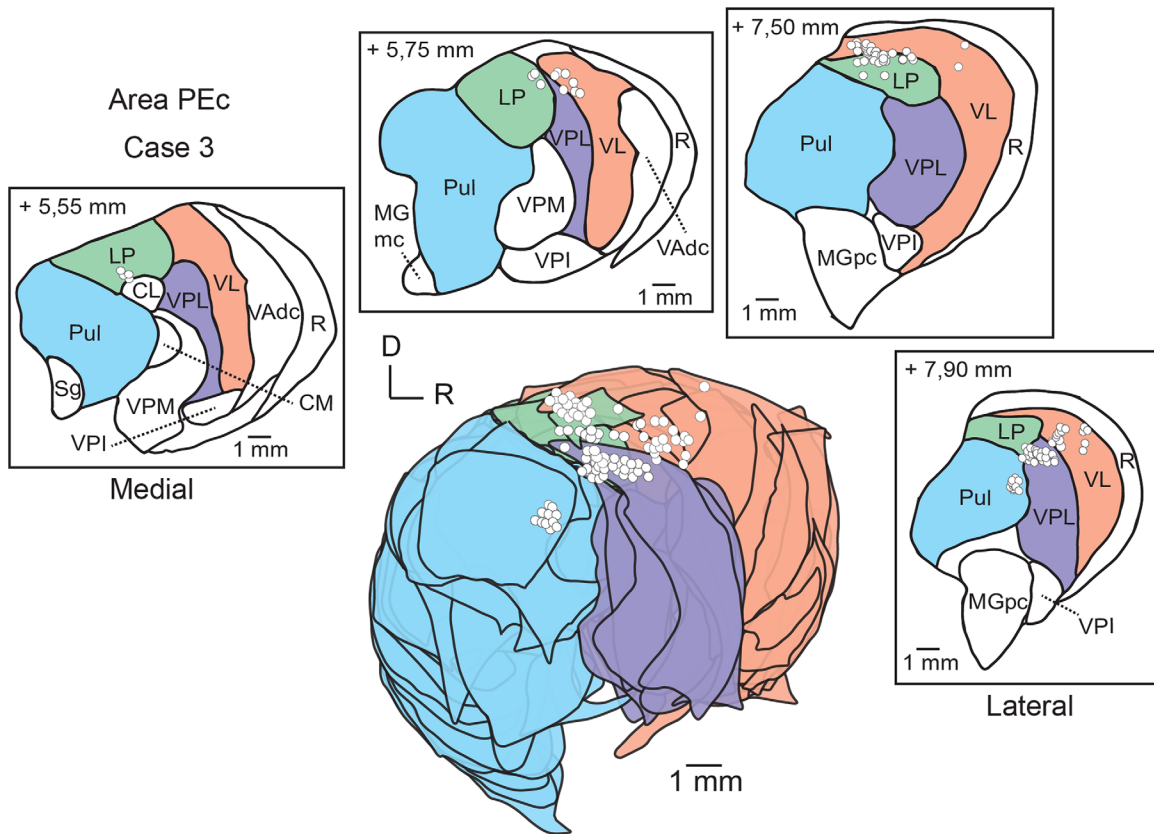


FIGURE 4 Typical case with thalamic afferents to area PEc. Four parasagittal sections from Case 3 are reported. The white circles represent the labeled cells. At the center, a reconstruction of the most involved thalamic nuclei is shown, obtained by overlapping all sections at our disposal. The thalamic nuclei that contain labeled cells are highlighted with various colors: green for LP, blue for Pul, red for VL, and purple for VPL. For the nomenclature of thalamic nuclei, see the list of abbreviations. Other details and abbreviations as in Figures 1–3 [Color figure can be viewed at wileyonlinelibrary.com]

distributions of labeled cells within these nuclei. In Figure 8, we reconstructed each of these nuclei by superimposing coronal sections from all cases available; brains originally sectioned in parasagittal planes were first re-sliced into coronal views, following 3D reconstructions in CARET.

Figure 8a shows the distribution of labeled cells in the LP nucleus. Cells were distributed in the lateral region of LP, whether PEc or PE was injected. The labeling after PEc injections appeared to cover a larger proportion of this nucleus, compared to PE.

The Pul nucleus is traditionally subdivided into four parts: medial, lateral, anterior, and inferior (Olszewski, 1952; Snider & Lee, 1961; Grieve, Acuña, & Cudeiro, 2000). Figure 8b shows that both PEc and PE mainly receive from the medial Pul. Area PEc, in addition, may receive a numerically small projection from the anterior Pul. Cells projecting to PE were distributed more dorsally, with respect to those projecting to PEc.

Figure 8c shows that cells projecting to area PEc are strictly segregated to the dorsal part of the VPL nucleus, whereas those projecting to PE are more widely distributed. According to Rausell, Bickford, Manger, Woods, and Jones (1998), VPL represents the whole body except the head (see Figure 8c right), which is represented in VPM. Labeled cells projecting to PEc are located in the parts of VPL that most likely

represent the trunk and the proximal portions of the limbs (in particular, the legs). Cells projecting to PE, in addition, appeared to also be located in the representations of more distal parts of the limbs. The VPM nucleus did not project to PEc or PE.

Figure 8d shows the distribution of labeled neurons in the VL nucleus. Projections to PEc and PE are very similar, involving the dorsal-most part of the nucleus and, far more sparsely, the ventral part. Comparison with the somatotopic map proposed by Vitek, Ashe, DeLong, and Alexander (1994) suggests that the labeled cells are located in parts of VL mostly representing the trunk and legs, although the ventral group of cells appears to overlap with the region of face representation.

4 | DISCUSSION

The present study defined the thalamo-cortical connections of the posterior parietal areas PEc and PE (Pandya & Seltzer, 1982). We have found that these areas receive major thalamic afferents from the posterior and lateral regions of the thalamus (namely, the VL, VPL, LP, and Medial Pul nuclei), and minor afferents from the medial and intralaminar regions. There have been previous studies investigating the

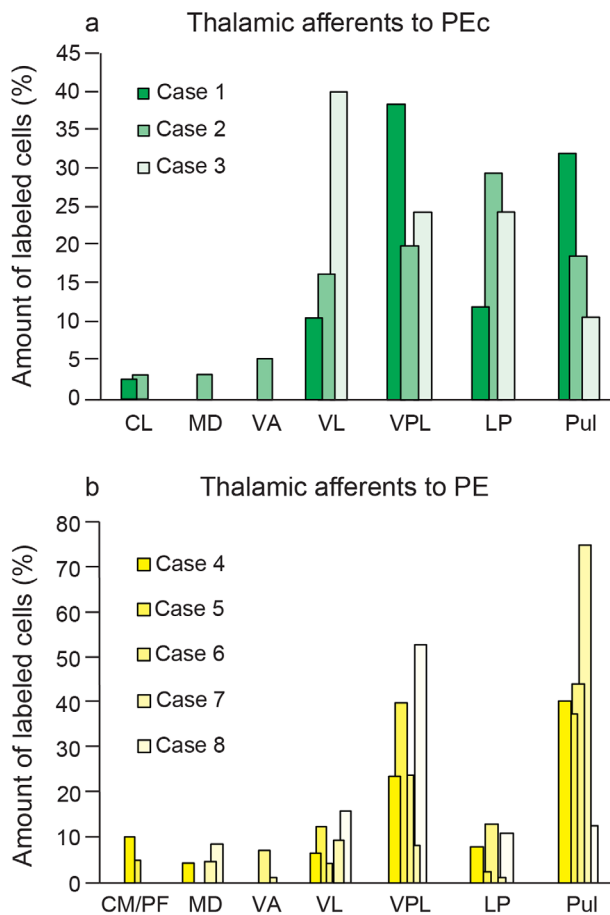


FIGURE 5 (a) Thalamic afferents to area P_{Ec}. Percentage of labeled cells in the thalamic nuclei after injections confined within the cyto-architectonic limits of area P_{Ec}. Only labeling that represented on average > 1% of thalamic afferents are reported. (b) Thalamic afferents to area P_E. Percentage of labeled cells in the thalamic nuclei after injections confined within the cyto-architectonic limits of area P_E. Only labeling that represented on average > 1% of thalamic afferents are reported. For the nomenclature of thalamic nuclei, see list of abbreviations and Table 2 [Color figure can be viewed at wileyonlinelibrary.com]

thalamic connections of the superior parietal lobule (Yeterian & Pandya, 1985; Schmahmann & Pandya, 1990; Cappe et al., 2007; Padberg et al., 2009). The present study refined and extended the observations of these earlier studies by making use of a larger series of injection sites, which allowed us to study P_{Ec} and P_E separately, while considering the entire extents of these areas.

4.1 | Major thalamic afferents

Areas P_{Ec} and P_E receive the majority of their thalamic afferents from the posterior and lateral regions of the thalamus (Mai & Forutan, 2012). The posterior thalamus is dominated by the Pul complex, which account for about a quarter of its total mass (Grieve et al., 2000; Mai & Forutan, 2012), and it is traditionally subdivided into four sectors, each with specific functional properties (Olszewski, 1952; Snider & Lee, 1961; Grieve et al., 2000; Mai & Forutan, 2012;

see Figure 8b). The anterior Pulvinar is reported to have somatosensory functions (Grieve et al., 2000); the lateral and inferior nuclei contain visually responsive cells, which are organized retinotopically (Kaas & Lyon, 2007), and the Medial Pul contains visual cells which are not retinotopically organized (Mathers & Rapisardi, 1973; Grieve et al., 2000), as well as cells responding to reaching activity (Acuña, Cudeiro, Gonzalez, Alonso, & Perez, 1990) and auditory stimuli (Yirmiya & Hocherman, 1987). The Medial Pul also seems to be involved in directing attention and in recognizing visual salience (Andersen, 1987; Laberge & Buchsbaum, 1990; Mesulam, 1990; Romanski, Giguere, & Bates, 1997). Immediately anterior to the Medial Pul is the LP nucleus. Given the difficulty in establishing a reliable anatomical boundary between the Medial Pul and the LP, these two nuclei are often considered as part of a single complex (Van Buren & Borke, 1972; Cooper, Riklan, & Rakic, 1974; Percheron, 2004); indeed, the few functional studies investigating LP in the macaque found similar functional characteristics in comparison with the Medial Pul (Acuña, Cudeiro, & Gonzalez, 1986; Acuña et al., 1990; Cudeiro, González, Pérez, Alonso, & Acuña, 1989).

Our results show that both the Medial Pul and the LP form major projections to areas P_{Ec} and P_E, although area P_E tends to receive comparatively less numerous afferents from LP (Figure 5). The strong Medial Pul inputs are in line with the role attributed to these areas in preparation/execution of reaching actions (Burbaud et al., 1991; Ferraina et al., 2001; Bremner & Andersen, 2012; Hadjimitsakis et al., 2015; Piserchia et al., 2017). The reason for the comparatively weaker LP inputs to P_E is unclear. Recent studies on the dopaminergic innervation (Sanchez-Gonzalez, 2005; García-Cabezas, Rico, Sánchez-González, & Cavada, 2007; García-Cabezas, Martínez-Sánchez, Sánchez-González, Garzón, & Cavada, 2009) have demonstrated that the LP nucleus is heavily innervated by dopaminergic fibers, while the Medial Pul is only mildly innervated. Since also the primary motor cortex and the nuclei of the “motor” thalamus receive strong dopaminergic input, these studies suggested that the LP nucleus is involved in the control of motor actions.

In a recent study, it has been found that area V6A, a visuo-motor area located further caudally, adjacent to P_{Ec} (see Figure 1), is strongly connected to the LP nucleus, and less so to the Medial Pul (Gamberini et al., 2016), further emphasizing the view that different balances in the thalamic inputs contribute to the functional differences among superior parietal lobule areas. Thus, the thalamic input from the LP nucleus becomes comparatively more significant from rostral to caudal (i.e., from area P_E to area V6A), while that from Medial Pul progressively decreases. Interestingly, the LP input increases according to the incidence of visually responsive cells in its cortical target: such cells are virtually absent in P_E (Mountcastle et al., 1975), form approximately 40% of the population in P_{Ec} (Breveglieri et al., 2008) and 65% in V6A (Gamberini, Galletti, Bosco, Breveglieri, & Fattori, 2011). Based on these observations, and taking into account the observations discussed in the paragraph above, we suggest that LP input mainly contributes to visuo-motor information.

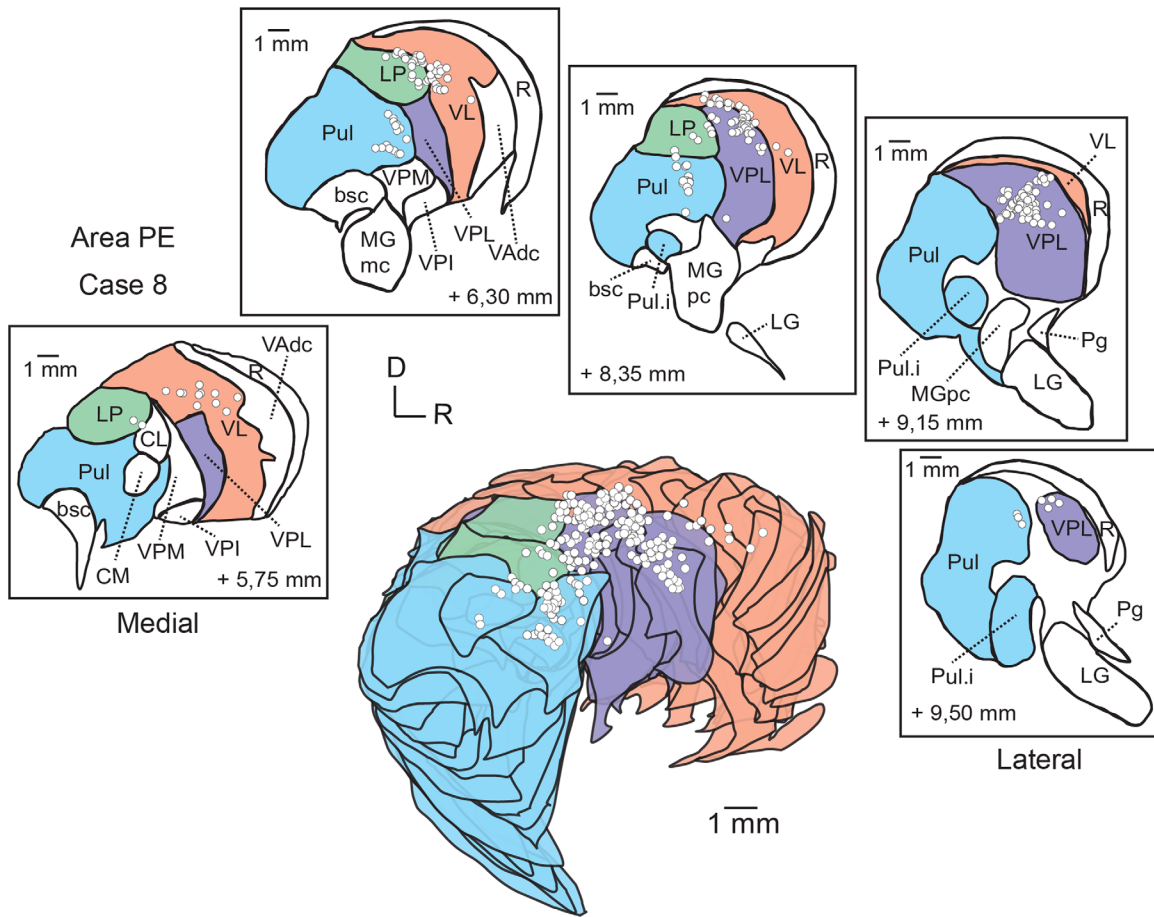


FIGURE 6 Typical case with thalamic afferents to area PE. Five parasagittal sections from Case 8 are reported. For the nomenclature of thalamic nuclei and tracts, see the list of abbreviations. Other details and abbreviations as in Figure 4 [Color figure can be viewed at wileyonlinelibrary.com]

Nuclei in the lateral region of the thalamus are strongly connected with both areas PEc and PE. Our results show that, for area PE, the inputs coming from the “sensory” subdivision of the lateral thalamus (Mai & Forutan, 2012) are more numerous than those from the “motor” subdivision, while for area PEc, they appear to be more balanced (Figure 7). This finding is in line with the functional properties of the two cortical areas, which suggest that PEc controls the interaction of the four limbs with the environment (Bakola et al., 2010), for which an integration between motor and sensory (visual and somatic) information is required (Gamberini, Dal Bò, Breveglieri, et al., 2017), whereas area PE is involved in the preparation of limb movement (Burbaud et al., 1991; Bremner & Andersen, 2012), a function that requires a strong somatosensory input, in particular proprioception, to control the posture to accomplish a correct limb movement.

The VPM and VPL are two of the nuclei composing the “sensory” thalamus. Together, they contain a complete and topographically organized representation of the body, with the head represented in VPM and the trunk and limbs in VPL (Rausell et al., 1998). We found that neither PEc nor PE received thalamic inputs from VPM, while receiving strong afferents from the portion of VPL which represents the trunk and the proximal parts of the limbs.

Interestingly, the portion of VPL representing the distal part of the limbs projected only to area PE. These observations agree with the somatosensory representation in areas PEc and PE, in that PEc represents only the trunk and the proximal parts of the four limbs (Breveglieri et al., 2006) and PE also the hands and feet (Padberg et al., 2007; Krubitzer & Disbrow, 2008).

The “motor” sector of the lateral thalamus is formed by the VA and VL nuclei (Mai & Forutan, 2012). VA formed only minor projections, which were not constantly present in all cases we studied. In contrast, the VL nucleus is strongly connected with both PEc and PE. According to Vitek et al. (1994), VL contains a motor topographical map of the whole body, including the head. After PEc and PE injections labeled cells in VL were mainly located in the dorsal part of the nucleus, likely overlapping with the representations of the trunk and legs, but a few cells were also observed in the ventral part of the nucleus, which represents the face (Figure 8d). No labeled cells were found in the putative arm representation. This cell distribution is somewhat surprising, given that in both PEc and PE cells are responsive to forelimb movements (PEc: Bhattacharyya et al., 2009; Hadjimitsakis et al., 2015; Piserchia et al., 2017; PE: Burbaud et al., 1991; Ferraina et al., 2009; Bremner and Andersen, 2012), and to tactile and proprioception

Regional subdivision of the thalamic afferents to PEc and PE

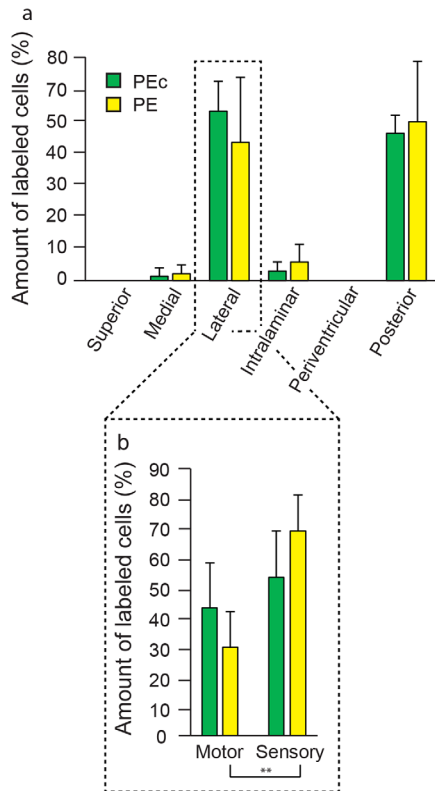


FIGURE 7 Regional subdivision of thalamic afferents to areas PEc and PE. (a) Average percentages of thalamic cells labeled in the six thalamic regions described by Mai and Forutan (2012) after injections in areas PEc and PE. (b) Average percentages of labeled cells in the Lateral region of the thalamus, subdivided in "Motor" and "Sensory" thalamus according to Mai and Forutan (2012). Vertical bar: SD; ** $p < .01$ [Color figure can be viewed at wileyonlinelibrary.com]

stimulations of forelimbs (PEc: Brevéglieri et al., 2006; PE: Padberg et al., 2007; Krubitzer & Disbrow, 2008). Our tracer injections covered the entire extent of area PEc, and the vast majority of the extent of area PE, in particular the antero-lateral part of the area where the forelimb is represented (Krubitzer & Disbrow, 2008). Therefore, we expected to find many labeled cells in the sectors of VL representing arm and hand, but this was not apparent in our data. A similar situation was observed by Bakola et al. (2010, 2013), who reported an emphasis of somatosensory and premotor/motor leg-field cortical projections to PEc and PE. It could be that both thalamo-cortical and cortico-cortical networks are involved in the control of movements performed with the four limbs, typical of non-human primates moving in natural habitat. A cortico-thalamo-cortical loop could be engaged in the control of more stereotyped movements, as those activated in locomotion, that mainly involve the legs, while an alternative cortico-cortical network would be mainly activated when the grasping of an object is requested. Alternatively, this apparent discrepancy may reflect the difficulty in comparison across studies which used different methods.

4.2 | Minor thalamic afferents

In addition to the major thalamic afferents described above, recognized in all our cases, we found minor and variable afferents from the MD, VA, CL, and CM/PF nuclei. The MD nucleus, which sends minor afferents to both areas PEc and PE, is reported to be involved in the control of saccades (Watanabe & Funahashi, 2004) and in learning and decision-making functions (Mitchell, 2015). Saccadic activity has been reported in PEc (Raffi, Ballabeni, Maioli, & Squatrito, 2008), but to our knowledge not in area PE, and nothing is known about a possible involvement of PEc and/or PE in learning and decision-making processes. The VA nucleus, which sends a few afferents to both areas PEc and PE, is described as a node of a loop involved in the induction, execution, and control of principal aspects of voluntary movements, in particular when multiple alternatives are possible (Mushiaké & Strick, 1995; Middleton & Strick, 2000; Sommer, 2003). The CL nucleus and CM/PF complex send few afferents to areas PEc and PE, respectively. CL is possibly involved in the execution of cognitive functions (Van Der Werf, Witter, & Groenewegen, 2002), and CM/PF seems to have a role in movement regulation (Mai & Forutan, 2012).

4.3 | Comparison with previous studies

Previous studies focused on the thalamic connections of superior parietal lobule were based on few injections, which in most cases did not encompass the complete extent of a cytoarchitecturally defined area (Yeterian & Pandya, 1985; Schmahmann & Pandya, 1990; Cappe et al., 2007; Padberg et al., 2009). Table 3 shows a comparison of the present observations (column 5) with those of previous studies (columns 1–4). In Table 3, we only show data from injections of retrograde tracers (as those used in this work) located in a specific cortical area of the superior parietal lobule, avoiding data from injections of anterograde tracers and/or that involved more than one area. The nomenclature adopted in older studies was harmonized with that used in the present work (see Table 2).

Table 3 shows that the thalamo-cortical afferents we observed for area PEc were very similar to those of Yeterian and Pandya (1985), although specific differences (absence of labeled neurons in the R nucleus, and their presence in the VPL nucleus) were observed. Our conclusions differ more substantially from those of Schmahmann and Pandya (1990), possibly due to the more comprehensive sample obtained in the present study.

With respect to the thalamic afferents of area PE, our results differ from the previous literature in several ways (see Table 3). For example, we did not observe afferents from the Anterior Pulvinar, which were reported by earlier studies. Other aspects of our study reflect earlier observations, such as the presence of major afferents from the Medial Pul, and the LP and VPL nuclei. Overall, our conclusions are in closer agreement with those of Cappe et al. (2007). Although some of the discrepancies could be due to the fact that earlier studies did not cover the entire extent of area PE, other factors, such as the use of different criteria for parcellation of the thalamus, are likely to also play a role in explaining such differences.

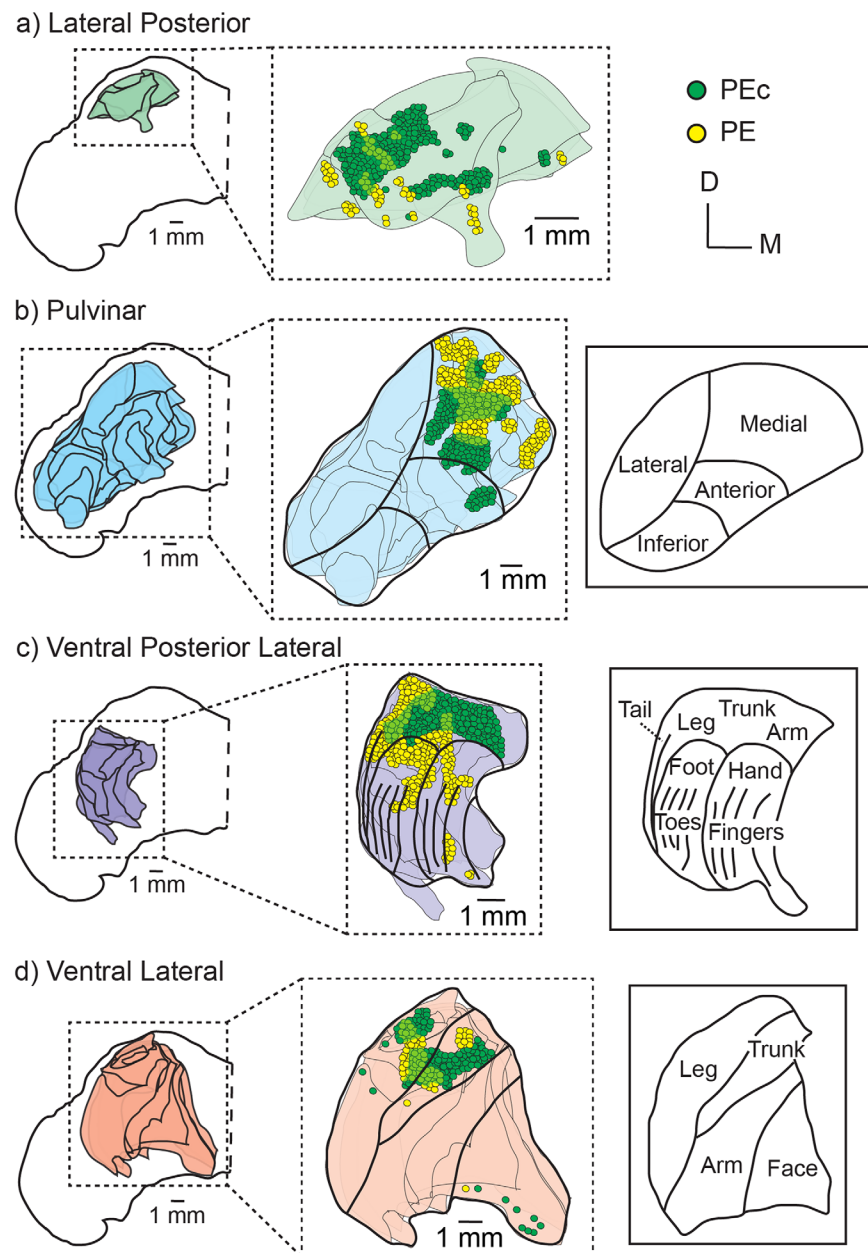


FIGURE 8 Distribution of labeled cells in LP, Pul, VPL, and VL nuclei. (a–d) To the left, the outline of the most external limit of the thalamus in a typical coronal section, with a reconstruction of LP, Pul, VPL, VL nuclei (enlarged at the center), and their subdivision (on the right) according to Grieve et al. (2000) (Pul), Rausell et al. (1998) (VPL), and Vitek et al. (1994) (VL) are shown. The subdivisions of Pul, VPL, and VL are also reported at the center of the figure (black contour) where they are morphed on the shape of specific thalamic nucleus in order to facilitate the allocation of labeled cells. Yellow and green dots represent labeled cells sending projections to PE and PEc, respectively. Other details and abbreviations as in Figures 1–3 [Color figure can be viewed at wileyonlinelibrary.com]

In humans, several studies that use DTI and resting-state fMRI techniques allowed subdividing the thalamus in clusters, each comprising various nuclei (Mastropasqua, Bozzali, Spanò, Koch, & Cercignani, 2015; O'Muircheartaigh, Keller, Barker, & Richardson, 2015; Yuan et al., 2016; Hwang, Bertolero, Liu, & D'esposito, 2017; Kumar, van Oort, Scheffler, Beckmann, & Grodd, 2017). These studies show that different clusters are connected with different cortical regions, and confirm the present and previous works on the macaque monkey in showing

that the clusters that include VL, VPL, LP, and Pul are connected with the posterior parietal cortex. However, the limits of the neuroimaging techniques in discerning the border of cortical and subcortical architectonic subdivisions do not allow a direct comparison of the thalamo-cortical connections of areas PEc and PE in macaques and humans. Furthermore, the great difference in extent and location of areas 5 and 7 in macaques and humans would make this comparison unreliable (Brodmann, 1909; Amunts & Zilles, 2015).

TABLE 3 Comparison with previous studies on the macaque

	PEc			PE				
	1	2	5	1	2	3	4	5
Anterior Pul	+	+++	+	++	+++	+	+++	-
Lateral Pul	-	+	-	+++	+	-	-	-
Medial Pul	+++	-	+++	++	-	++	-	+++
CL	+	+	+	-	++	+	-	-
CM/PF	-	+	-	-	++	+	-	+
LP	+++	+++	+++	+++	+++	+++	+++	++
MD	++	+	+	-	+	++	-	+
R	++	-	-	++	-	-	-	-
VA	-	-	+	-	-	-	-	+
VL	+++	+	+++	+++	+	-	+	++
VPI	-	-	-	-	-	-	+	-
VPL	-	+	+++	+++	++	+++	+++	+++

1: Yeterian and Pandya (1985) (retrograde).

2: Schmahmann and Pandya (1990) (anterograde/retrograde).

3: Cappe et al. (2007) (anterograde/retrograde).

4: Padberg et al. (2009) (retrograde).

5: Present study (retrograde).

-: no connections.

+: weak connections.

++: moderate connections.

+++ : high connections.

For the extended nomenclature of the thalamic nuclei, see the list of abbreviations.

5 | CONCLUSIONS

The thalamic inputs to areas PEc and PE reported here confirm the sensory-motor integration nature of these posterior parietal areas (Mountcastle et al., 1975; Burbaud et al., 1991; Breveglieri et al., 2006, 2008; Padberg et al., 2007; Krubitzer & Disbrow, 2008; Bremner & Andersen, 2012). The thalamic afferents to these areas are largely similar, in that they both originate mainly from regions of the thalamus which represent trunk, upper limbs and lower limbs, particularly the legs and the proximal parts of both limbs, but also show differences. These observations well agree with the functional roles proposed for PEc and PE, with the first suggested to control the interaction of the four limbs with the environment (Bakola et al., 2010), and the second to be involved in the preparation/execution of limbs movement (Burbaud et al., 1991; Ferraina & Bianchi, 1994; Lacquaniti et al., 1995; Kalaska, 1996; Ferraina et al., 2009; Bremner & Andersen, 2012). The thalamic inputs to PEc and PE also suggest the existence of cortico-thalamo-cortical circuits supporting a certain degree of motor automatism, particularly important in locomotion.

ACKNOWLEDGMENTS

The authors would like to acknowledge S. Bakola for participating in some of the experiments and initial analyses, and thank M. Verdosci, F. Campisi, and G. Placenti for technical assistance, and G. Beghelli for contributing in the re-slicing process.

CONFLICT OF INTEREST

The authors declare that they have no conflict of interest.

ROLE OF AUTHORS

All authors had full access to all the data in the study and take responsibility for the integrity of the data and the accuracy of the data analysis. Study concept and design: MG, CG. Acquisition of data: DI, MG, LP, MR. Analysis and interpretation of data: DI, MG, CG. Drafting of the manuscript: DI, MR, CG. Critical revision of the manuscript for important intellectual content: MR. Obtained funding: MR, CG. Administrative, technical, and material support: LP. Study supervision: CG.

REFERENCES

- Acuña, C., Cudeiro, J., & Gonzalez, F. (1986). Lateral posterior (LP) and pulvinar unit activity related to intentional upper limb movements directed to spatially separated targets, in behaving *Macaca Nemestrina* monkeys. *Revue Neurologique*, 142, 354–361.
- Acuña, C., Cudeiro, J., Gonzalez, F., Alonso, J. M., & Perez, R. (1990). Lateral-posterior and pulvinar reaching cells - comparison with parietal area 5a - a study in behaving *Macaca Nemestrina* monkeys. *Experimental Brain Research*, 82, 158–166.
- Amunts, K., & Zilles, K. (2015). Architectonic mapping of the human brain beyond Brodmann. *Neuron*, 88, 1086–1107.
- Andersen, R. A. (1987). Inferior parietal lobule function in spatial perception and visuomotor integration. In F. Plum, V. B. Mountcastle, & S. R.

- Geiger (Eds.), *Handbook of Physiology*. The Nervous System. Higher Functions of the Brain. (Sect. 1, Vol. V, Chapt. 12, pp. 483–518). Bethesda, MD: American Physiological Society.
- Bakola, S., Gamberini, M., Passarelli, L., Fattori, P., & Galletti, C. (2010). Cortical connections of parietal field PEc in the macaque: Linking vision and somatic sensation for the control of limb action. *Cerebral Cortex (New York, N.Y. : 1991)*, *20*, 2592–2604.
- Bakola, S., Passarelli, L., Gamberini, M., Fattori, P., & Galletti, C. (2013). Cortical connectivity suggests a role in limb coordination for macaque area PE of the superior parietal cortex. *The Journal of Neuroscience*, *33*, 6648–6658.
- Battaglia-Mayer, A., Ferraina, S., Genovesio, A., Marconi, B., Squatrito, S., Molinari, M., ... Caminiti, R. (2001). Eye-hand coordination during reaching. II. An analysis of the relationships between visuomanual signals in parietal cortex and Parieto-frontal association projections. *Cerebral Cortex (New York, N.Y. : 1991)*, *11*, 528–544.
- Bhattacharyya, R., Musallam, S., & Andersen, R. A. (2009). Parietal reach region encodes reach depth using retinal disparity and vergence angle signals. *Journal of Neurophysiology*, *102*, 805–816.
- Bremner, L. R., & Andersen, R. A. (2012). Coding of the reach vector in parietal area 5d. *Neuron*, *75*, 342–351.
- Breveglieri, R., Galletti, C., Gamberini, M., Passarelli, L., & Fattori, P. (2006). Somatosensory cells in area PEc of macaque posterior parietal cortex. *The Journal of Neuroscience*, *26*, 3679–3684.
- Breveglieri, R., Galletti, C., Monaco, S., & Fattori, P. (2008). Visual, somatosensory, and bimodal activities in the macaque parietal area PEc. *Cerebral Cortex (New York, N.Y. : 1991)*, *18*, 806–816.
- Brodman, K. (1909). *Vergleichende Lokalisationslehre der Großhirnrinde in ihren Prinzipien dargestellt auf Grund des Zellenbaues*. Leipzig: Barth JA.
- Burbaud, P., Doegle, C., Gross, C., & Bioulac, B. (1991). A quantitative study of neuronal discharge in areas 5, 2, and 4 of the monkey during fast arm movements. *Journal of Neurophysiology*, *66*, 429–443.
- Cappe, C., Morel, A., & Rouiller, E. M. (2007). Thalamocortical and the dual pattern of corticothalamic projections of the posterior parietal cortex in macaque monkeys. *Neuroscience*, *146*, 1371–1387.
- Chen, J., Reitzen, S. D., Kohlenstein, J. B., & Gardner, E. P. (2009). Neural representation of hand kinematics during prehension in posterior parietal cortex of the macaque monkey. *Journal of Neurophysiology*, *102*, 3310–3328.
- Cooper, S., Riklan, M., & Rakic, P. (1974). *The pulvinar - LP complex: I*. Springfield, Ill: C. C. Thomas.
- Cudeiro, J., González, F., Pérez, R., Alonso, J. M., & Acuña, C. (1989). Does the pulvinar-LP complex contribute to motor programming?. *Brain Research*, *484*, 367–370.
- Duffy, F. H., & Burchfiel, J. L. (1971). Somatosensory system: Organizational hierarchy from single units in monkey area 5. *Science (New York, N.Y.)*, *172*, 273–275.
- Ferraina, S., & Bianchi, L. (1994). Posterior parietal cortex: Functional Properties of neurons in area 5 during an instructed-delay reaching task within different parts of space. *Experimental Brain Research*, *99*, 175–178.
- Ferraina, S., Battaglia-Mayer, A., Genovesio, A., Marconi, B., Onorati, P., & Caminiti, R. (2001). Early Coding of Visuomanual Coordination During Reaching in Parietal Area PEc. *Journal of Neurophysiology*, *85*, 462–467.
- Ferraina, S., Brunamonti, E., Giusti, M. A., Costa, S., Genovesio, A., & Caminiti, R. (2009). Reaching in depth: Hand position dominates over binocular eye position in the rostral superior parietal lobule. *The Journal of Neuroscience*, *29*, 11461–11470.
- Gallyas, F. (1979). Silver staining of myelin by means of physical development. *Neurological Research*, *1*, 203–209.
- Gamberini, M., Galletti, C., Bosco, A., Breveglieri, R., & Fattori, P. (2011). Is the medial posterior parietal area V6A a single functional area?. *The Journal of Neuroscience*, *31*, 5145–5157.
- Gamberini, M., Fattori, P., & Galletti, C. (2015). The medial parietal occipital areas in the macaque monkey. *Visual Neuroscience*, *32*, E013.
- Gamberini, M., Bakola, S., Passarelli, L., Burman, K. J., Rosa, M. G. P., Fattori, P., & Galletti, C. (2016). Thalamic projections to visual and visuomotor areas (V6 and V6A) in the Rostral Bank of the parieto-occipital sulcus of the Macaque. *Brain Structure and Function*, *221*, 1573–1589.
- Gamberini, M., Dal Bò, G., Breveglieri, R., Briganti, S., Passarelli, L., Fattori, P., & Galletti, C. (2017). Sensory properties of the caudal aspect of the macaque's superior parietal lobule. *Brain Structure and Function*, <https://doi.org/10.1007/s00429-017-1593-x>.
- Gamberini, M., Passarelli, L., Bakola, S., Impieri, D., Fattori, P., Rosa, M. G. P., & Galletti, C. (2017). Claustral afferents of superior parietal areas PEc and PE in the macaque. *The Journal of Comparative Neurology*, *525*, 1475–1488.
- García-Cabezas, M. Á., Rico, B., Sánchez-González, M. Á., & Cavada, C. (2007). Distribution of the dopamine innervation in the macaque and human thalamus. *Neuroimage*, *34*, 965–984.
- García-Cabezas, M. Á., Martínez-Sánchez, P., Sánchez-González, M. Á., Garzón, M., & Cavada, C. (2009). Dopamine innervation in the thalamus: Monkey versus rat. *Cereb Cortex*, *19*, 424–434.
- Grieve, K. L., Acuña, C., & Cudeiro, J. (2000). The primate pulvinar nuclei: Vision and action. *Trends in Neurosciences*, *23*, 35–39.
- Hadjidimitrakis, K., Dal Bo', G., Breveglieri, R., Galletti, C., & Fattori, P. (2015). Overlapping representations for reach depth and direction in caudal superior parietal lobule of macaques. *Journal of Neurophysiology*, *114*, 2340–2352.
- Hwang, K., Bertolero, M. A., Liu, W. B., & D'Esposito, M. (2017). The human thalamus is an integrative hub for functional brain networks. *The Journal of Neuroscience*, *37*, 5594–5607.
- Ilinsky, I. A., & Kultas-Ilinsky, K. (1987). Sagittal cytoarchitectonic maps of the *Macaca mulatta* thalamus with a revised nomenclature of the motor-related nuclei validated by observations on their connectivity. *The Journal of Comparative Neurology*, *262*, 331–364.
- Johnson, P. B., Ferraina, S., Bianchi, L., & Caminiti, R. (1996). Cortical networks for visual reaching: Physiological and anatomical organization of frontal and parietal lobe arm regions. *Cerebral Cortex (New York, N.Y. : 1991)*, *6*, 102–119.
- Jones, E. G., Coulter, J. D., & Hendry, S. H. (1978). Intracortical connectivity of architectonic fields in the somatic sensory, motor and parietal cortex of monkeys. *The Journal of Comparative Neurology*, *181*, 291–347.
- Kaas, J. H., & Lyon, D. C. (2007). Pulvinar contributions to the dorsal and ventral streams of visual processing in primates. *Brain Research Reviews*, *55*, 285–296.
- Kalaska, J. F. (1996). Parietal cortex area 5 and visuomotor behavior. *Canadian Journal of Physiology and Pharmacology*, *74*, 483–498.
- Krubitzer, L., & Disbrow, E. (2008). The evolution of parietal areas involved in hand use in primates. In J. Kaas, & E. Gardner (Eds), *The senses: A comprehensive reference* (pp. 183–214). London: Elsevier.
- Kumar, V. J., van Oort, E., Scheffler, K., Beckmann, C. F., & Grodd, W. (2017). Functional anatomy of the human thalamus at rest. *Neuroimage*, *147*, 678–691.
- Laberge, D., & Buchsbaum, M. S. (1990). Positron emission tomographic measurements of pulvinar activity during an attention task. *Journal of Neuroscience*, *6*, 613–619.

- Lacquaniti, F., Guigon, E., Bianchi, L., Ferraina, S., & Caminiti, R. (1995). Representing spatial information for limb movement: Role of area 5 in the monkey. *Cerebral Cortex (New York, N.Y. : 1991)*, 5, 391–409.
- Luppino, G., Ben Hamed, S., Gamberini, M., Matelli, M., & Galletti, C. (2005). Occipital (V6) and parietal (V6A) areas in the anterior wall of the parieto-occipital sulcus of the macaque: A cytoarchitectonic study. *The European Journal of Neuroscience*, 21, 3056–3076.
- Mai, J. K., & Forutan, F. (2012). Thalamus. In J. K. Mai, & G. Paxinos (Eds), *The human nervous system* (3rd ed., pp. 618–677). Amsterdam: Academic Press.
- Maimon, G., & Assad, J. A. (2006). Parietal area 5 and the initiation of self-timed movements versus simple reactions. *The Journal of Neuroscience*, 26, 2487–2498.
- Marconi, B., Genovesio, A., Battaglia-Mayer, A., Ferraina, S., Squatrito, S., Molinari, M., ... Caminiti, R. (2001). Eye-hand coordination during reaching. I. Anatomical relationships between parietal and frontal. *Cerebral Cortex (New York, N.Y. : 1991)*, 11, 513–527.
- Markov, N. T., Misery, P., Falchier, A., Lamy, C., Vezoli, J., Quilodran, R., ... Knoblauch, K. (2011). Weight consistency specifies regularities of macaque cortical networks. *Cerebral Cortex (New York, N.Y. : 1991)*, 21, 1254–1272.
- Mastropasqua, C., Bozzali, M., Spanò, B., Koch, G., & Cercignani, M. (2015). Functional anatomy of the thalamus as a model of integrated structural and functional connectivity of the human brain in vivo. *Brain Topography*, 28, 548–558.
- Matelli, M., Govoni, P., Galletti, C., Kutz, D. F., & Luppino, G. (1998). Superior area 6 afferents from the superior parietal lobule in the macaque monkey. *The Journal of Comparative Neurology*, 402, 327–352.
- Mathers, L. H., & Rapisardi, S. C. (1973). Visual and somatosensory receptive fields of neurons in the squirrel monkey pulvinar. *Brain Research*, 64, 65–83.
- Mesulam, M. M. (1990). Large-scale neurocognitive networks and distributed processing for attention, language, and memory. *Annals of Neurology*, 28, 597–613.
- Middleton, F. A., & Strick, P. L. (2000). Basal ganglia and cerebellar loops: Motor and cognitive circuits. *Brain Research. Brain Research Reviews*, 31, 236–250.
- Mitchell, A. S. (2015). The mediodorsal thalamus as a higher order thalamic relay nucleus important for learning and decision-making. *Neuroscience and Biobehavioral Reviews*, 54, 76–88.
- Mountcastle, V. B., Lynch, J. C., Georgopoulos, A., Sakata, H., & Acuña, C. (1975). Posterior parietal association cortex of the monkey: Command functions for operations within extrapersonal space. *Journal of Neurophysiology*, 38, 871–908.
- Mushiake, H., & Strick, P. L. (1995). Pallidal neuron activity during sequential arm movements. *Journal of Neurophysiology*, 74, 2754–2758.
- Olszewski, J. (1952). *The thalamus of the Macaca Mulatta. An atlas for use with the stereotaxic instrument*. Basel: Karger.
- O'Muirheartaigh, J., Keller, S. S., Barker, G. J., & Richardson, M. P. (2015). White matter connectivity of the thalamus delineates the functional architecture of competing thalamocortical systems. *Cerebral Cortex*, 25, 4477–4489.
- Padberg, J., Franca, J. G., Cooke, D. F., Soares, J. G. M., Rosa, M. G. P., Fiorani, M., ... Krubitzer, L. (2007). Parallel evolution of cortical areas involved in skilled hand use. *Journal of Neuroscience*, 27, 10106–10115.
- Padberg, J., Cerkevich, C., Engle, J., Rajan, A. T., Recanzone, G., Kaas, J., & Krubitzer, L. (2009). Thalamocortical connections of parietal somatosensory cortical fields in macaque monkeys are highly divergent and convergent. *Cerebral Cortex*, 19, 2038–2064.
- Palmer, S. M., & Rosa, M. G. P. (2006). Quantitative analysis of the cortico-cortical projections to the middle temporal area in the marmoset monkey: Evolutionary and functional implications. *Cerebral Cortex*, 16, 1361–1375.
- Pandya, D. N., & Seltzer, B. (1982). Intrinsic connections and architectonics of posterior parietal cortex in the rhesus monkey. *The Journal of Comparative Neurology*, 204, 196–210.
- Percheron, G. (2004). Thalamus. In G. Paxinos, & J. K. Mai (Eds), *The human nervous system* (pp. 439–468). San Diego: Academic Press.
- Pischerchia, V., Breveglieri, R., Hadjidimitrakis, K., Bertozzi, F., Galletti, C., & Fattori, P. (2017). Mixed body/hand reference frame for reaching in 3d space in macaque parietal area PEC. *Cerebral Cortex (New York, N.Y. : 1991)*, 27, 1976–1990.
- Raffi, M., Squatrito, S., & Maioli, M. G. (2002). Neuronal responses to optic flow in the monkey parietal area PEC. *Cerebral Cortex*, 6, 639–646.
- Raffi, M., Ballabeni, A., Maioli, M. G., & Squatrito, S. (2008). Neuronal responses in macaque area PEC to saccades and eye position. *Neuroscience*, 156, 413–424.
- Rausell, E., Bickford, L., Manger, P. R., Woods, T. M., & Jones, E. G. (1998). Extensive divergence and convergence in the thalamocortical projection to monkey somatosensory cortex. *The Journal of Neuroscience*, 18, 4216–4232.
- Romanski, L. M., Giguere, M., & Bates, J. F. (1997). Topographic organization of medial pulvinar connections with the prefrontal cortex in the rhesus monkey. *Journal of Comparative Neurology*, 332, 313–332.
- Rosa, M. G. P., Palmer, S. M., Gamberini, M., Tweedale, R., Piñon, M. C., & Bourne, J. A. (2005). Resolving the organization of the New World monkey third visual complex: The dorsal extrastriate cortex of the marmoset (*Callithrix jacchus*). *Journal of Comparative Neurology*, 483, 164–191.
- Sakata, H., Takaoka, Y., Kawarasaki, A., & Shibutani, H. (1973). Somatosensory properties of neurons in the superior parietal cortex (area 5) of the rhesus monkey. *Brain Research*, 64, 85–102.
- Sanchez-Gonzalez, M. A. (2005). The primate thalamus is a key target for brain dopamine. *Journal of Neuroscience*, 25, 6076–6083.
- Schmahmann, J. D., & Pandya, D. N. (1990). Anatomical investigation of projections from thalamus to posterior parietal cortex in the rhesus monkey: A WGA-HRP and fluorescent tracer study. *The Journal of Comparative Neurology*, 295, 299–326.
- Seelke, A. M. H., Padberg, J. J., Disbrow, E., Purnell, S. M., Recanzone, G., & Krubitzer, L. (2012). Topographic Maps within Brodmann's Area 5 of Macaque Monkeys. *Cerebral Cortex (New York, N.Y. : 1991)*, 22, 1834–1850.
- Shi, Y., Apker, G., & Buneo, C. A. (2013). Multimodal representation of limb endpoint position in the posterior parietal cortex. *Journal of Neurophysiology*, 109, 2097–2107.
- Snider, R. S., & Lee, J. C. (1961). *A stereotaxic atlas of the monkey brain (Macaca mulatta)*. Chicago: University of Chicago Press.
- Sommer, M. E. (2003). The role of the thalamus in motor control. *Current Opinion in Neurobiology*, 13, 663–670.
- Squatrito, S., Raffi, M., Maioli, M. G., & Battaglia-Mayer, A. (2001). Visual motion responses of neurons in the caudal area PE of macaque monkeys. *The Journal of Neuroscience*, 21, RC130.
- Tanné, J., Boussaoud, D., Boyer-Zeller, N., & Rouiller, E. M. (1995). Direct visual pathways for reaching movements in the macaque monkey. *Neuroreport*, 7, 267–272.
- Tanné-Gariépy, J., Rouiller, E. M., & Boussaoud, D. (2002). Parietal inputs to dorsal versus ventral premotor areas in the macaque monkey: Evidence for largely segregated visuomotor pathways. *Experimental Brain Research*, 145, 91–103.

- Taoka, M., Toda, T., & Iwamura, Y. (1998). Representation of the midline trunk, bilateral arms, and shoulders in the monkey postcentral somatosensory cortex. *Experimental Brain Research*, 123, 315–322.
- Taoka, M., Toda, T., Iriki, A., Tanaka, M., & Iwamura, Y. (2000). Bilateral receptive field neurons in the hindlimb region of the postcentral somatosensory cortex in awake macaque monkeys. *Experimental Brain Research*, 134, 139–146.
- Van Buren, J. M., & Borke, R. C. (1972). *Variations and connections of the human thalamus*. Berlin: Springer.
- Van Der Werf, Y. D., Witter, M. P., & Groenewegen, H. J. (2002). The intralaminar and midline nuclei of the thalamus. Anatomical and functional evidence for participation in processes of arousal and awareness. *Brain Research. Brain Research Reviews*, 39, 107–140.
- Van Essen, D. C., Drury, H. A., Dickson, J., Harwell, J., Hanlon, D., & Anderson, C. H. (2001). An integrated software suite for surface-based analyses of cerebral cortex. *Journal of the American Medical Informatics Association*, 8, 443–459.
- Vitek, J. L., Ashe, J., DeLong, M. R., & Alexander, G. E. (1994). Physiologic properties and somatotopic organization of the primate motor thalamus. *Journal of Neurophysiology*, 71, 1498–1513.
- Watanabe, Y., & Funahashi, S. (2004). Neuronal activity throughout the primate mediodorsal nucleus of the thalamus during oculomotor delayed-responses. II. Activity encoding visual versus motor signal. *Journal of Neurophysiology*, 92, 1756–1769.
- Yeterian, E. H., & Pandya, D. N. (1985). Corticothalamic connections of the posterior parietal cortex in the rhesus monkey. *The Journal of Comparative Neurology*, 237, 408–426.
- Yirmiya, R., & Hocherman, S. (1987). Auditory- and movement-related neural activity interact in the pulvinar of the behaving rhesus monkey. *Brain Research*, 402, 93–102.
- Yuan, R., Di, X., Taylor, P. A., Gohel, S., Tsai, Y. H., & Biswal, B. B. (2016). Functional topography of the thalamocortical system in human. *Brain Structure & Function*, 221, 1971–1984.

How to cite this article: Impieri D, Gamberini M, Passarelli L, Rosa MGP, Galletti C. Thalamo-cortical projections to the macaque superior parietal lobule areas PEc and PE. *J Comp Neurol*. 2018;526:1041–1056. <https://doi.org/10.1002/cne.24389>